UPPSALA
UNIVERSITET

Parallel electric fields in space

Observations by Cluster satellites inside the auroral zone at altitudes above the main acceleration region

Erik Bergman

Master of Science Thesis

Department of Astronomy and Space Physics
Uppsala University

February, 2003

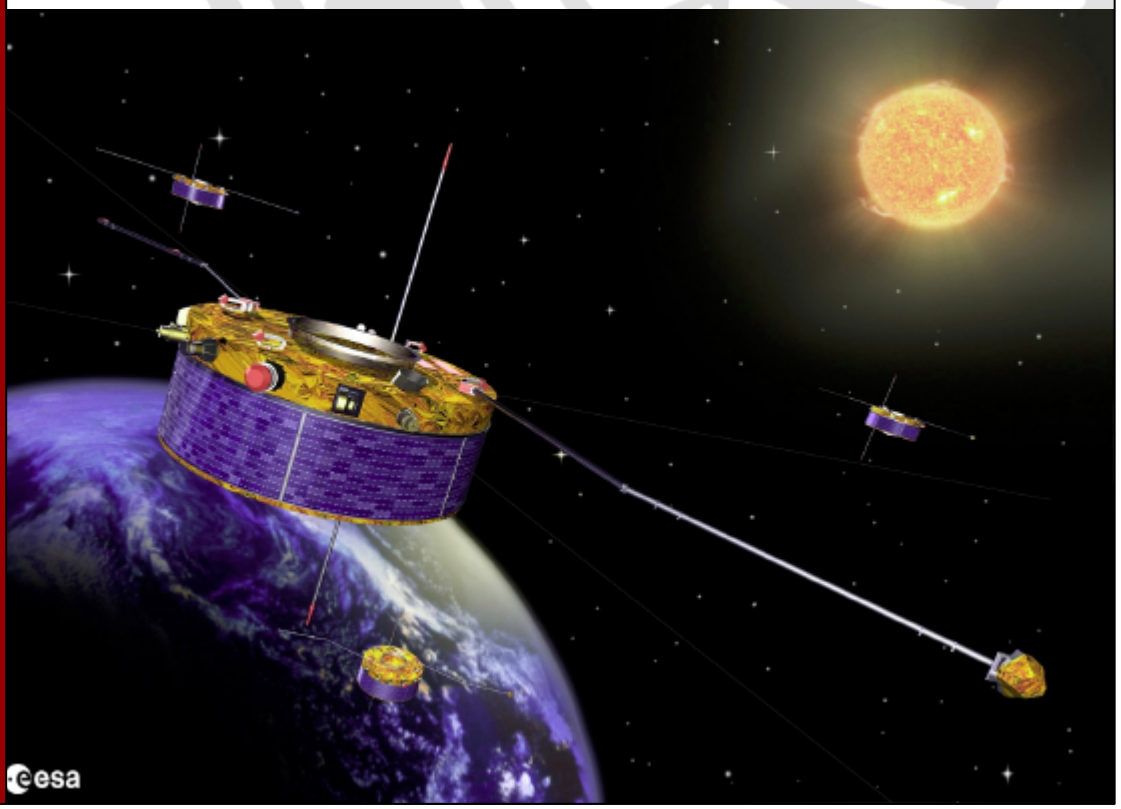

UPPSALA UNIVERSITET

Engineering Physics Programme
Uppsala University School of Engineering

UPTEC F 03 017	Date of issue 2003-02-26
Author Erik Bergman	
Title (English) Parallel electric fields in space – Observations by Cluster satellites inside the auroral zone at altitudes above the main acceleration region	
Title (Swedish)	

Abstract

In this study the four ESA Cluster satellites have been used for finding and investigating small electric fields (~1 mV/m) parallel to the magnetic field in the night-side auroral region at altitudes of about 4.5 Earth radii. The direction of the parallel electric fields at this altitude can tell something about which electric potential model is more plausible - the U or the O potential.

About 500 hundred events have been looked at and 57 of these have been studied closer. Five of these events were selected and analysed in detail. In total six parallel electric fields were found. All were upwards and had an amplitude between 0.5 – 1.5 mV/m. In addition three double layers and one solitary wave have been found, which give support to the parallel electric fields. Also an event showing the break-up of waves into double layers was discovered.

Several interpretations are possible based on the results from this altitude. It can be related to a U-potential or the lower part of an O-potential, or it could be a U-potential on top an O-potential. The lack of downward parallel electric fields could be explained by that they are too small to be measured by Cluster or that the O-potential has already closed at lower altitudes. Also there is a possibility that the results are due to the wake effect.

Keywords Parallel electric fields, Space plasma physics, Auroral arcs, Cluster satellites	
Supervisor(s) Andris Vaivads	
Examiner Annika Olsson	
Project name	Sponsors
Language English	Security
ISSN 1401-5757	Pages 102
Supplementary bibliographical information	

School of Engineering, Studies Office

Visiting address: Lägerhyddsvägen 1, The Ångström laboratory, Uppsala

Postal address: Box 536, SE-751 21, Uppsala, Sweden

Phone: +46-(0)18-4713003

Fax: +46-(0)18-4713000

E-mail: kansli@uth.uu.se

Acknowledgments

This Master of Science Thesis has been conducted at The Department of Astronomy and Space Physics at Uppsala University.

First and foremost I would like to thank my instructors, Andris Vaivads and Annika Olsson, for their invaluable support. I would like to thank Mats André for arranging this thesis project. In addition I want to thank Anders Eriksson, Pekka Janhunen, Forrest Mozer, and Per-Arne Lindqvist for inputs.

Contents

Chapter 1

Introduction

Auroral physics is one piece of the gigantic magnetospheric puzzle, which is governed by the solar-terrestrial environment. To explain the aurora an understanding of the electric fields parallel to the magnetic field is needed. The introduction in this report is quite extensive and will start with a "wide" approach about the magnetospheric physics incorporating a historic review and the basic physics in the area. Then Earth's magnetosphere and auroras will be discussed. Finally the introduction will narrow down to specifics about electric fields, why they are so important, and how different electric potential models for aurora look like.

1.1 The Myth and Beauty of Auroras

The wondrous and mighty displays of light in the sky, for us known as the Aurora or the Northern Lights, have through the centuries inspired and baffled mankind. Different explanations for the show in the sky have made their mark in folklore and religion, especially in the northern part of our globe where the observations of aurora displays are more common. There are also so called Southern Lights that usually hover above unpopulated Antarctica and the polar sea areas. Sometimes it can be seen in New Zealand and southern Australia.

The legends and beliefs triggered by the aurora have remarkable similarities in the northern and southern hemisphere. In Europe and North America various people thought that the light in the sky was reflections of campfires from people in the north. The Maori of New Zealand believed that the light came from huge bonfires lit by descendants of ancestors that traveled far to the south and got trapped by snow and ice.

The ever-changing forms in the sky were explained in various ways. The Eskimos of the lower Yukon River in Alaska saw the souls of their favorite animals like deer, seal, salmon and beluga whales. The Finns saw magical fire-foxes racing in the sky with sparks flying from their gleaming furs. For the Swedes it was a folk dance called Polka and for the Scots it was merry dancers. In Estonia the aurora was the glow from a celestial wedding with the shine coming from the horses and the sleds. The Samís of northern Sweden, Norway, Finland and Russia described the aurora as "Girls running around the fireplace dragging their pants".

Throughout history, the aurora has terrified people of many cultures, especially those living south of the north auroral zone, where the aurora is more rare and more likely to be red. In 507 AD Romans awoke to what they thought, a fierce battle in the sky with glowing armies at the same time as the Longobards attacked their empire. In the late Middle Ages, the Europeans were panic stricken by a great aurora, which they were convinced of being attacking armies. An artists impression of the armies in the sky above Europe is seen in Fig. 1.1.

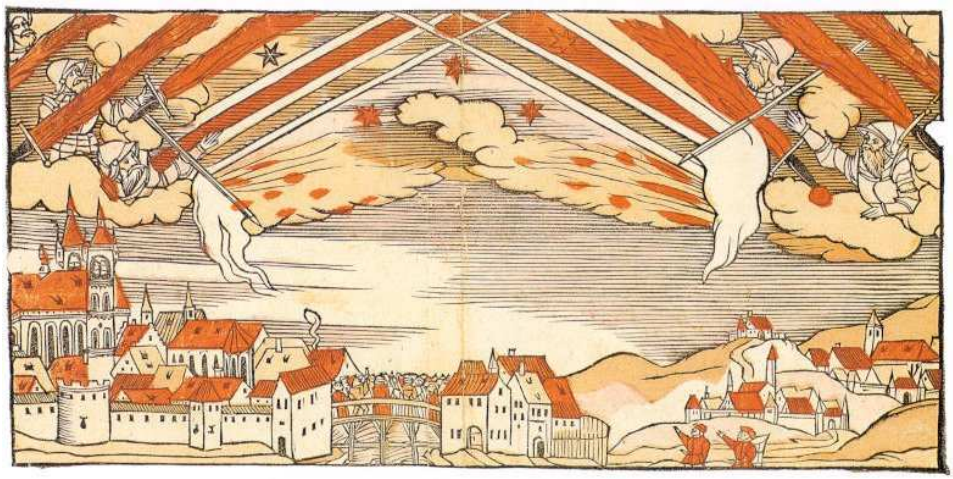

Figure 1.1: Armies in the sky over a terrified Bamberg, Germany in 1560. [Savage, C., 1994]

1.2 The Early Investigators

From early on philosophers tried to explain the aurora more scientifically. In 593 BC, a Greek philosopher named Anaximenes saw "inflammable exhalations from the Earth" as a cloud of burning gas. A century later Hippocrates of Chios proposed that the vapors were not on fire but rather lit by stray sunlight. When Aristotle approached the subject a century later he retarded further development for nineteen centuries due to his influence. For him it was basic truth that the heavens were perfect and unchanging. It was only in the near earth zone that anything could move or change and it was here that he located the source of the aurora.

The explanation of the phenomenon as earthly fumes remained way into the 18th century. A Swede named Samuel von Triewald even "proved" it experimentally in the 1740s. In a dark room he let refracted light shine through vapors rising from a glass of Cognac. An aurora could be seen - colored light was dancing over the screen. He confidently proclaimed that he had created an artificial aurora.

At the same time Edmond Halley wondered if the mysterious light in the sky could be a direct result of the Earth's magnetism. Maybe atoms of magnetic matter were circulating the Earth and between the poles of this great magnet. Halley's theory was strengthened by an observation made by a Swede, Olof Hiorter (Anders Celsius' brother-in-law). On 1 March 1741 he saw an aurora and simultaneously a great movement of his magnetic needle. He continued making readings every hour, and concluded after 6638 readings that the lights were associated with magnetic disturbances. In 1768 another Swede, Johann Carl Wilcke, discovered that the auroral rays were aligned with "the magnetic force".

A French physicist by the name of Jean Jacues d'Ortous de Mairan did not believe that the aurora had its source in the Earth. Just as Anaxagoras he looked for the answers in the Sun. He thought that the phenomenon was caused by the Sun's atmosphere, which he imagined as a fluid. He was certain that this fluid flowed close to Earth and got caught by the rotation and then got distributed to the poles where it showed as aurora. Skeptics asked why the aurora was so unpredictable and Mairan's thoughts went to the dark spots on the Sun. He wrote: "Is it not likely that a kind of precipitation of particles from the solar atmosphere causes the spots that so often appear on the surface of the Sun". And could not one discover some analogy between the frequency, the cessations and the returns of these spots, and the appearances, returns and cessations of the...[aurora]?"

In 1779 Benjamin Franklin made a presentation for the Royal Academy of Sciences on the nature of the aurora. He suggested that the lights were electrical discharges. At the end of the eighteenth

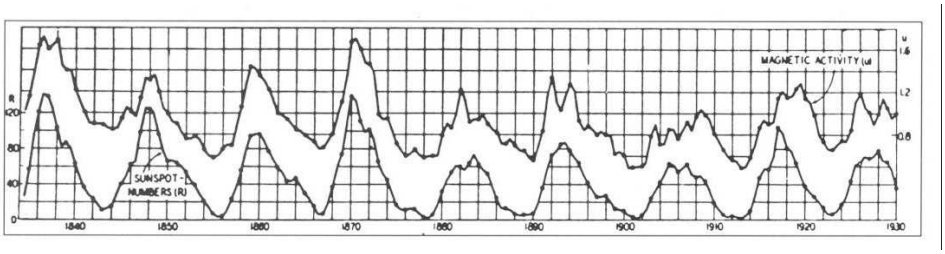

Figure 1.2: Graph showing the correlation between the number of sunspots and magnetic storms. [Savage, C., 1994]

century all the major ingredients needed to form a correct explanation had been thrown into the pot; earthly vapor, Earth's magnetism, the solar atmosphere and electricity.

In 1805 Alexander von Humboldt set up his magnetic instruments in a rented stone cottage on the outskirts of Berlin. For over a year Humboldt and his assistant recorded all the small changes of a magnetic needle with a microscope. After 13 months of half-hourly readings they not only found regular daily oscillations but also occasional violent fluctuations - magnetic storms - and often they were accompanied by auroras. The First World War stopped Humboldt for a few years. After that he commenced his research and also compared his data with colleagues in Paris and Freiburg. What he found was remarkable - the magnetic disturbances occurred at the same time at all three locations - these magnetic storms were not local phenomena. Humboldt shared his thoughts with a local astronomer, Carl Gauss, who immediately turned his talent to Earth's magnetic field. After improving instruments for measuring magnetic fields he set up a network of observatories in Germany, Sweden and Italy, which were linked to those in Russia. In 1838 he finally developed a technique to calculate Earth's magnetic field at any point of the globe.

In Germany an amateur astronomer named Samuel Schwabe had been studying the dark spots on the Sun for thirty years. Year by year he tabulated the data and a pattern emerged: a wave-like curve with a period of roughly 10 years. Humboldt's partner, Edward Sabine, discovered a connection between Schwabe's data and his own data over the number of annual magnetic storms, they followed the same cyclic ups and downs, as can be seen in Fig. 1.2. Sabine reported his discovery in 1852.

In 1820 a Dane by the name Hans Christian Oerstedt showed that a magnetic needle showed a disturbance when it was held near an electric wire. Eleven years later Michael Faraday demonstrated the opposite effect - by moving a wire over a magnet a current was induced. Electricity and magnetism were twin aspects to the same force. Faraday suggested that this electromagnetism could travel like a wave and therefore the magnetic energy could be dispersed through space. Despite this many scientists were reluctant to acknowledge the possibility of solar influence.

At the turn of the century a Norwegian, Kristian Birkeland, was setting up an experiment that hopefully would prove his theory. Could it be that streams of electrons were emitted from sunspots and traveled through space towards Earth and perhaps these electrons ultimately were caught by Earth's magnetic field and directed towards the poles. In his experiment he sent electrons towards a magnetized sphere which was suspended in partial vacuum (see Fig. 1.3). To his astonishment bright rings of light appeared over the globe's north and south poles. Birkeland revealed his auroral theory in the early years of the 20th century. Birkeland's explanation was a block-buster. But there was a problem, if the Sun sent a steady beam of electrons towards the Earth would it not tear itself apart due to electric repulsion. Sydney Chapman wondered if the matter from the Sun was in the form of a very thin highly ionized and neutral gas, a plasma. This plasma would not be torn apart. This simple idea took over his life and he started to develop the math needed to the describe it.

A modern description of a plasma, taken from a book on space plasma physics, can look like this: *"A plasma is a gas of charged particles, which consists of equal numbers of free positive and negative charge carriers. Having roughly the same number of charges with different signs in the*

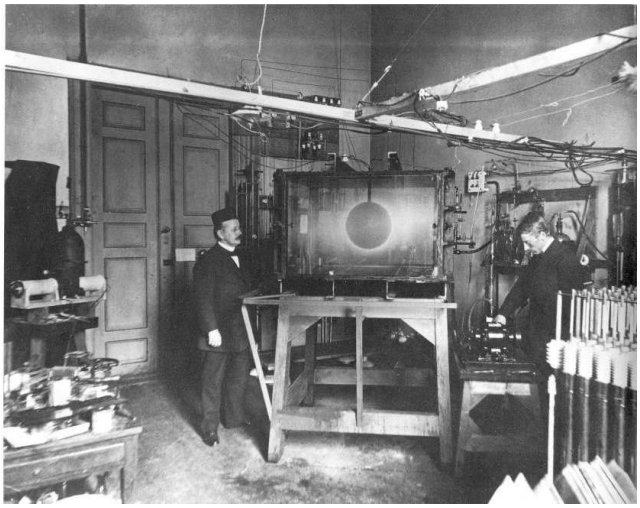

Figure 1.3: Birkeland (left) oversees an experiment in which electrons are sent towards a magnetized sphere. [Savage, C., 1994]

same volume element guarantees that the plasma behaves quasineutral in the stationary state. On average a plasma looks electrically neutral to the outside, since the randomly distributed particle electric charge fields mutually cancel." [Baumjohann and Treumann, 1996]

1.3 The Solar-Terrestrial Environment

So where do the precipitating particles (mostly electrons and protons) come from that cause the aurora? Some of them surely originate from the ionosphere but a large part of the particles are supplied by the Sun via the solar wind. Our Sun's corona is pouring out a steady stream of plasma in all directions and some of it is bound to hit Earth. This plasma consists of approximately equal amounts of electrons and ions where the ion component is made up of 95 % protons, a few percent double ionized helium and traces of heavier elements. In addition to particles the solar wind also carries a magnetic field originating from the Sun - the IMF (Interplanetary Magnetic Field). The solar wind mostly originates from areas with open magnetic field lines, that is field lines that extend virtually indefinitely out in space, but can also come from areas with closed magnetic fields in the form of Coronal Mass Ejections (CME). When the supersonic solar wind hits Earth's magnetic field a bow shock forms that looks much like the bow shock from a stone in a stream. In addition to this bow shock the magnetosphere gets squashed at the day-side and drawn out on the night-side, see Fig. 1.4 a).

A magnetic substorm is triggered by the IMF when it has a component that is directed southward, opposite the direction of the Earth's magnetic field at the dayside. When this happens a phenomenon called reconnection takes place. The IMF's and Earth's magnetic fields connect and the result is an opening along a wide equatorial belt which enables slow, hot, and dense plasma from the solar wind to penetrate the magnetosphere. These charged particles bombard the atmosphere at high latitudes in the dayside. The resulting electric current heats up the atmosphere resulting in large amounts of ionospheric ions being pumped into the magnetosphere. These particles together with particles from the solar wind is stored in the plasma sheet (see Fig. 1.4 b). The transfer of magnetic energy from the solar wind radically alters the shape of the magnetosphere. The interconnected IMF and Earth's magnetic field lines are swept back over the nightside of the magnetosphere pouring energy into the lobes. The swelling lobes squash the plasma sheet, which becomes thinner and thinner and at some distance downstream (on the nightside) a second reconnection takes place allowing the

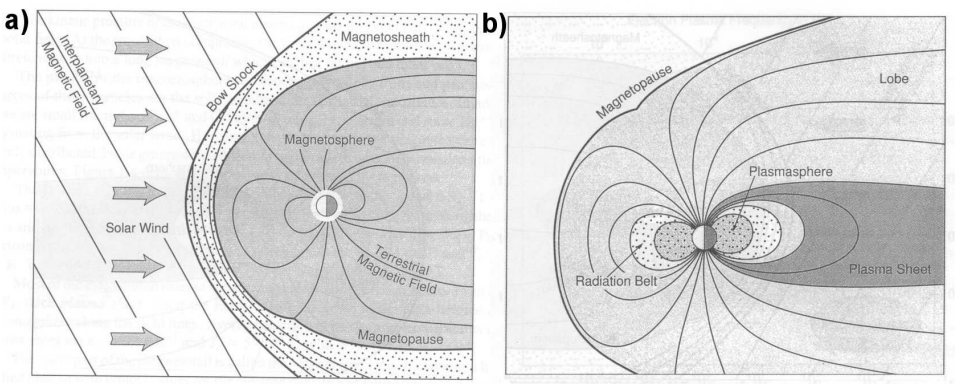

Figure 1.4: a) Topography of the solar-terrestrial environment. b) The magnetosphere [Baumjohann and Treumann, 1996]

IMF field to continue its journey through space. This second reconnection allows Earth's magnetic field to snap back to its original configuration. When this happens enormous amounts of energy is released and the ions and electrons stored in the plasma sheet are injected into the inner parts of the magnetosphere. Some of these particles, guided by magnetic field lines, end up over the poles stimulating increased auroral emissions in the ionosphere. The orientation of the IMF turns southward fairly often, so on average substorms occur a few times every day and last for between one and three hours.

The ionosphere forms an electrically conducting layer in the upper atmosphere. It consists of a mix of neutral atoms and molecules of the atmosphere, like oxygen and nitrogen, and electrons and ions. The ionosphere stretches from the bottom at about 80 km to over 800 km.

The auroral emissions take place in the ionosphere and are the results of transitions in energy levels for different ions and atoms. In excited species an electron jumps from a higher energy orbital to a lower energy orbital and gives of a photon with a wavelength corresponding to the energy difference of the levels. The major visual emissions are those from atomic oxygen; 630.0 nm (blood red), and 557.7 nm (yellow-green), and from singly ionised molecular nitrogen: 427.8 nm (blue). The red emissions, coming from low energy electrons, dominate the regions above 200 km, while green line emissions, coming from high energy electrons, dominate between 100 and 200 km. Below 100 km there is a mix of bluish emissions from N_2^+ and reddish from N_2 and O_2^+.

There is always an auroral oval crowning the south pole and north pole of our globe. These ovals are located between 65 and 75 and between -65 and -75 degrees magnetic latitude, referred as the auroral zone. There are always particles precipitating causing auroral emissions in the whole electromagnetic spectrum from microwaves to gamma rays. There is usually a background diffuse aurora in the lower latitude part of the auroral zone caused by low energetic precipitating particles (~100 eV - ~1 keV). The bright arcs and other forms that can be seen are products from beams or sheets of energetic electrons that are usually narrowly focused in energy, 1 to 10 keV.

Auroras come in many different colors, shapes, and sizes. Arcs and rays can have a vertical extent of hundreds of kilometers, starting around 100 km and up to 600 km along the magnetic field lines. These curtains can have a small horizontal size of ~100 meters, or they can be so large that they cover the whole sky. They can be virtually stable for minutes and then suddenly start to wave, with patches disappearing and appearing again.

1.4 Electric Fields in Space

Bright arcs are caused by energetic electrons that are accelerated by electric fields. Electric fields perpendicular to the magnetic field, hence forward called perpendicular electric fields, allows electrons and ions to gyrate around a specific magnetic field line and thus drifting with it. While the perpendicular electric fields only make the electrons gyrate, the electric fields parallel to the magnetic field, referred to as parallel electric fields, accelerate electrons along the magnetic field lines. To get an expression for the effect of magnetic and electric fields on charged particles the single particle motion must be considered.

The equation of motion for a particle with a charge q is governed by the Coulomb force (in an electric field), and the Lorentz force (in a magnetic field). Neglecting collisions and gravitation (as can be done in most of the magnetosphere) the governing equation is

$$m\frac{d\mathbf{v}}{dt} = q(\mathbf{E} + \mathbf{v} \times \mathbf{B}) \tag{1.1}$$

Here v denotes the velocity and m the mass of the particle. In Eq. 1.1 it can be seen that the force acting on the particle due to the electric field $\mathbf{E}$ is always in the direction of the electric field vector, but the force stemming from the magnetic field $\mathbf{B}$ is always directed perpendicular to the velocity direction of the particle. This means that the electric field can energise a particle while the magnetic field only makes it gyrate around the magnetic field line. By taking the dot product of v with both sides of Eq. 1.1 we get the resulting energy conservation equation.

$$\mathbf{v} \cdot m\frac{d\mathbf{v}}{dt} = \mathbf{v} \cdot q(\mathbf{E} + \mathbf{v} \times \mathbf{B}) \Rightarrow \frac{d}{dt}\left(\frac{mv^2}{2}\right) = q(\mathbf{v} \cdot \mathbf{E}) \tag{1.2}$$

The magnetic field influence vanishes because $\mathbf{v}$ is perpendicular to $\mathbf{v} \times \mathbf{B}$. It is easily seen that the only way to change the kinetic energy of a charged particle is energisation by an electric field. That shows the importance of electric fields in particle acceleration. Parallel electric fields are efficient accelerators that accelerate charged particles along the magnetic field lines and are widely believed to play a major role in the production of auroral particles [Fälthammar, C.-G., 1983].

As long as the electric field parallel to the magnetic field, is zero the 'frozen in field condition' is satisfied [Fälthammar, C.-G., 1983].

$$\nabla \times \mathbf{B}(\mathbf{E} \cdot \mathbf{B}/B^2) = \nabla \times \mathbf{E}_{\|} = 0 \tag{1.3}$$

This means that any two elements of plasma that are on the same magnetic field line will still be on that same line an instant later. If the parallel electric field is non-zero this condition does not apply any longer. Magnetic field lines are then cut off and a decoupling of the motions of magnetically connected plasmas occur. This is another reason why parallel electric fields are important in space physics.

1.5 Discrete Aurora

Discrete auroral arcs are typically bright and localised structures. They are usually elongated in the east-west direction and narrow in the north-south direction. The typical north-south scale size is about 5 km, but it can range between 100 m - 80 km. Discrete auroral arcs are caused by precipitating magnetospheric electrons from the plasmasheet. The peak energy usually has a maximum value near the center of the arc, and decreases north and south of the centre, resulting in an inverted-V form of the electron energy spectrum when observed by satellites crossing the arc. Parallel electric fields at about 1-2 R_E, are generally agreed to be responsible for the acceleration of down-going inverted-V electrons and also for up-going ion-beams.

The existence of upward directed parallel electric fields above auroral arcs was theoretically suggested by Alfvén in 1958 [Alfven, H., 1958], and the first indications of parallel fields in the auroral

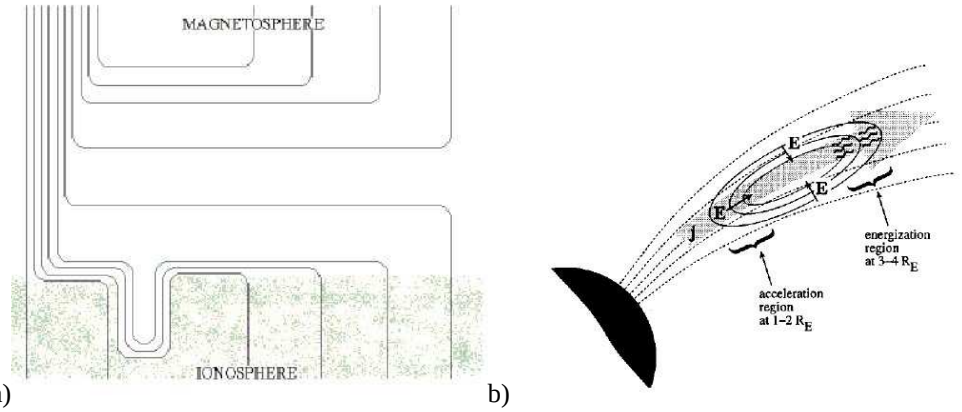

a) b)

Figure 1.5: a) U-shaped model that is a bit asymmetric and thus has a S-shaped feature as well [Mozer and Hull, 2001]. b) O-shaped model [Janhunen et al, 2001]

acceleration region came from electron spectra measurements by a sounding rocket [McIlwain, C. E., 1960]. The first real evidence came from measurements of very large perpendicular electric fields in the acceleration region done by the S3-3 satellite [Mozer et al, 1977]. The conclusion was that parallel electric fields must exist because no strong perpendicular electric fields are observed in the ionosphere. This lead to the suggested U-shaped potential model [Carlqvist and Boström, 1970], as a description of the geometry of the electric potentials.

Direct observations of parallel electric fields have also been done. Measurements done in studies using FAST and Viking satellites have shown evidence of large parallel electric fields at high altitudes (up to 14 000 km, ~2.2 R_E) [Lindqvist and Marklund, 1990, Ergun et al, 2001].

1.6 Different Potential Models

It is not exactly clear how the electric fields responsible for auroral electron acceleration are distributed along the magnetic field lines. The U-shaped potential model has long been used for explaining the electron acceleration. In the classical model the bottom of the U is located in the acceleration region, at about 1-2 R_E, and the flanks of the potential contours goes up along the magnetic field lines only to close again in an U in the other hemisphere. In a more geometrically asymmetric case the U-shape would look more S-shaped, as can be seen in Fig. 1.5 a. The S-model assumes an upward field-aligned current in the region. The low altitude boundary have features that are called fingers, which extend to lower altitudes. If a spacecraft passes one of these fingers it will observe large perpendicular fields, eventually a parallel field, and in the middle low plasma density. The low plasma density is due to a lack of cold plasma, which almost entirely has been accelerated in order to carry the field aligned current [Mozer and Hull, 2001].

Many observations in the acceleration region supports the U-shaped model. However, there are not many detailed studies of electric fields at altitudes above the main acceleration region. In a study at high altitudes (~4 R_E), using Polar satellite data [Janhunen et al, 1999], the lack of perpendicular fields lead to the suggestion of a closed U-shaped potential forming an O-potential below 4 R_E (see Fig. 1.5 b). Thus, in the lower part of both the open U-shaped model and the O-shaped model the characteristics are the same. Only an O-shaped potential structure would not give any net acceleration to electrons crossing the structure. Electrons with enough energy to pass the top part of the O will have the same energy after passing the whole structure as it initially had, while low energy electrons will be filtered out. Somewhere the electrons have to gain energy in order to cause the intensity measured at lower altitudes. To fix the intensity problem it has been proposed that

there are plasma waves above the main acceleration region causing parallel energisation of electrons [Janhunen and Olsson, 2000]. The wave-particle interaction is assumed to be resonant so that only middle-energy electrons (100 - 1000 eV) are affected. In the upper part of the potential structure the electrons are slowed down and thus given more time to be affected by the plasma waves, resulting in a gain of energy.

Both the O-shaped and the U-shaped models are quasistatic descriptions, even though the O-shaped model needs support from waves. There are also descriptions of acceleration models that are based entirely on waves that can be important. In these descriptions different plasma waves are responsible for the auroral particle acceleration.

1.7 What We Are Looking For and Where

What happens above the main acceleration zone is currently not well known. Electric fields have not been studied so much in this region. This is an investigation aimed at searching for parallel electric fields in the auroral zone at altitudes above the main acceleration region. At this altitude the models have different predictions on how the parallel electric fields look like. The O-shaped potential structure will result in a positive electric field and the U-shaped in a negative, in the northern hemisphere (the opposite on the southern hemisphere). A picture showing the predicted signatures for the two models can be seen in Fig. 1.6. A comparison of models with respect to parallel electric fields is the motivation for this paper.

For this study we use data from Cluster spacecrafts with their sensitive electric field instruments. When the Cluster satellites are in the auroral zone they have an altitude of about 4.5 R_E, which is above the main acceleration region at 2-3 R_E. The Polar satellite has been used to investigate [Mozer and Hull, 2001] electric fields in this region. In some cases data have shown indications of small parallel DC electric fields [Janhunen, private communication]. However, the quality of the Polar electric field instrument may not be enough to reliably measure these small electric fields.

Distances between magnetic field lines scale approximately as $B^{-1/2}$ in a dipole field like the Earth's. At Cluster altitude (~4.5 R_E) the magnetic field strength is about 500 nT and at the ionosphere where the aurora is produced it is about 50 000 nT. Thus ionospheric distances multiplied by 10 equals distances at Cluster altitude. Accordingly the typical 5 km north-south scale size of discrete auroral arcs mapped to Cluster altitude is ~50 km. Hence at Cluster speed of ~5 km/s we would expect parallel electric field structures of ~10 seconds.

The expected magnitude of the downward electric field is something like 0.1-10 mV/m, but with Cluster it may not be possible to measure fields smaller than 1 mV/m. The small expected magnitude makes the direct measurements of parallel electric fields very difficult; the spacecraft must be properly aligned with respect to the magnetic field and there are several instrumental effects that can influence the measurements. The alignment of the spacecraft is especially important in an environment where the perpendicular fields are on the average 10 times greater. This will be discussed in the data handling section. Any evidence of parallel fields would be important results, and by studying the sign of the parallel fields in a large sample of events it might be possible to draw a conclusion on what model is more plausible.

The following section will deal with different theories of how DC parallel electric fields are maintained in space. Then the instruments that are used on Cluster and the handling of data are described. Finally the strategy for choosing events and the results from those events are discussed.

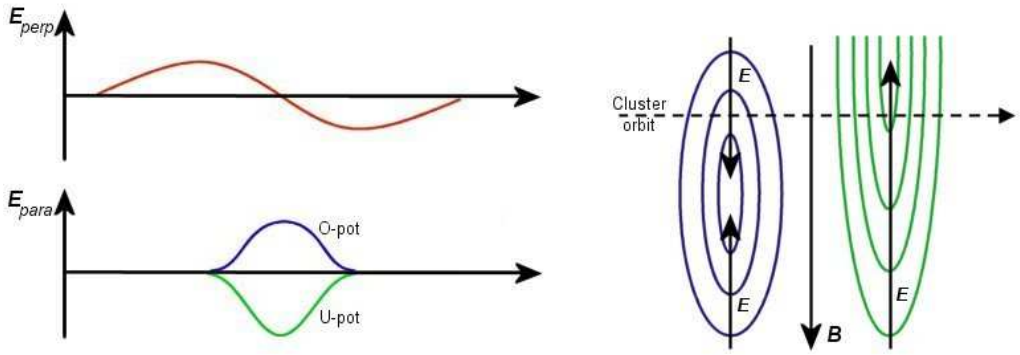

Figure 1.6: To the left the idealized electric field signatures when crossing a U-shaped and an O-shaped potential structure. The parallel electric fields have opposite signs.

Chapter 2

Maintaining DC Parallel Electric Fields

There are different theories on how parallel electric fields are maintained, and the most important quasistatic theories are described in this section. By quasistatic we mean that the potential structures responsible for discrete auroral arcs are not changing as an electron passes through. Therefore both the time scale (how rapidly the potential structure changes) and the spatial scale (the size of the structure) are considered. It has been found that temporal electric field fluctuations around 0.5 Hz are experienced as quasistatic by energetic auroral electrons but as waves by ions for a large part of the acceleration region [Block and Fälthammar, 1990]. An interesting aspect of how electrons and ions see different fields is that it leads to selective acceleration of the particles.

2.1 Anomalous Resistivity

Anomalous resistivity was early on suggested as a mechanism for supporting parallel electric fields. The main idea is that resistivity occurs somewhere along a magnetic field line. The magnetospheric plasma is collisionless, so a regular resistivity, due to electrons colliding with ions, is not possible. Instead waves can be responsible for the resistivity, which therefore is called anomalous resistivity. When charged particles have to transverse such a region, a quasistatic parallel electric field, in accordance with Ohm's law, is built up. Ions and electrons are scattered by waves and can interact differently with them, for example heating ions in the perpendicular direction and electrons in the parallel direction.

Wave turbulence is thought to be caused by auroral current-driven instabilities. When the drift velocity between electrons and ions comes close to the electron thermal speed, a number of plasma instabilities can arise. The most common referred instabilities for creating strong anomalous resistivity is the ion-acoustic instability, the Buneman instability, and the cyclotron instability. The end state of current-driven instabilities need not even be turbulence, but can also be electric double layers [Fälthammar, C.-G., 1983, Lysak, R.L., 1990].

2.2 Double Layers

Parallel electric fields may be continuously distributed in space, but simulations and laboratory work have suggested that the fields, at least partly, could be built up by a series of small steps, called weak double layers (WDL), or by large steps called strong double layers (SDL). The WDLs can be a part of large potential drop, but can hardly account for the whole potential drop of several kilovolts needed to produce intense auroral arcs [Marklund, G., 1993]. However, there are suggestions that one or two SDLs can be responsible for the whole potential drop.

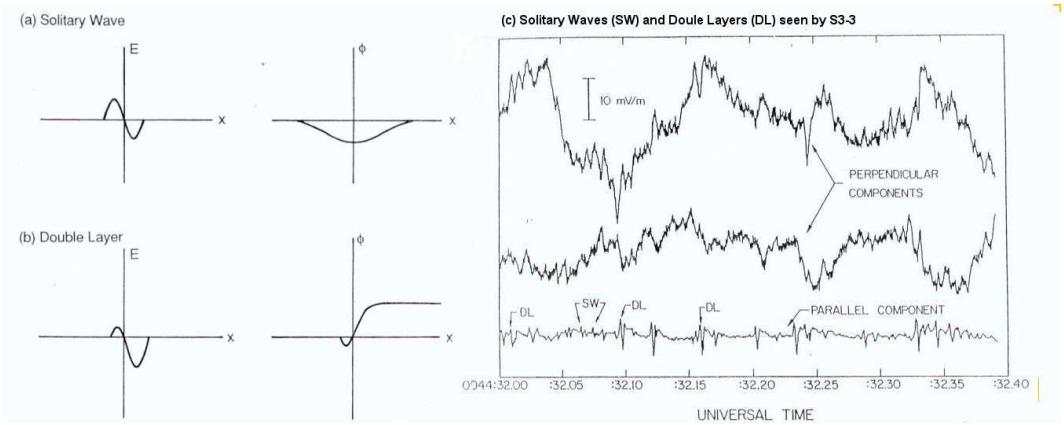

Figure 2.1: Diagrams a) and b) shows the electric field and potential signatures for a solitary wave and a double layer respectively. In c) an example of real data is shown. It is electric field data from the S3-3 satellite decomposed in perpendicular and parallel components with marked solitary waves and double layers. [Lysak, R.L., 1990]

Double layer fields are very thin space charge structures that are characterized by a localized spike of the electric field in one direction and a following spike in the other direction. The structures are local electrostatic potential minima, related to upward-going density holes, that propagate with typical speeds of 10 - 30 km/s [Eriksson and Boström, 1993]. If the opposing spikes are of the same magnitude the integration of the electric field does not result in a net potential, these structures are called solitary waves. If the opposing spikes are of different magnitude, the net potential drop over the structure is non-zero, this is called a double layer. A schematic drawing of the solitary wave and the double layer can be viewed in Fig. 2.1 a) and b), and an example from the S3-3 satellite showing both features is seen in c).

The formation of a weak double layer can be explained in the following way. Let us assume a one-dimensional plasma with an upward field-aligned current carried by down-going electrons, as illustrated in Fig. 2.2. Somewhere in this plasma there is a local potential minima, a potential well, which is stationary on the electron time scale. Electrons without enough kinetic energy to pass the potential structure will be deflected back. This reflection leads to an excess negative charge above the structure and a positive below. The electric fields at P and R in Fig. 2.2 a) are free to propagate along the field line, while the local minima stays virtually confined. Now the electric field at Q is mainly upwardly directed, and it is meaningful to consider the net potential drop - a weak double layer.

2.3 Magnetic Mirror Force

Another theory for maintaining parallel electric fields is based on the magnetic mirror force. Here the parallel electric field is the result of the mirror force working on ions and electrons with different velocity distributions. The first adiabatic invariant, the magnetic moment, must be considered in order to understand how the magnetic mirror force leads to a parallel electric field.

$$\mu = \frac{W_\perp}{B} = \frac{m v_\perp^2}{2B} \tag{2.1}$$

Here $W_\perp$ is the perpendicular energy and $v_\perp$ is the perpendicular velocity, the speed at which the charged particle gyrates around the magnetic field line. Adiabatic invariants hold for slow changes in the system, and they can be considered constant for the time-scales we are looking at. In the case

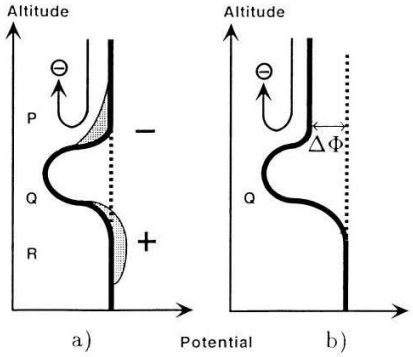

Figure 2.2: The formation of a weak double layer. A potential well in the presence of an upward current reflects downgoing electrons and results in an excess negative charge at P, which leads to an asymmetric potential structure with a net potential drop - a double layer. [Eriksson and Boström, 1993]

of the magnetic moment, it will be constant as long as the magnetic field's temporal change is small during the gyroperiod (the time for the particle to make a full orbit around the magnetic field line) and the spatial change is small over the scales comparable to the gyroradius.

The pitch angle of a particle is defined as

$$\alpha = \arctan\left(\frac{v_\perp}{v_\parallel}\right) \tag{2.2}$$

and depends on the ratio between the perpendicular and parallel velocity components. Using the pitch angle as defined in Eq. (2.2) and replacing $v_\perp$ by $v\sin\alpha$, the magnetic moment, Eq. (2.1), can be rewritten as

$$\mu = \frac{mv^2\sin^2\alpha}{2B} \tag{2.3}$$

Since the magnetic moment and the kinetic energy (and therefore velocity) is constant, only the pitch angle can change when the magnetic field increases or decreases. The pitch angle of a particle at different locations is therefore directly related to the magnetic field-strength at those locations according to

$$\frac{\sin^2\alpha_2}{\sin^2\alpha_1} = \frac{B_2}{B_1} \tag{2.4}$$

If we know the pitch angle at some location, then this quantity can be calculated for all other locations.

As a particle moves towards the Earth along a field-line, the magnetic field-strength increases, and thus the pitch angle increases according to Eq. 2.4. The energy is transferred from the parallel component to the perpendicular component. This is achieved by the parallel component of the gradient force

$$\mathbf{F}_\nabla = -\mu\nabla B \tag{2.5}$$

At some point the pitch angle reaches 90° and all the energy is in the perpendicular plane - this is called the *mirror point*. Then the particle is pushed back and gain speed in the upward parallel direction. In Fig. 2.3, the mirroring of a charged particle in a converging magnetic field is depicted.

Let us assume that at some specific location the velocity space distributions of ions and electrons differ. For example this could be due to wave activity that by resonance can affect ions and electrons differently. This wave activity may lead to electrons getting larger parallel energy than the ions, and thus a smaller pitch angle. Where we start the B-field is the same for both species, but the pitch

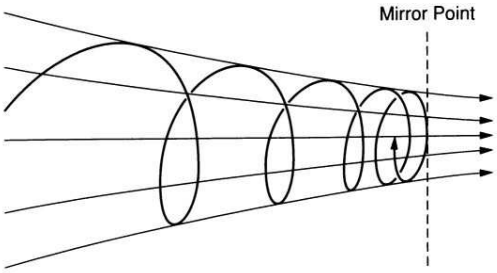

Figure 2.3: The mirroring of a charged particle in a converging magnetic field. The dashed line denotes the mirror point. [Baumjohann and Treumann, 1996]

angles differ. According to Eq. 2.4 then, the mirror point of the electrons will be at a location with stronger magnetic field than for the ions. In order to maintain quasi-neutrality a parallel electric field forms to balance the mirror effect.

Chapter 3

Cluster and its Instruments

In this study we use data from the Cluster satellites. The four identical Cluster satellites (a cut-away of the spacecraft can be seen in Fig. 3.1) were launched in the summer of 2000 by the European Space Agency. Their mission is to complete a detailed investigation in the near-Earth space on how the Sun and Earth interact. By employing four satellites and flying them in formation, it is possible to distinguish temporal and spatial changes of measured properties in a way that has not been possible before.

3.1 Instruments

Four out of eleven Cluster instruments are used in this investigation; EFW - Electric Field and Wave experiment, FGM - Flux Gate Magnetometer, EDI - Electron Drift Instrument, CIS - Cluster Ion Spectrometry experiment. The EFW, which measures the electric field directly, is the key instrument for this study. It is the only instrument on Cluster that is able to measure parallel electric fields. Beside the electric field it also measures the electron density, which is an important parameter when analysing the data. The FGM measures the ambient magnetic field which is essential for constructing the used coordinate system. Data from the EDI and CIS instruments are used for reference purposes. They help us to tell how reliable the measurements from the EFW are.

3.2 EFW - Electric Field and Wave Experiment

3.2.1 Set-up

The EFW experiment has four spherical sensors located at the end of 44 meter long wire booms. A schematic illustration of the booms is seen in Fig. 3.2. The booms are located in the spinplane of the satellite and are kept stretched out by the centrifugal force due to the spinning of the spacecraft. Each boom unit is a small self-contained package that contains a deployment mechanism and a multiconductor cable with the spherical sensor at the end. The spheres are 8 cm in diameter and made of aluminum. They are coated with an electrically conducting paint, that also allows the sensor to keep a suitable temperature. [Gustafsson et al, 1977]

3.2.2 Measured Quantities

The four probes can individually operate in voltage mode to measure the electric field, or in current mode to measure the density and temperature of the plasma. In voltage mode, or electric-field mode (when the probe is given a constant bias current), the potential differences on the two orthogonal double probe pairs provide the electric field in two directions in the spinplane (as seen in Fig. 3.2). The electric field component in the spin axis direction is not measured. In order to get the total field

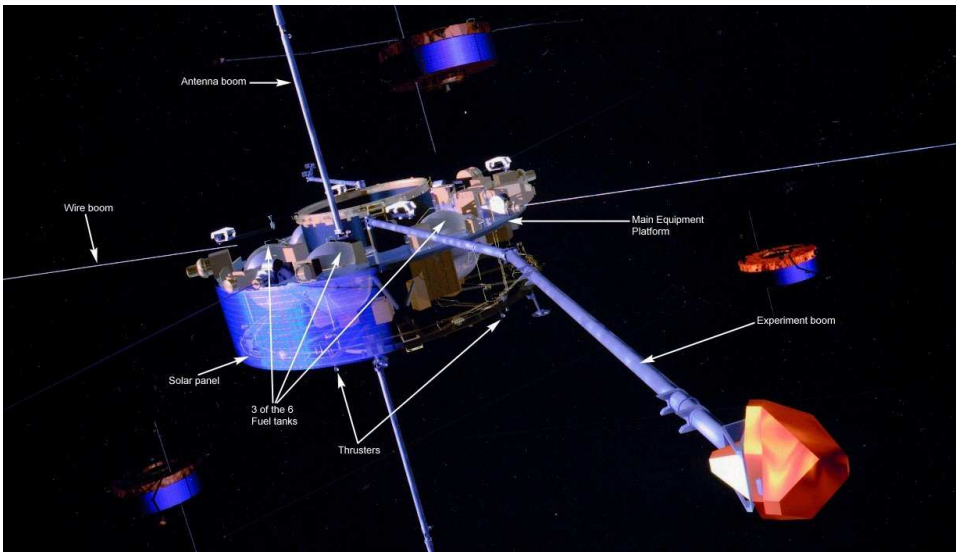

Figure 3.1: A cut-away of the Cluster spacecraft showing some of the parts. [ESA]

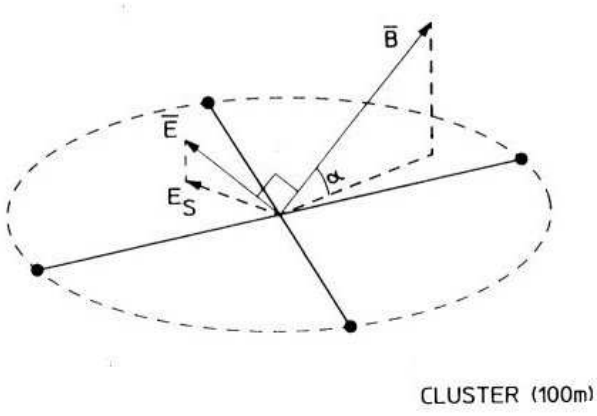

Figure 3.2: Two crossed double probes measure the projection of the electric field to the spin-plane, E_s. The angle α is the angle between the magnetic field vector and the spinplane. [Pedersen et al, 1998]

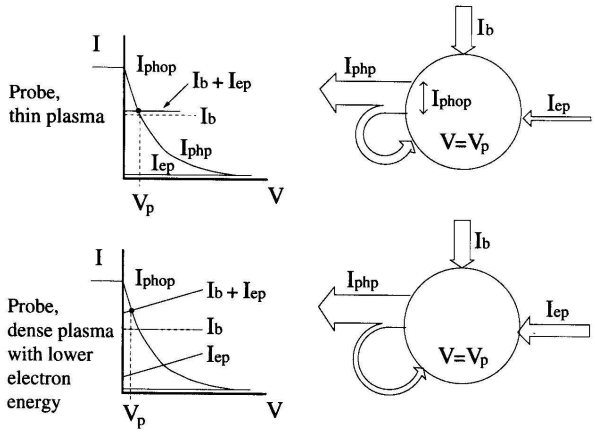

Figure 3.3: Schematic illustration of the probe current balance between emitted photoelectrons and collected plasma electrons. [Pedersen et al, 2001]

vector, the component along the spin axis must be constructed using assumptions. The most common assumption is that the parallel electric field is zero, $\mathbf{B} \cdot \mathbf{E} = 0$, which is not a good strategy when looking for exactly those parallel fields. How this is solved is discussed in section 4.3. In current mode, or Langmuir mode, the probes are operated with voltage bias that allows measurements of plasma density. The reason for this is that a positively charged probe collects a current proportional to the plasma density if the electron temperature stays constant. Variations in plasma density will lead to proportional variations in the collected current. The plasma temperature and density are calculated from the current-voltage characteristics of the plasma, which is measured by stepping the voltage bias [Gustafsson et al, 1977].

A probe (and spacecraft) will always come to a positive potential in a magnetospheric plasma due to the emission of photoelectrons. The photoelectrons actually provide the necessary contact between the probe and the local plasma surrounding. A natural bi-product from the measurements by double probes is the spacecraft potential which in its turn provides information about plasma density variations. This is not the same measurement as in the described Langmuir mode.

3.2.3 Bias Currents and Electric Fields

For proper measurements by the electric field instrument the probes need to be fed electrons by a high impedance current source in order to bring them close to the plasma potential. This bias current (carried by the electrons) is necessary for creating the optimum impedance. By changing the bias current we move along the voltage-current characteristic curve, and can choose a point that gives the lowest impedance.

If the impedance between the probes and their local plasma environment is comfortable, the electric field is then simply the voltage difference between the probe pair divided by their “effective length”. The “effective length” is somewhat shorter than the physical separation of the sensors, caused by a partial short-circuiting of the electric field by the wire booms.

The advantage of spherical probes is the spherical geometry that provides better symmetry. The photoemission does not vary so much during the spin period, which is important when measuring electric fields in a plasma. With just one pair of probes the spinplane component of the electric field can only be determined if it does not change during the spin period. Having two crossed double probes (as for Cluster) the electric field in the spinplane can be determined continuously. It is assumed that the spatial dimensions of the potential structures are much larger than the double

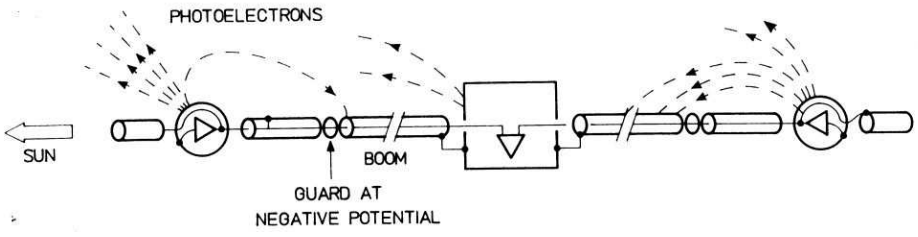

Figure 3.4: A probe pair with one of the probes aligned towards the Sun. The negatively biased guards minimise the effect of the sunward electric field caused by asymmetric photoelectron losses to the wire boom. [Pedersen et al, 1998]

probe dimensions. This is the same as saying that the field is more or less constant over the distant between the double probes.

An apparent sunward electric field can arise when the spinplane of the satellite is close to the sun direction. This is due to asymmetric emissions of photoelectrons from the probes. Because areas facing the Sun are affected, a probe located away from the Sun will loose more photoelectrons to the boom wire, which is positive (same potential as the spacecraft), than the other probe in the pair located towards the Sun. This can be seen in picture 3.4. By putting a negatively biased guard at the outer end of the wire boom this effect can be minimized.

Fig. 3.3 is a schematic illustration of the probe current balance in a thin and a dense plasma. The major difference between the two cases is the magnitude of the probe electron current, I_{ep}, where the dense plasma provides more electrons to the probe. Note that the arrows in the picture point in the direction of the electrons, which is opposite the direction of the currents by definition. The negative bias current (I_b), which forces electrons on the probe, plus the electron current collected from the ambient plasma (I_{ep}), balance the escaping photoelectrons (I_{php}). This causes the probe to be at a potential V_p close to that of the plasma, where the resulting potential is determined by the balance of plasma electron current, photoemission current, and bias current [Pedersen et al, 2001].

3.3 Other instruments

As mentioned earlier the EFW instrument is the key instrument for this study. The other three instruments used in this study - FGM, EDI, and CIS - are only briefly described in the following sections.

3.3.1 FGM - Flux Gate Magnetometer

The measurement of the magnetic field is a vital part of all space physics missions. It is in itself important for studies of the magnetosphere, and it is also an important component of all other measurements in order to analyze them in the magnetospheric context. We use the magnetic field vector to construct the coordinate system; one parallel axis (pointing along the magnetic field vector), and two perpendicular axis.

The FGM instrument consists of two triaxel fluxgate magnetometers; one that is located on the end of a 5.2 m radial boom to avoid as much interference from the spacecraft as possible, and another that is located inside the spacecraft [Daly, P. W., 2002]. Each magnetometer consists of three sensors that are orthogonally arranged in order to construct the total magnetic vector.

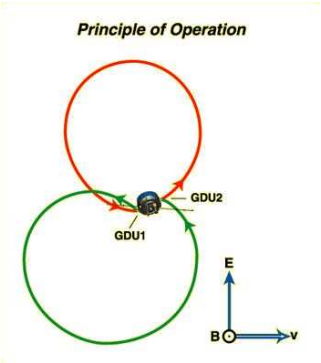

Figure 3.5: The EDI operation principle. Two electron beams are send away perpendicular to the magnetic field and received on the other side of the spacecraft. [from EDI homepage]

3.3.2 EDI - Electron Drift Instrument

The electron drift instrument is the other instrument capable to directly measure the electric field. It can only measure perpendicular electric fields (that can be compared to EFW). It has some difficulties in the turbulent auroral region and is therefore not able to provide high time resolution data.

Measurements are based on the displacement of a weak beam of test electrons after a gyration in the surrounding electric and magnetic field. The displacement allows for both the electric field and the magnetic gradient to be independently derived [Daly, P. W., 2002].

The electron beam returns to the spacecraft only if its fired in one of two exact directions. Two electron beams are independently swept by separate units on each side of the spacecraft in the plane perpendicular to the magnetic field (it is therefore unable to measure any parallel component of the electric field), until they are detected on the other side of the spacecraft (see Fig. 3.5).

One electron gun and one detector is paired up and they constitute one single unit called a gun/detector unit (GDU). The two GDUs are mounted on opposite sides of the spacecraft in order to detect each other's beams.

3.3.3 CIS - Cluster Ion Spectrometry Experiment

If the ion velocity vector is known then the perpendicular electric field can be derived given the magnetic field vector. CIS is capable to deliver velocity vectors for different ions.

The CIS experiment is an ionic plasma spectrometry package capable of measuring full three-dimensional ion distributions [Daly, P. W., 2002]. It consists of two instruments, a Hot Ion Analyser (HIA) and a time-of-flight ion COmposition DIstribution Function (CODIF). The CODIF is a mass-resolving spectrometer capable of obtaining distribution functions for the major ion species. This means that it can provide velocity vectors for different ions, due to its energy-per-charge analyser. The HIA instrument does not have mass resolution but it has a larger dynamic range. It selects incoming ions according to energy-per-charge ratio by deflection, and analyses the selected ions with a fast imaging particle detection system, which is based on electron multipliers and position-encoding discrete anodes. The result is a velocity vector that can be used to, for example, derive the electric field if the magnetic field vector is known. How this is done will be described in the section about data handling.

Chapter 4

Handling the data

The data from the instruments on the Cluster satellites is stored in a database, from where it easily can be accessed by different data manipulating programs. For this project MATLAB has been used to retrieve and handle the data. The MATLAB-code especially written for this project can be found in section A. There are no references to the code in the text, instead the MATLAB code has references back to the text.

4.1 Coordinate Systems

Electric field data from EFW are given in a local reference frame that spins with the spacecraft. In order for the data to be more easily handled a nonspinning coordinate system is used, where the z-axis still is aligned with the spin vector but the x-axis is in the spinplane pointing in the direction that is closest to the Sun. This reference frame is referred to as the DeSpun Coordinate system (DSC).

The data from the other used instruments (magnetic field data from FGM, electric field data from EDI, and ion velocity data from CIS) is given in the Geocentric Solar Ecliptic coordinate system (GSE). In this reference frame the $\hat{z}_{GSE}$ is directed "north", perpendicular to the Sun-Earth ecliptic plane (the plane in which Earth orbits the Sun), and $\hat{x}_{GSE}$ is in the Earth-Sun direction. Given small tilt-angles of the spacecraft's spinplane the DSC and GSE coordinates are practically the same, except that $\hat{z}_{GSE} = -\hat{z}_{DSC}$ (the satellite is upside down) and $\hat{y}_{GSE} = -\hat{y}_{DSC}$ have different sign. The two coordinate systems are illustrated in Fig. 4.1.To allow FGM, EDI, and CIS data to be used together with EFW data, they are transformed into DSC.

Other "house keeping" data, like phase angle of the spin, altitude, and Invariant LATitude (ILAT), are also read from the database but need no further manipulation and are used as is.

4.2 FAC - Field Aligned Coordinate System

Since we look at electric fields parallel and perpendicular to the ambient magnetic field, it is practical to use a Field Aligned Coordinate system (FAC). The FAC is constructed in the following way:

$$\hat{\perp}_1 = norm(\mathbf{B} \times \hat{z}) \tag{4.1}$$

$$\hat{\perp}_2 = norm(\hat{\perp}_1 \times \mathbf{B}) \tag{4.2}$$

$$\hat{\parallel} = norm(\mathbf{B}) \tag{4.3}$$

Fig. 4.2 shows the constructed FAC system. The unity vector, $\hat{\perp}_1$, is perpendicular to both the magnetic field ($\mathbf{B}$) and to the spin axis ($\hat{z}$), and is therefore always in the spinplane. The unity vector, $\hat{\perp}_2$, is perpendicular to both the magnetic field and the first perpendicular unity vector. Finally the parallel unity vector, $\hat{\parallel}$, is directed along the magnetic field vector. The advantage with the constructed

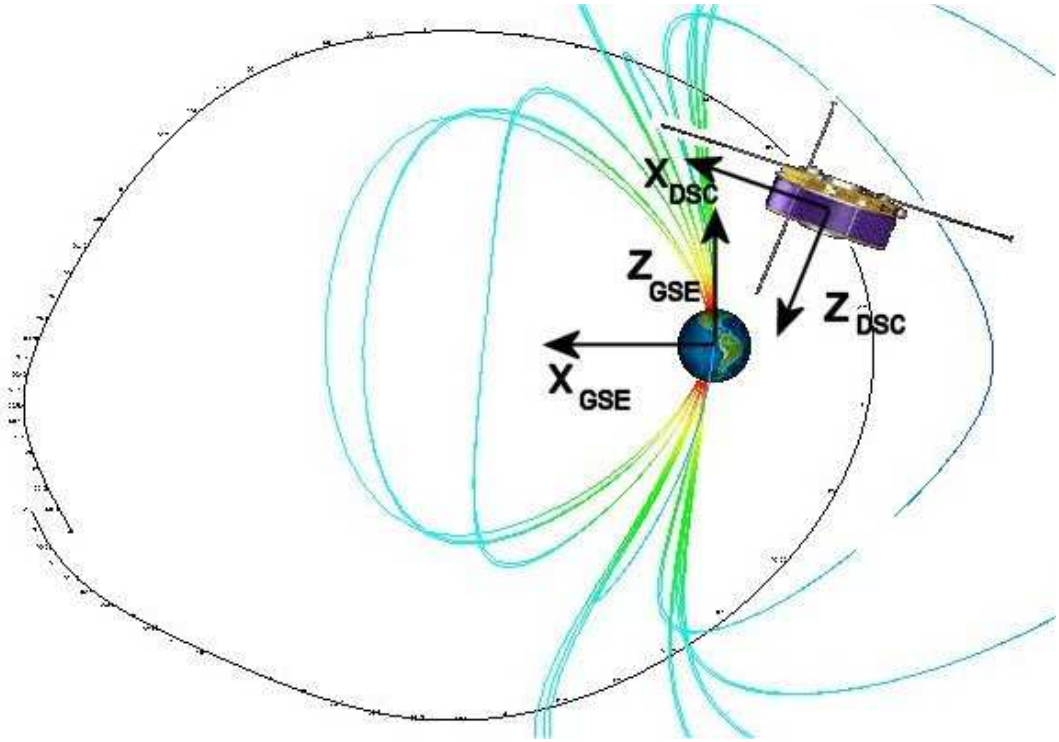

Figure 4.1: A simple schematic of the the GSE and DSC coordinate systems.

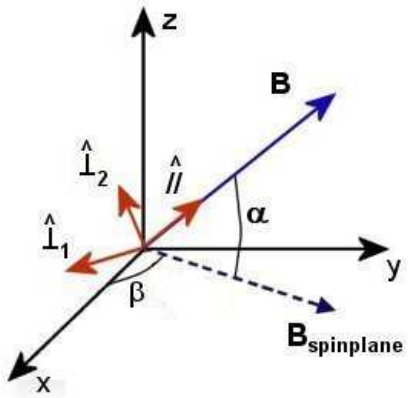

Figure 4.2: The field aligned coordinate system (FAC) with its two perpendicular components and parallel component. z is the spin axis and y, z, and $\hat{\perp}_1$ is in the spinplane. α is the spinplane angle.

FAC system is that the first perpendicular component of the electric field is always in the spinplane and thus always can be measured reliably by EFW. When the magnetic field is at a small angle to the spinplane, hence called the spinplane angle (α in Fig. 4.2), also the parallel component can be more reliably measured. The drawback is that the second perpendicular component cannot be reliably measured by EFW. At an angle of zero degrees one parallel and one perpendicular component will be in the spinplane and give the best possible conditions for analysis.

4.3 Calculations and Assumptions of the Full E-field vector

The spinplane angle is crucial because the reliability of the parallel electric field measurements is depending on it. The spinplane angle is calculated from the magnetic field data as

$$\alpha = \arcsin \frac{B_z}{|\mathbf{B}|} \tag{4.4}$$

Because the double probes of the EFW only can measure electric fields in the spinplane there will always be one component missing from the dataset, the z component. One criteria to reliably measure the parallel electric fields is therefore that the spinplane angle is small. The spinplane angle can also be used as a survey parameter that tells something about how the direction of the magnetic field changes. Because sun direction can affect the EFW measurements another angle is also computed. It is the angle, β, between the Sun and the magnetic field in the spinplane (see Fig. 4.2):

$$\beta = \arctan \frac{B_y}{B_x} \tag{4.5}$$

In order to derive the full electric field vector it is necessary to make some assumptions. The assumption commonly used is to say that the parallel electric field is zero, $E_{\parallel} = 0 \Rightarrow \mathbf{E} \cdot \hat{\parallel} = 0$. Using this relation the z-component can be derived as

$$E_z = -\frac{(E_x \hat{\parallel}_x + E_y \hat{\parallel}_y)}{\hat{\parallel}_z} \tag{4.6}$$

The problem with this strategy is obviously that the $E_{\parallel}$ is equal to zero by definition, but it is a good way to get $E_{\perp_2}$at large spinplane angles. At small spinplane angles when $E_{\perp_2}$ is almost parallel to the spin axis this is not a good strategy. It is still useful, because it can be compared to $E_{\perp_2}$ measured by EDI and CIS (which both can measure this component even for small spinplane angles).

The second strategy to obtain the full electric field is to set the z-component of the electric field to zero. It is straight forward and it does not take any extra calculations. This strategy works well when deriving $E_{\parallel}$ at small spinplane angles, because then the z-component is almost perpendicular to the parallel direction and therefore does not affect the parallel component much.

The EDI and CIS instruments can only measure the perpendicular components of the electric field, no matter what the spinplane angle is. In the EDI case it is because the electron beam is emitted and received in the plane perpendicular to the magnetic field. In the CIS case it is because the electric field is derived from the measured velocity vector using the relation

$$\mathbf{E} = -\mathbf{v} \times \mathbf{B} \tag{4.7}$$

and thus the derived electric field always is perpendicular to the magnetic field.

The third way to obtain the full electric field is to set the second perpendicular component to zero, $E_{\perp_2} = 0 \Rightarrow \mathbf{E} \cdot \hat{\perp}_2 = 0$. With this third strategy the z-component is derived as

$$E_z = -\frac{(E_x \hat{\perp}_{2,x} + E_y \hat{\perp}_{2,y})}{\hat{\perp}_{2,z}} \tag{4.8}$$

	$E_z = 0$	$E_\parallel = 0$	$E_{\perp_2} = 0$
$\mathbf{E} \cdot \hat{\parallel} =$	$E_\parallel^{E_z=0}$	0	$E_\parallel^{E_{\perp_2}=0}$
$\mathbf{E} \cdot \hat{\perp}_1 =$	$E_{\perp_1}$	$E_{\perp_1}$	$E_{\perp_1}$
$\mathbf{E} \cdot \hat{\perp}_2 =$	$E_{\perp_2}^{E_z=0}$	$E_{\perp_2}^{E_\parallel=0}$	0

Table 4.1: Resulting FAC components using different assumptions. See also MATLAB code erik_Epp.m in the appendix.

Why do we set $E_{\perp_2} = 0$ if $E_{\perp_2}$ is one of the components that can be directly measured by CIS and EDI? The reason is that the parallel component we now get gives an indication on how the parallel component obtained using the assumption $E_z = 0$ is affected by an electric field that is in the second perpendicular direction. Under the assumption that $E_{\perp_2} = 0$ the parallel component depends on the spinplane angle α.

$$E_{E_\parallel}^{\perp_2=0} = -E_{\perp_2} \tan \alpha \tag{4.9}$$

If the parallel component, derived using the assumption $E_z = 0$, follows the parallel component, derived using $E_{\perp_2} = 0$, then the contribution to the parallel component, using $E_z = 0$, comes almost entirely from an electric field in the second perpendicular direction, not from the real parallel electric field.

All this manipulation with the components is necessary just because the z-component is missing from the EFW data. When the spinplane angle is nonzero the measured electric field in the spinplane can be due to a real field in the parallel direction or a larger real field in the second perpendicular direction. By looking at components derived using different assumptions it is easier to decide if the measured parallel field is to be trusted or not. An overview of the assumptions and the resulting electric field components is available in table 4.1.

Overview plots based on the described data handling have been used in this study. The overview plots all have 10 minutes worth of data, which in most cases correspond to a spinplane angle roughly between -5 and 5 degrees. The reason for the selected angles is that $\tan(5) \approx 10\%$. The real parallel electric field should be at least 10% of the perpendicular to be measurable. For smaller spinplane angles the real parallel electric field can be even smaller.

One overview plot can be seen in the top half of Fig. 5.3. The first panel shows the spinplane angle (Eq. 4.4) which is approximately the negative of the θ angle seen in the quicklook plots (see Fig. 5.2). The following three panels shows the three electric field components in the FAC system. The first perpendicular component is real data from all three instruments (EFW, EDI, and CIS), but the second perpendicular component uses the $E_\parallel = 0$ assumption for the EFW data. For the parallel component the assumption that $E_z = 0$ has been used for EFW, and the assumption that $E_{\perp_2} = 0$ for EDI and CIS data. There is an offset present that moves the whole EFW curve down a bit - this is not a DC field. The offset effect will be discussed in the section on instrumental effects. The fifth panel shows the spacecraft potential that corresponds to the plasma density. The sixth panel shows the angle between the Sun and the magnetic field in the spinplane (Eq. 4.5).

4.4 Filter

In order to comprehend plots based on longer periods of data (for example the 10 minutes overview plots) a low pass filter is applied. There are lots of waves with large amplitudes and with frequencies up to 10 Hz (180 Hz in Burst Mode). We are mainly interested in DC parallel electric fields, which is why the filter is applied.

The cut-off frequency for the filter was decided to 0.7 Hz, which provided a reasonably smooth curve in most cases. It also filters the wake effect at 1 Hz, that is caused every time a probe is behind the spacecraft with respect to an up-going ion beam. With a spin period of 4 seconds and with 4

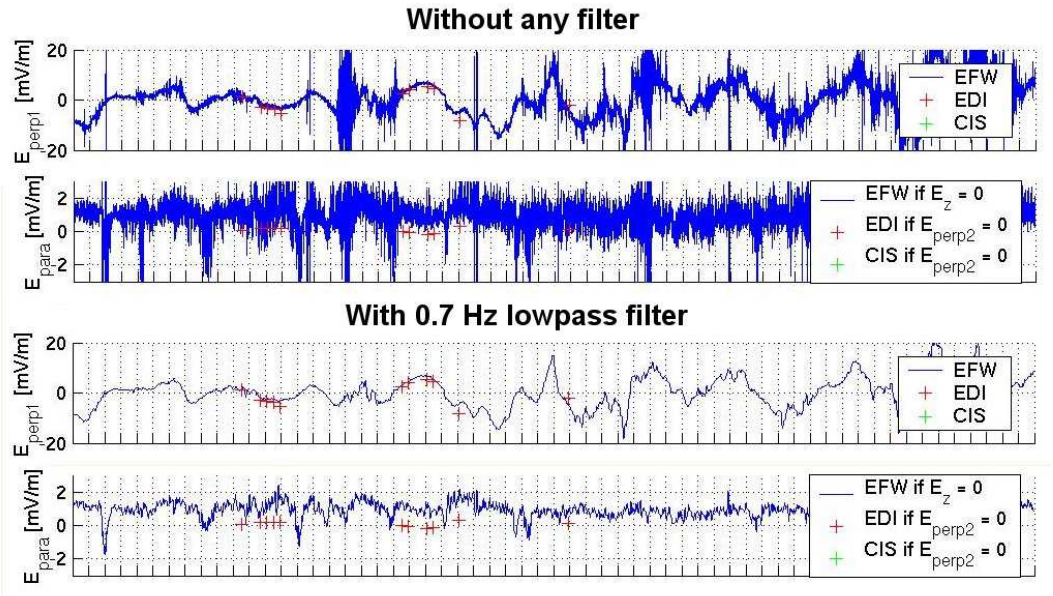

Figure 4.3: Demonstration of the filter effect on two components.

probes, the wake effect shows up in cycles of 1 second, resulting in 1 Hz. Deeper explanation of the wake effect and the drawback of filtering can be found in the section on instrumental effects.

In Fig. 4.3 the effect of the low-pass filter is demonstrated. The first perpendicular and parallel components are rather “messy” at the top, but after filtering at 0.7 Hz the plots are much easier to comprehend.

Chapter 5

Selection Strategy

The Cluster orbits are fixed with respect to stars so that the perigee (the ellipse's turn-point that is closest to Earth) orbit the Earth in one year. To get data from night-side auroral crossings, where discrete auroras are more frequent, the perigee needs to be on the night-side, which it is roughly from January to May. The changes of the orbit during this period can be viewed in Fig. 5.1. The satellites pass the auroral oval almost entirely in the south-north direction.

The spinplane angle of the satellite (angle between B and the spinplane) crosses zero two times close to perigee. First close to or inside the southern auroral zone and then close to or inside the northern one. One orbit takes ~57 hours (~2.4 days), which leads to about 128 orbits in the time period from January to May. Because the spinplane angle crosses zero twice close to perigee it sums up to about 256 events. In total about 500 zero crossings from the years 2001 and 2002 have been identified using quicklook plots provided by CSDSWEB (Cluster Science Data System WEB). An example of a quicklook plot can be seen in Fig. 5.2. The elevation angle of $\mathbf{B}$ seen in the second panel is in GSE coordinates. It is close to the spinplane angle with opposite sign.

57 events were selected for closer inspection based on low-frequency wave activity and data availability. The low frequency electric field wave activity can be seen in the fifth panel in Fig. 5.2.

The 57 events were divided into four sub categories in the following way:

- 16 "No activity" - When there is no or small activity of neither the first perpendicular nor the parallel electric field component. This is usually because the satellite is in the plasmasphere (see Fig. 1.4 b), which is a non turbulent region, and located at lower latitude than the auroral zone.

- 23 "No perp activity" - When there is some activity in the parallel component but no or small activity in the perpendicular component. Signatures as depicted in Fig. 1.6 with $E_{\perp}$ changing sign is the target so a perpendicular component is needed.

- 5 "Too active" - When there is so much activity and turbulence that the analysis becomes extremely difficult. These events can be interesting when more is known about small parallel electric fields. These plots are therefore available in section B.3 in the appendix.

- 13 "Good" - When there is activity and the plots are as easy as possible to comprehend. All these plots can be found in section B.2 in the appendix.

Overview plots were used to look at these 57 events and decide which category they would go into. One of these overview plots, which is an example of a "good" event, can be seen in the top half of Fig. 5.3. The bottom half of Fig. 5.3 shows examples of the three other categories.

The first three categories will not be further dealt with. From the 13 "good" events 5 were selected for closer study, and they will be referred to as "selected" events. This last selection is based on the same loose criterion as for the "good" ones; the "selected" events are just the clearest

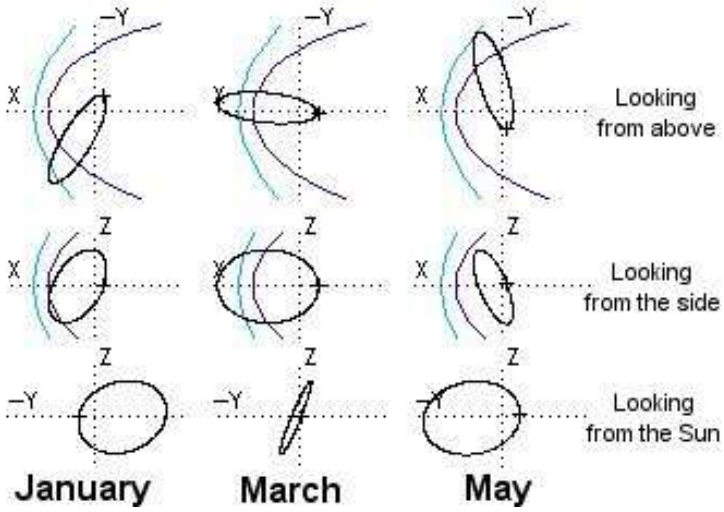

Figure 5.1: Development of the Cluster orbit from January to May, when the perigee of the ellipse allows night-side auroral crossings. The blue curve is the bowshock and the purple curve is the magnetopause.

of the “good”. Overview plots from the “too active” can be found in section B.3 and from the “good” in section B.2. These two categories have plots from one satellite. All the plots from the “selected” events can be found in section B.1.

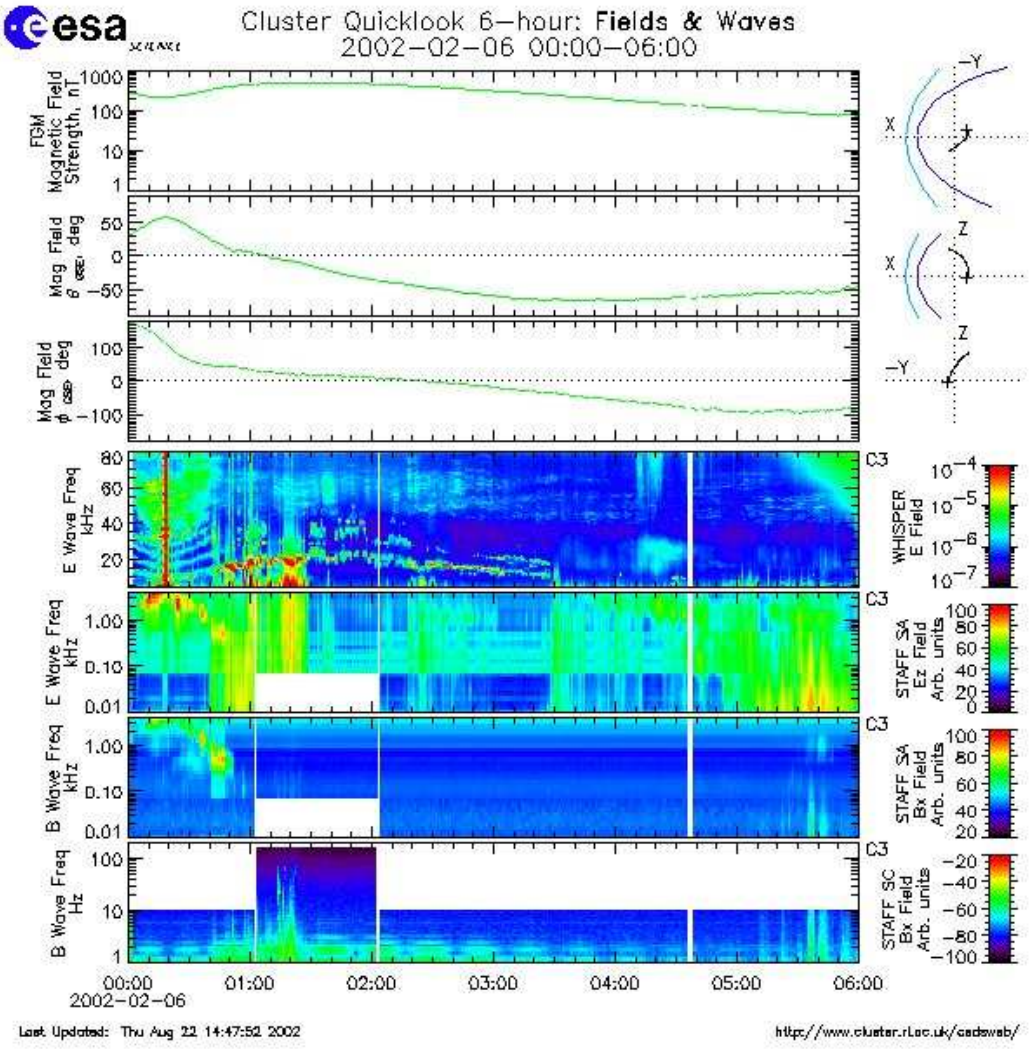

Figure 5.2: Example of a quicklook plot from the CSDS homepage. In this case there is a block of data missing in panel 5 at low frequencies around zero spinplane angle (at 01:00-02:00 UT). This is not actually missing data, instead this is the signature of a burst mode.

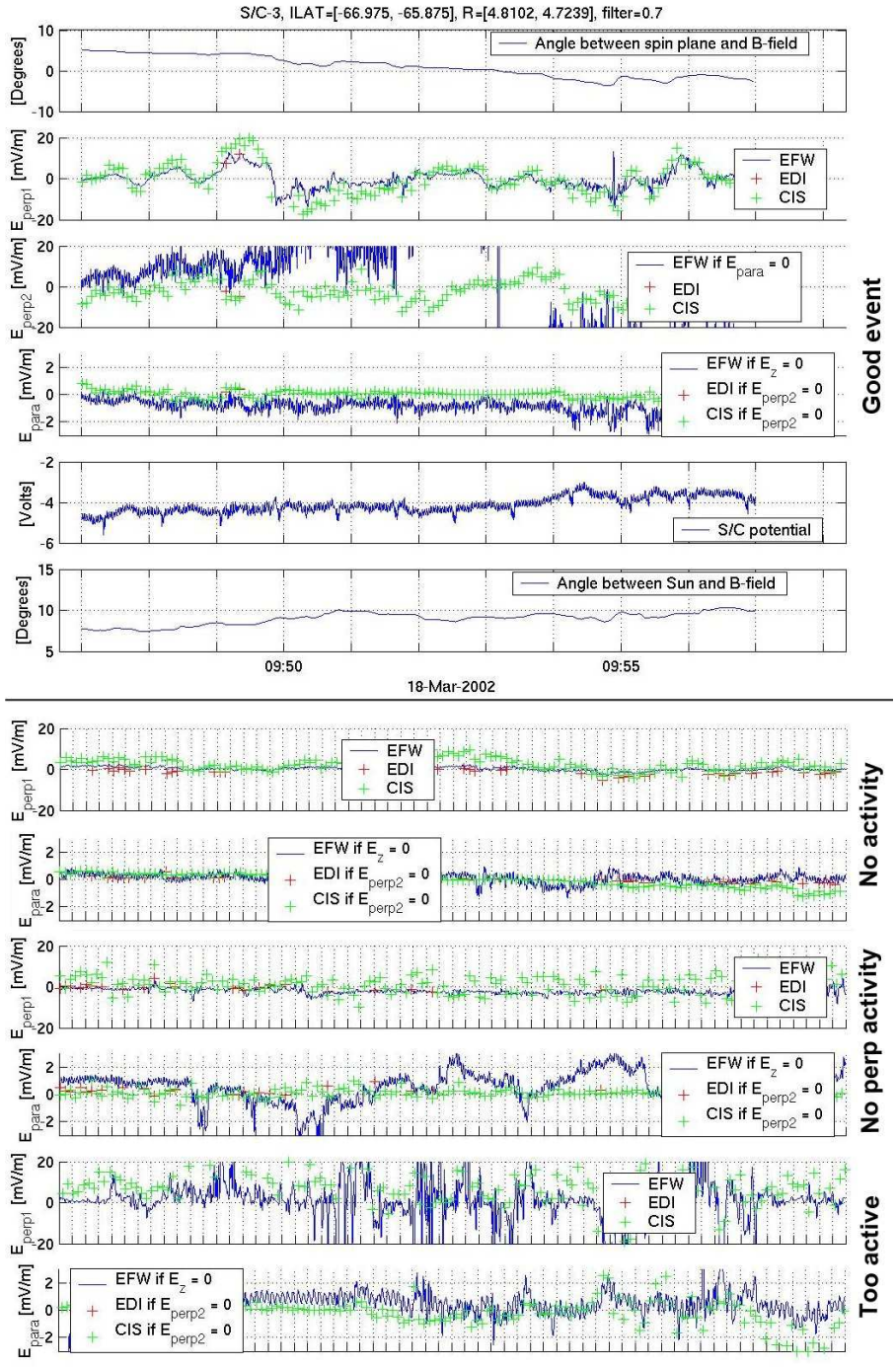

Figure 5.3: The top part shows the total overview plot of a “good” event. The bottom part shows the parallel and first perpendicular component from the three other sub categories; no activity, no perpendicular activity, and too active.

Chapter 6

Results from “Selected” Events

The following five events have been studied closer in the search for parallel electric fields:

1. 2002-01-10, 19:00-19:10 UT - SH, S/C-3
2. 2002-02-06, 01:10-01:20 UT - NH, S/C-2, 3, 4
3. 2002-02-17, 22:47-22:57 UT - NH, S/C-3
4. 2002-03-06, 14:24-14:34 UT - NH, S/C-2, 3, 4
5. 2002-03-18, 09:47-09:57 UT - SH, S/C-3

UT is universal time, S/C is spacecraft, and SH and NH is southern and northern hemisphere respectively. The events are not dealt with one at a time. Instead the different found features are discussed separately, with some examples taken from these five events. All plots are not shown here, but they can all be seen in the appendix.

6.1 Parallel DC Electric Fields

We especially look for the parallel DC fields when the perpendicular E component simultaneously changes sign. A predicted signature can be seen in Fig. 1.6. The structures found in this investigation usually have a size of roughly 10 seconds. If the structures are stable it corresponds to a distance of ~50 km which mapped to the ionosphere becomes 5 km. This is consistent with the north-south scale size of discrete auroral arcs mentioned in the introduction. If the structures are moving towards the spacecraft they are larger, and if they are moving away they are smaller, than the calculated size.

The second selected event (2002-02-06, 01:10-01:20 UT - NH) has a few interesting structures with parallel DC fields correlated with sign change of perpendicular electric component. These structures are labeled from 1 to 5 in the overview plot from S/C-3 seen in Fig. 6.1. Here it can be seen that in the first perpendicular component the field component derived from CIS data does not agree very well, while EFW and EDI follow each other quite nicely. This is a reliability check of EFW data. The overview plots from S/C-2 and 4 show similar structures. In the overview plots it is only possible to identify candidates. Due to the filtering the structures 1 to 5 seen in the overview plot (Fig. 6.1) can be the results of wake effects or waves and not real quasi-static parallel electric fields. To analyze further and to get the size of a structure it is necessary to zoom in closer.

In Fig. 6.2 a zoomed in part of structure 1 in Fig 6.1 from S/C-2 is shown. This plot is lacking data from EDI and CIS but is chosen because it shows three distinct features; a dip in the parallel electric field, typical wake effect signatures, and a sharp dip in the spacecraft potential at the same time as the amplitude goes off scale. The dip in the parallel electric field at 01:10:17-01:10:25 is about 1.5 mV/m and 8 seconds long which corresponds nicely to a discrete auroral arc scale size.

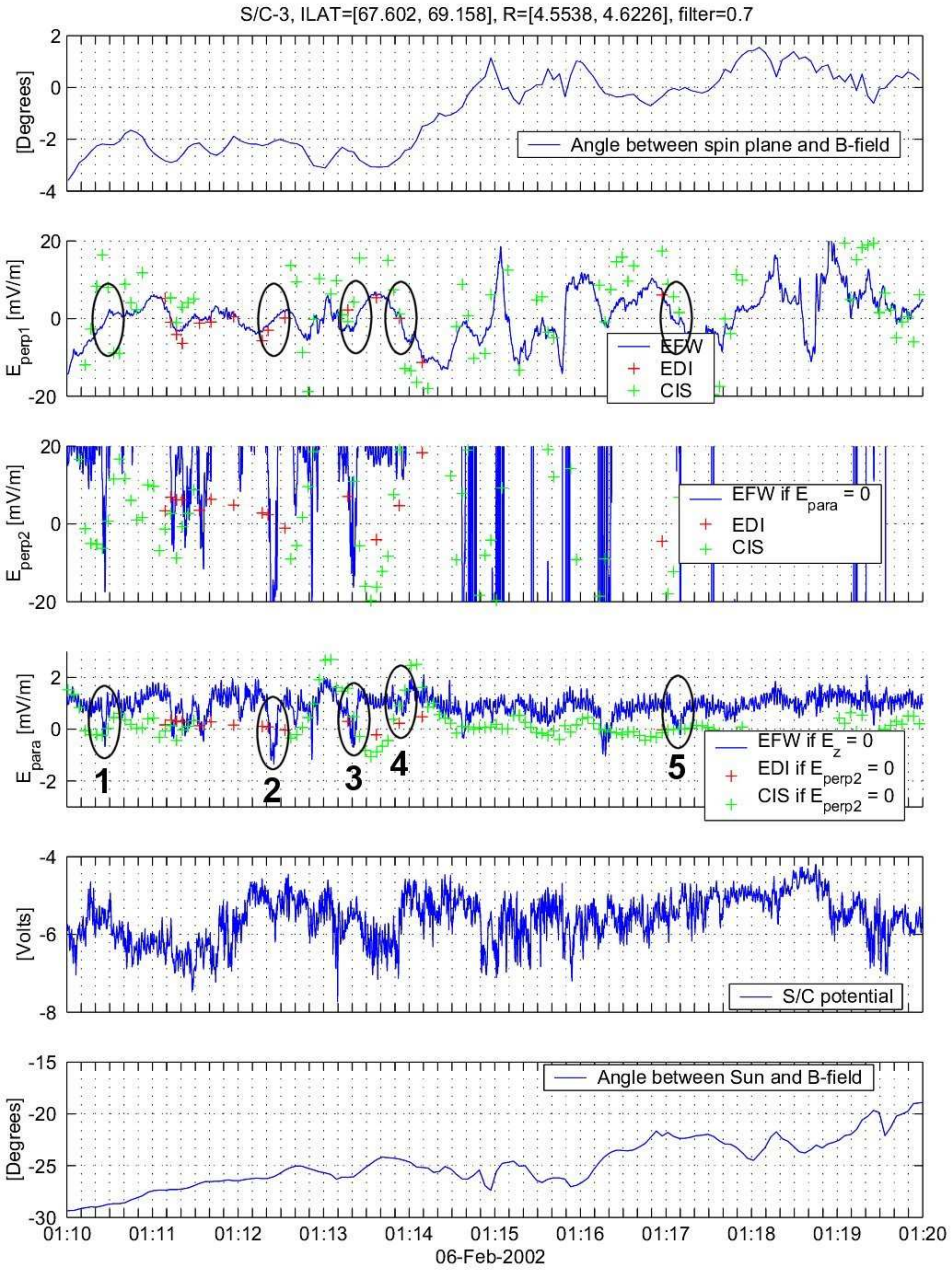

Figure 6.1: Overview plot from S/C-3 on 2002-02-06 showing five parallel DC electric fields associated with a sign change in $E_{\perp_1}$. Panel 1 shows the angle between the spinplane and the B-field. Panel 2 shows the perpendicular E component in the spinplane. Panel 3 shows the second perpendicular E component. Panel 4 shows the parallel E component. Panel 5 shows the spacecraft potential. Panel 6 shows the angle between the B-field and the sun direction (in the spinplane).

The five large negative peaks with 1 second cycle at 01:10:19-01:10:23 UT are probably due to a wake, which might be the result from an upward flowing ion-beam. See further discussion of wake effects in section 7.1. This is nice because upward ion-beams (together with precipitating inverted-V electrons) are associated with discrete auroral arcs. The amplitudes seen in the overview plot can often look larger than the amplitudes seen when zoomed in due to the filtering of wake effects or large AC electric fields. The last feature is the dip in the spacecraft potential, which is caused by a dip in the plasma density. This can be a signature of weak double layers or solitary waves. In the next section this will be pursued further. In structure 1 S/C-4 also sees the parallel electric field, 12 seconds long and ~1 mV/m, and wake at 01:10:20-01:10:32 UT (see plot in section B.1.2 on page 69). S/C-3 on the other hand only sees the ion-beam induced wake effect in structure 1 at 01:10:25-01:10:28 UT (see plot in section B.1.2 on page 63).

Structure 2 in Fig 6.1 is very similar to structure 1 with the exception that it is S/C-4 that sees a wake without a dip in the parallel field at 01:12:19-01:12:23 UT (see plot in section B.1.2 on page 70). S/C-2 sees a 6 seconds dip of ~1 mV/m in the parallel electric field with wake at 01:12:19-01:12:25 UT (see plot in section B.1.2 on page 58). S/C-3 sees a 7 seconds dip of ~1 mV/m with wake at 01:12:21-01:12:28 UT (see plot in section B.1.2 on page 64). This structure is somewhat disturbed by WHISPER on S/C-3, which is on during the last 2 seconds. Interference from WHISPER is discussed in section 7.3.

Structure 3 in Fig 6.1 is seen by S/C-2 and S/C-3 but is only due to wake effect, on S/C-2 at 01:13:15-01:13:21 UT (see plot in section B.1.2 on page 59) and on S/C-3 at 01:13:10-01:13:24 UT (see plot in section B.1.2 on page 65)

In structure 4 in Fig 6.1 all spacecrafts see a field that is only 1 second long. On S/C-2 at 01:13:52 (see plot in section B.1.2 on page 60), on S/C-3 at 01:13:55 UT (see plot in section B.1.2 on page 66), and on S/C-4 at 01:13:53 (see plot in section B.1.2). It looks like wake effect so it could be a “thin” ion-beam.

In structure 5, S/C-3 sees a 12 seconds parallel electric field of ~1 mV/m at 01:17:03-01:17:15 UT (see plot in section B.1.2 on page 67), S/C-2 only wake at 01:17:03-01:17:10 UT (see plot in section B.1.2), and S/C-4 sees both features at 01:17:02-01:17:07 UT with a 5 seconds parallel electric field of ~1 mV/m. All the parallel fields in this second event is in the range 0.5-1.5 mV/m.

The first event (2002-01-10, 19:00-19:10 UT - SH) has one 10 second parallel electric field of about 1 mV/m (with weak double layers as well, which will be discussed in next section) seen by S/C-3 at 19:05:10-19:05:20 UT (see plot in section B.1.1 on page 53).

The third event (2002-02-17, 22:47-22:57 UT - NH) has one 10 second parallel electric field seen by S/C-3 at 22:47:50-22:48:00 UT (see plot in section B.1.3 on page 74), that is only about 0.5 mV/m at an spinplane angle of -3.3 degrees. It is therefore hard to say if it can be trusted. But it is centered around the sign-change of the perpendicular component and does not seem to follow the derived EDI and CIS parallel components (which means that it should not come from a field in the second parallel direction).

The fourth event (2002-03-06, 14:24-14:34 UT - NH) has no distinct parallel fields , but some wave activity have been found, which will be discussed in section 6.3.

The fifth event (2002-03-18, 09:47-09:57 UT - SH) is similar to the third event with a small 10 second parallel electric field seen by S/C-3 at 09:52:54-09:53:04 UT (see plot in section B.1.5 on page 85) of about 0.5 mV/m centered around a sign-change of the perpendicular component. Here the spinplane angle is smaller, 0.4 degrees, so it is more believable than the parallel electric field in the third event. S/C-4 does not see this field (see plot in section B.1.5)

All six found DC parallel electric fields are upward (peak for SH and dip for NH), including those that are questionable. Table 6.1 summarizes the six DC parallel electric fields.

6.2 Double Layers and Solitary Waves

This study was primarily aimed at looking for parallel DC electric fields. Some of the identified events showed signs of solitary structures, WDLs (weak double layers) or SWs (solitary waves).

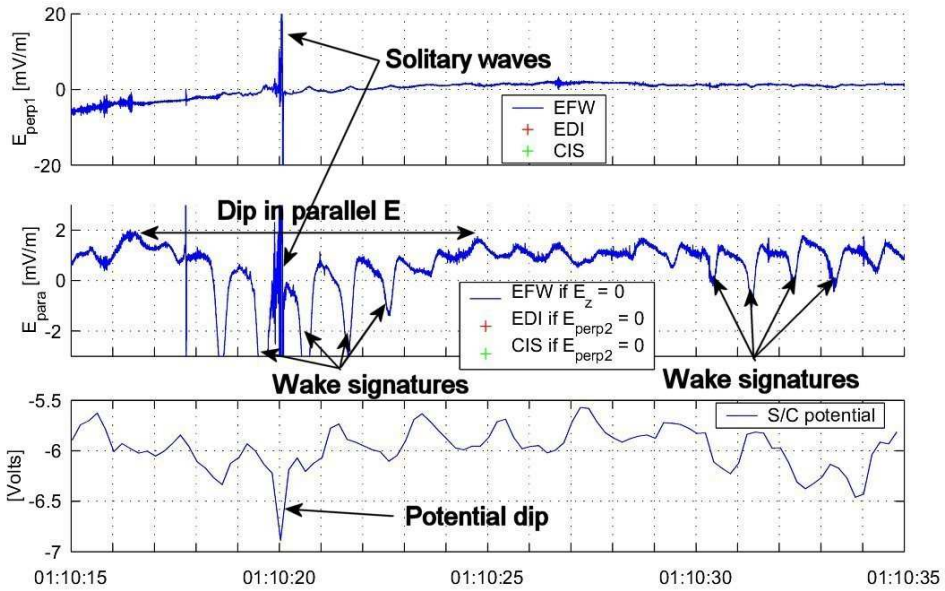

Figure 6.2: S/C-2 on 2002-02-06 showing a parallel DC electric field and wake at 01:10:17-01:10:25 UT, a potential dip at 01:10:20 UT, and a solitary wave structure at 01:10:20 UT.

Event	Time [UT]	S/C	Hemisphere	Duration [s]	Ampl [mV/m]
1	2002-01-10, 19:05:10-19:05:20	3	SH	10	1
2	2002-02-06, 01:10:17-01:10:25	2	NH	8	1.5
2	2002-02-06, 01:10:20-01:10:32	4	NH	12	1
2	2002-02-06, 01:12:19-01:12:25	2	NH	6	1
2	2002-02-06, 01:12:21-01:12:28	3	NH	7	1
2	2002-02-06, 01:17:03-01:17:15	3	NH	12	1
2	2002-02-06, 01:17:02-01:17:07	4	NH	5	1
3	2002-02-17, 22:47:50-22:48:00	3	NH	10	0.5
5	2002-03-18, 09:52:54-09:53:04	3	SH	10	0.5

Table 6.1: Summary of the six found DC parallel electric fields.

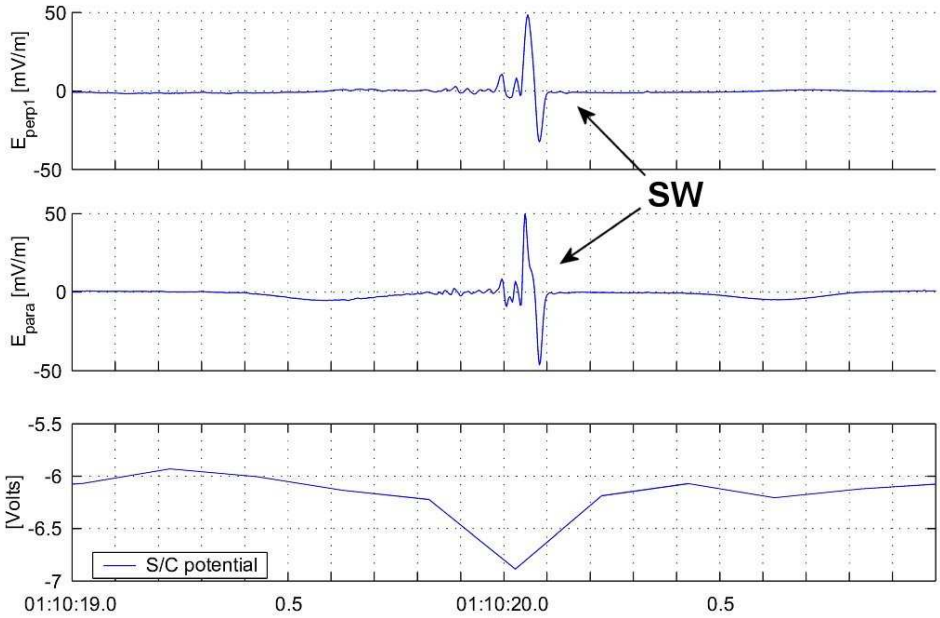

Figure 6.3: S/C-2 on 2002-02-06 showing a solitary wave (SW) associated with a potential dip.

This is interesting since WDLs might give a small contribution to the total potential drop causing the auroral acceleration [Eriksson and Boström, 1993].

Fig. 6.3 shows a zoom of the plot in Fig. 6.2, where the solitary structure can be seen at 01:10:20.0-20.1 UT. It is inside structure 1 from the second event (2002-02-06, 01:10-01:20 UT - NH) on S/C-2 (see also plot in section B.1.2 on page 57). An integration of the parallel electric field over the structure will give a value close to zero. Thus the solitary structure is a SW, with a peak-to-peak amplitude of 100 mV/m. The expected dip in the spacecraft potential can also be seen. SWs and WDLs are expected to propagate upwards at roughly 20 km/s [Eriksson and Boström, 1993]. This yields a field aligned extension of about 2 km for this 0.1 second SW. Previously observed solitary structures from the S3-3 and Viking satellites have typical field aligned dimensions of 50-250 m and potential drops of up to 5 V [Eriksson and Boström, 1993]. The SW found here is about an order of magnitude larger in field aligned extension compared to previous studies.

Fig. 6.4 shows 30 seconds and 2 seconds zooms of two DLs. It is from the first event (2002-01-10, 19:00-19:10 UT - SH) on S/C-3 (see also plots in section B.1.1 on page 53 and B.1.1 on page 54). The first DL at 19:05:17.0-17.5 UT is seen in both the perpendicular and the parallel electric field components. Integrating the parallel component with a peak-to-peak amplitude of 50 mV/m yields 4 mVs/m. Assuming a typical speed of 20 km/s would give a potential drop of 80 V. This is 16 times higher than the 5 V found before at lower altitudes. The second DL at 19:05:17.6-18.0 UT is seen only in the parallel component with a peak-to-peak amplitude of 30 mV/m and results in a potential drop of 50 V. Both DLs have a field aligned extension of about 7 km (assuming velocity of 20 km/s) and are associated with a dip in the spacecraft potential.

Another DL was found in the fourth event (2002-03-06, 14:24-14:34 UT - NH) by S/C-3 at 14:28:09.2-09.6 UT (see Fig. 6.5 and also in section B.1.4 on page 76 and B.1.4 on page 77). This DL has a peak-to-peak amplitude of 15 mV/m and the same dimension of about 8 km, but the resulting potential drop is only about 10 V.

The four found solitary structures all start with a positive peak. Assuming upward propagation of the solitary structures this gives converging electric field - consistent with ion holes - on the northern hemisphere, and diverging on the southern. Table 6.2 summarizes the four solitary structures.

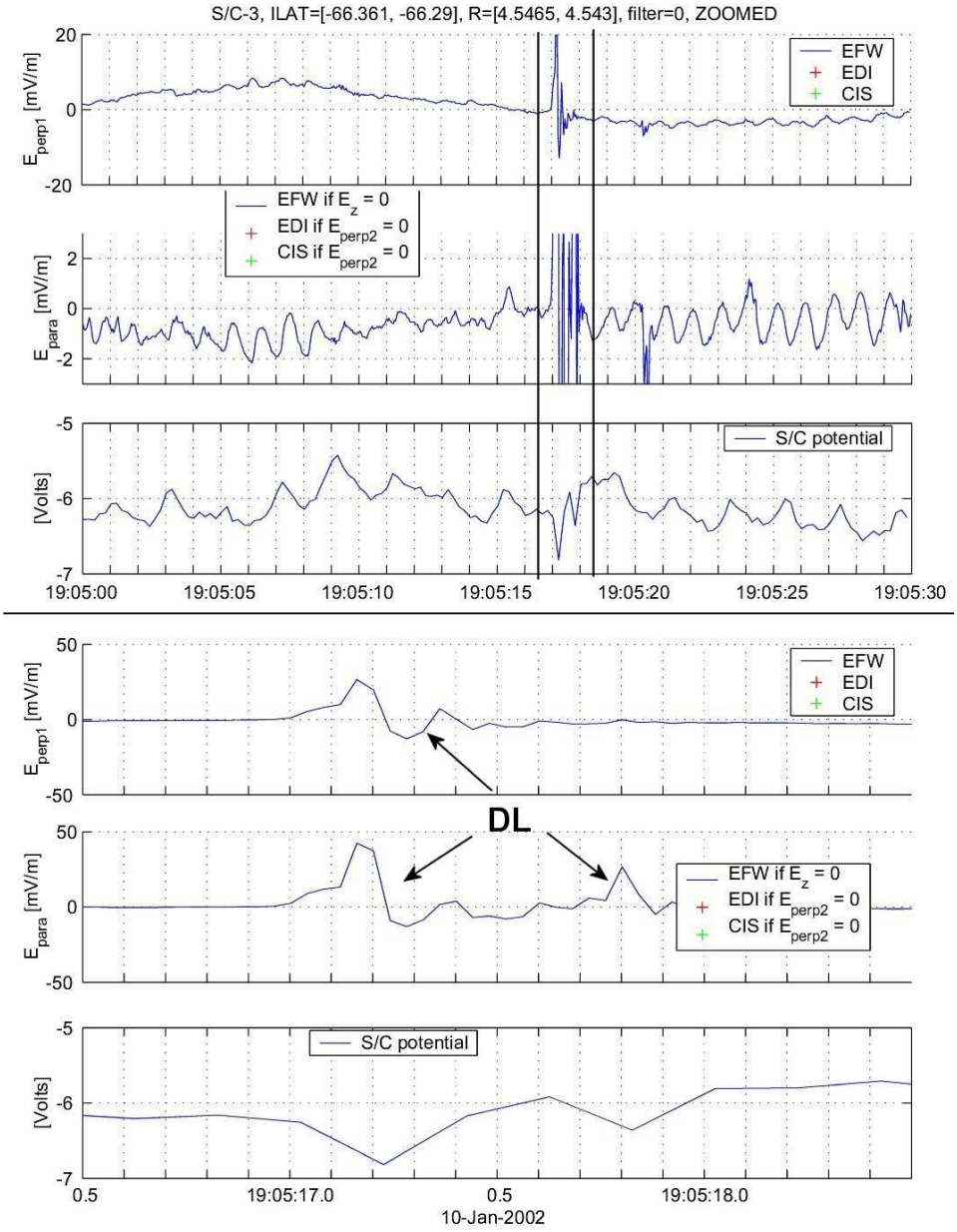

Figure 6.4: S/C-3 on 2002-01-10 on southern hemisphere. Upper part shows a small positive parallel DC electric field and the lower part shows a zoom of double layers (DL) associated with potential drops at 19:05:17.

Event	Time [UT]	S/C	Hemisphere	Conv/Div	P-P [mV/m]	Pot drop [V]
1	2002-01-10, 19:05:17.0-17.5	3	SH	Diverging	50	80
1	2002-01-10, 19:05:17.6-18.0	3	SH	Diverging	30	50
2	2002-02-06, 01:10:20.0-20.1	2	NH	Converging	100	0
4	2002-03-06, 14:28:09.2-09.6	3	NH	Converging	15	10

Table 6.2: Summary of the four found solitary structures. Upward propagation at 20 km/s is assumed.

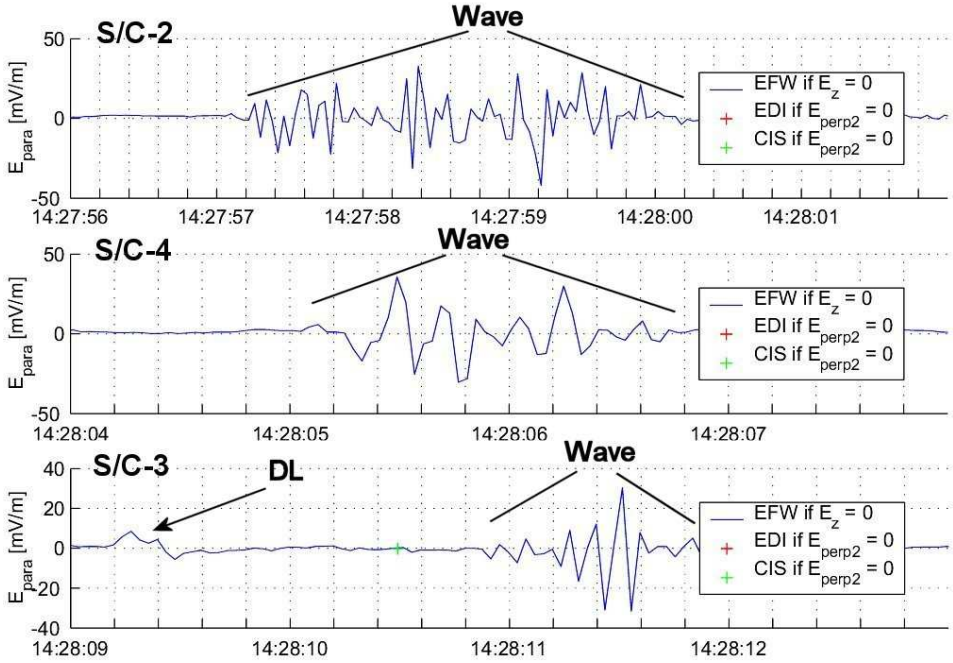

Figure 6.5: Break-up of waves into double layers on 2002-03-06.

6.3 Waves

In addition to quasi-static parallel electric fields, waves might also be able to accelerate auroral particles. One example of wave activity was found by S/C-2, 3, and 4 in the fourth event (2002-03-06, 14:24-14:34 UT - NH) at about 14:28 UT. The evolution of the wave can be seen in Fig. 6.5. S/C-2 sees it first centered around 14:27:59 UT (see plot in section B.1.4 on page 77). A few seconds later the activity has diminished and is seen by S/C-4 centered around 14:28:06 UT (see plot in section B.1.4 on page 83). When S/C-3 sees it at 14:28:11 UT (see plot in section B.1.4 on page 80) the wave activity is almost gone and it is starting to brake up into solitary structures. This is quite interesting because the end state of current-driven instabilities (waves) could be electric double layers, as mentioned in the introduction.

Chapter 7

Instrumental Effects

There are some instrumental effects that can introduce false electric fields. This section is not intended to cover all possible instrumental effects that could occur, but to address the most important ones; wake effect, offsets, and WHISPER interference.

7.1 Physical and Potential Wakes

A wake effect can cause 1-second-cycle spikes in electric fields. The physical wake effect is caused by a probe going through the plasma wake of the satellite body. If there are cold ions present (for example a cold ion beam) then the ions cannot get around the body of the spacecraft fast enough to provide the same plasma surroundings for the probe pair. There will be a lack of protons in the wake behind the spacecraft. The electrons are lighter and faster and manage to get in behind the spacecraft. The result is that the plasma in the wake has a lower potential than it should. It is relatively easy to pick out these wake effect structures in data as has been shown, see Fig 6.2 and corresponding text in section 6.1. However, cleaning out the wake effect from data is a difficult process. The electric potential wake effect is harder to detect. Not much is known about its effect on the measured fields. This effect comes from the fact that the spacecraft has a positive potential that extends much further in the plasma than the physical shape of the spacecraft. Ions can be hindered somewhat by the potential structure and irregularities can arise between probes.

7.2 Offsets

There are small offsets in the measured electric field data. These are pretty constant, but can vary depending on the plasma environment and time. The small offsets of 1-2 mV/m are caused as a result of asymmetric emissions of photoelectrons from the probes when they are in the sunward direction. It is easy enough to see the offset by inspection so nothing has been done to remove it from the data.

7.3 Interference from WHISPER

The WHISPER (Waves of HIgh frequency and Sounder for Probing of the Electron density by relaxation) instrument has a sounder that is an active wave experiment. When the sounder is on, electric field measurements are disturbed with waves. There are a few different ways to check if the sounder is active. One sign that the sounder is active is a characteristic dip in the spacecraft potential. It has been checked that only one of the investigated structures on one spacecraft is disturbed by WHISPER.

Chapter 8

Discussion and Conclusions

What happens above the main acceleration zone is currently not well known. Electric fields have not been studied so much in this region. We have used the Cluster spacecraft with its sensitive electric field instrument to search for parallel electric fields in the auroral zone at altitudes above the main acceleration region (Cluster satellites cross the auroral zone at an altitude of ~4.5 R_E). At this altitude the models have different predictions on how the parallel electric fields look like.

The measurement of parallel electric fields with the EFW instrument is limited to times when the angle between the spinplane of the spacecraft and the magnetic field is close to zero. 57 out of a total of 500 events with a close-to-zero angle were studied based on low-frequency wave activity and data availability. Five out of the 57 events bore signatures of DC electric fields parallel to the magnetic field. Six signatures of parallel DC electric fields with amplitude about 1 mV/m were found in the five selected events; one in 2001, and five in 2002. The reason for finding only one in 2001 and five in 2002 is probably due to low data availability in 2001 and that one of the events in 2002 had three signatures while all other events had only one or none. With the used selection strategy one could expect to find roughly two events per Cluster year.

It is very difficult to measure parallel electric fields with amplitudes around 1 mV/m. There are many things that could interfere with the measurements. We have checked for the main instrumental effects and other factors that can affect the results. Even so the found parallel electric fields seem to be real. Some but not all of the six parallel DC electric fields were combined with a wake effect from the spacecraft that results in false electric fields. When this happens it is harder to distinguish a possibly real electric field. In some cases fortunately more than one spacecraft sees the fields, and while one sees the wake another does not. Therefore we believe that the six found parallel electric fields are not the result of a wake-induced electric field even though some other clearly are.

The parallel fields are almost always centered around the sign change of the perpendicular component and they are all directed upwards (away from the Earth). Even the less reliable events show upward electric fields. In addition, other signatures of aurora - current and ion beams (not included in this paper) - show an upward direction in most cases. There is not a single indication of downward parallel fields associated with perpendicular sign change.

The results can be interpreted in several ways. Small (~1 mV/m) upward parallel electric fields could be blamed entirely on instrumental effects, but this is not so probable given that all the events are upward and on both hemispheres and are seen by multiple spacecraft in some cases. It could be U associated but it is not known how likely it is for these altitudes. It could also be lower part of an O, hence the potential have not begun to close at this altitude, or the lack of downward fields could mean that Cluster is measuring above the O-potential. Another possibility is that downward electric fields at this altitude is too small to be measured by EFW on Cluster (<1 mV/m). To resolve the question more events from a bigger range of altitudes, possibly using more sensitive instruments, should be studied.

In addition a solitary wave and three double layers have been found. The double layers are thought to contribute to the total potential drop that energises the auroral electrons and solitary waves

are usually found in combination. The peak-to-peak amplitudes of found solitary waves and double layers are between 15mV/m and 100 mV/m.The field aligned extent is ~8 km and potential drops are up to 80 V (assuming an upward speed of 20 km/s). These values are much larger compared to double layers, with amplitudes of about 5 V and a field line extension of about 100 m, earlier found at lower altitudes.

This project was intended to look at quasistatic electric fields. Despite this a very interesting wave event was found, showing the break-up of waves into double layers.

In further work it would be valuable to utilise the fact that there are multiple satellites more. For example, to make correlations between the satellites to get the size, speed and direction of the parallel DC electric fields. In addition one should look for parallel fields at other places, not only at the sign-change of a bi-polar perpendicular electric field structure. The few double layers and solitary waves that were found had much larger spatial extent and potential drop than the ones observed at lower altitudes. Further studies should answer whether this is a common feature and they should give a better understanding on how double layers and solitary waves fit into the bigger picture.

Appendix A

MATLAB Code

A.1 erik_Epp

```
function [E_pp] = erik_Epp(B_ds, E_ds)
%
% function [E_pp] = erik_Epp(B_ds, E_ds)
%
% Input:  B and E-fields in despun coordinates
% Output: E-field in parallel and perpendicular coord,
%   if EFW (E_ds miss the z component)
%   [E_pp] = [t  E_perp1  E_perp2  E_perp2_para=0  E_para_Ez=0  E_para_perp2=0]
%   if CIS or EDI (all components present)
%   [E_pp] = [t  E_perp1  E_perp2 E_para_perp2=0]
%
%   All references are to Parallel Electric Fields in Space
%   thesis paper by Erik Bergman, 2003
%
%   See Table 4.1 for definitions
%   E_perp1 if E_z = 0
%   E_perp2   if E_z = 0
%   E_perp2_para=0   if E_para = 0
%   E_para_Ez=0   if E_z = 0
%   E_para_perp2=0 if E_perp2 = 0
%


%See Eq. (4.1)
B_perp1 = av_norm(av_cross(B_ds, [0 0 1]));
%See Eq. (4.2)
B_perp2 = av_norm(av_cross(B_perp1, B_ds));
%See Eq. (4.3)
B_para = av_norm(B_ds);

% Interpolate the B data so we have the same number of points as the E data
B_perp1_h = [E_ds(:,1) interp1(B_perp1(:,1), B_perp1(:,[2 3 4]), E_ds(:,1), ...
'linear', 'extrap')];
B_perp2_h = [E_ds(:,1) interp1(B_perp2(:,1), B_perp2(:,[2 3 4]), E_ds(:,1), ...
'linear', 'extrap')];
B_para_h = [E_ds(:,1) interp1(B_para(:,1), B_para(:,[2 3 4]), E_ds(:,1), ...
'linear', 'extrap')];

% If E_ds miss z-comp then from EFW
if length(E_ds(1, :)) == 3
  % Assuming E_z = 0
  E_ds(:, 4) = 0;
  E_perp1 = av_dot(B_perp1_h, E_ds);
  E_perp2 = av_dot(B_perp2_h, E_ds);
  E_para = av_dot(B_para_h, E_ds);

  E_pp = E_perp1;
  E_pp(:, 3) = E_perp2(:, 2);
  E_pp(:, 5) = E_para(:, 2);
```

```
  % Assuming E_para = 0, see Eq. (4.6)
  E_ds(:, 4) = -(E_ds(:, 2) .* B_para_h(:, 2) + E_ds(:, 3) .* ...
B_para_h(:, 3)) ./ B_para_h(:, 4);
  E_perp2 = av_dot(B_perp2_h, E_ds);
  E_pp(:, 4) = E_perp2(:, 2);

  % Assuming E_perp2 = 0, see Eq. (4.10)
  E_ds(:, 4) = -(E_ds(:, 2) .* B_perp2_h(:, 2) + E_ds(:, 3) .* ...
B_perp2_h(:, 3)) ./ B_perp2_h(:, 4);
  E_para = av_dot(B_para_h, E_ds);
  E_pp(:, 6) = E_para(:, 2);

% Else from CIS or EDI
else
  E_perp1 = av_dot(B_perp1_h, E_ds);
  E_perp2 = av_dot(B_perp2_h, E_ds);

  % Assuming E_perp2 = 0, see Eq. (4.10)
  E_ds(:, 4) = -(E_ds(:, 2) .* B_perp2_h(:, 2) + E_ds(:, 3) .* ...
B_perp2_h(:, 3)) ./ B_perp2_h(:, 4);
  E_para = av_dot(B_para_h, E_ds);

  E_pp = E_perp1;
  E_pp(:, 3) = E_perp2(:, 2);
  E_pp(:, 4) = E_para(:, 2);
end
```

A.2 erik_plot

```
%
% erik_plot
%
%   Main program for making the overview plots
%   Data should already be loaded using routine erik_read_cluster
%
%   panel 1 - spinplane angle
%   panel 2 - perpendicular component in spinplane
%   panel 3 - perpendicular component out of spinplane
%   panel 4 - parallel component in spinplane
%   panel 5 - spacecraft potential
%   panel 6 - angle between Sun and B-field in spinplane
%

zoom = input('Zoomed in (1 = yes, 0 = no)?: ');
sc_no = input('Which S/C (1-4)?: ');
filter = input('LP filter freq (0 = no filter)?: ');
disp('Working...');

% Get the Cluster data (already loaded from disk)
command = sprintf('B_ds = B_fgm_%1.0f;\0',sc_no); eval(command);
command = sprintf('E_ds = E_vect_%1.0f;\0',sc_no); eval(command);
command = sprintf('EDI_ds = EDI_vect_%1.0f;\0',sc_no); eval(command);
command = sprintf('CIS_ds = CIS_v_%1.0f;\0',sc_no); eval(command);
command = sprintf('N_e = Ne_%1.0f;\0',sc_no); eval(command);
command = sprintf('SC_p = SCp_%1.0f;\0',sc_no); eval(command);
command = sprintf('ph = ph_vect_%1.0f;\0',sc_no); eval(command);
command = sprintf('E_12 = E_12_%1.0f;\0',sc_no); eval(command);
command = sprintf('E_34 = E_34_%1.0f;\0',sc_no); eval(command);
command = sprintf('LAT = LAT_vect_%1.0f;\0',sc_no); eval(command);
command = sprintf('R = R_vect_%1.0f;\0',sc_no); eval(command);

% Extract Invariant latitude and altitude
LAT_start = LAT(1, 2);
LAT_end = LAT(length(LAT), 2);
R_start = R(1, 2);
R_end = R(length(R), 2);

% Get the angles
theta_xy = erik_angle(B_ds, 'xy');
theta_x = erik_angle(B_ds, 'x');
theta_x = [E_ds(:,1) interp1(theta_x(:,1), theta_x(:,2), E_ds(:,1), ...
'linear', 'extrap')];

% Get date and time
start_time = E_ds(1,1);
date = datestr(datenum(fromepoch(start_time)));
date = date(1:11);

% Get EFW and EDI in FAC
```

```
E_pp = erik_Epp(B_ds, E_ds);
E_pp_EDI = erik_Epp(B_ds, EDI_ds);

% Calculate E-field from CIS data (E=-VxB)
E_pp_CIS = av_cross(CIS_ds, B_ds);
E_pp_CIS(:, 2) = E_pp_CIS(:, 2) * (-1e-3);
E_pp_CIS(:, 3) = E_pp_CIS(:, 3) * (-1e-3);
E_pp_CIS(:, 4) = E_pp_CIS(:, 4) * (-1e-3);

% Get CIS in FAC
E_pp_CIS = erik_Epp(B_ds, E_pp_CIS);

% Additional plots if zoom selected
if zoom == 1
  figure(2);
  clf;
  ph = erik_fixphase(ph, E_pp(:, 1));
  h2(1) = subplot(4, 1, 1); plot( ph(:, 2), E_pp(:, 5));
  set(gca ,'XTick', 0:45:360);
  curr_axis = axis;
  axis([curr_axis(1) curr_axis(2) -7 7]);
  ylabel('mV/m');
  strTitle = sprintf('phase vs E_p_a_r_a on S/C-%1.0f', sc_no);
  title(strTitle);
  theta = theta_x(:, 2) + ph(:, 2);
  h2(2) = subplot(4, 1, 2); plot(theta, E_pp(:, 5));
  set(gca ,'XTick', 0:45:360);
  curr_axis = axis;
  axis([curr_axis(1) curr_axis(2) -7 7]);
  ylabel('mV/m');
  strTitle = sprintf('Angle between B-field and spinning x-axis ...
vs E_p_a_r_a on S/C-%1.0f', sc_no);
  title(strTitle);


  h2(3) = subplot(4, 1, 3); plot(E_12(:,1), E_12(:, 2));
  curr_axis = axis;
  axis([curr_axis(1) curr_axis(2) -10 10]);
  ylabel('Volts');
  strTitle = sprintf('S/C-%1.0f, raw probe data',sc_no);
  title(strTitle);
  h2(4) = subplot(4, 1, 4); plot(E_34(:,1), E_34(:, 2));
  curr_axis = axis;
  axis([curr_axis(1) curr_axis(2) -10 10]);
  ylabel('Volts');
  add_timeaxis(h2([3 4]), date);
  legend(h2(3), 'E_1_2', 0);
  legend(h2(4), 'E_3_4', 0);

end

% Filter the data to get rid of wake effects
```

```
if filter ~= 0
  E_pp = av_tsfilt(E_pp, 0, filter, [], 3);
end

% Main plots
figure(1);
clf;
h(1) = subplot(6, 1, 1); plot(theta_xy(:,1), theta_xy(:, 2));
ylabel('[Degrees]');
grid;
strTitle = sprintf('S/C-%1.0f, ILAT=[%0.05g, %0.05g], R=[%0.05g, ...
%0.05g], filter=%0.5g\0',...
sc_no, LAT_start, LAT_end, R_start, R_end, filter);
if zoom == 1
  strTitle = [strTitle ', ZOOMED']
end
title(strTitle);

h(2) = subplot(6, 1, 2);
hold on;
plot(E_pp(:, 1), E_pp(:, 2));
plot(E_pp_EDI(:, 1), E_pp_EDI(:, 2), '+r');
plot(E_pp_CIS(:, 1), E_pp_CIS(:, 2), '+g');
hold off;
curr_axis = axis;
axis([curr_axis(1) curr_axis(2) -20 20]);
ylabel('E_p_e_r_p_1 [mV/m]');
grid;

h(3) = subplot(6, 1, 3);
hold on;
plot(E_pp(:, 1), E_pp(:, 4));
plot(E_pp_EDI(:, 1), E_pp_EDI(:, 3), '+r');
plot(E_pp_CIS(:, 1), E_pp_CIS(:, 3), '+g');
hold off;
curr_axis = axis;
axis([curr_axis(1) curr_axis(2) -20 20]);
ylabel('E_p_e_r_p_2 [mV/m]');
grid;

h(4) = subplot(6, 1, 4);
hold on;
plot(E_pp(:, 1), E_pp(:, 5));
plot(E_pp_EDI(:, 1), E_pp_EDI(:, 4), '+r');
plot(E_pp_CIS(:, 1), E_pp_CIS(:, 4), '+g');
hold off;
curr_axis = axis;
axis([curr_axis(1) curr_axis(2) -3 3]);
ylabel('E_p_a_r_a [mV/m]');
grid;

h(5) = subplot(6, 1, 5); plot(SC_p(:, 1), SC_p(:, 2));
```

```
ylabel('[Volts]');
grid;

h(6) = subplot(6, 1, 6); plot(theta_x(:, 1), theta_x(:, 2));
ylabel('[Degrees]');
grid;

add_timeaxis(h, date);
legend(h(1), 'Angle between spin plane and B-field', 0);
legend(h(2), 'EFW', 'EDI', 'CIS', 0);
legend(h(3), 'EFW if E_p_a_r_a = 0', 'EDI', 'CIS', 0);
legend(h(4), 'EFW if E_z = 0', 'EDI if E_p_e_r_p_2 = 0', ...
'CIS if E_p_e_r_p_2 = 0', 0);
legend(h(5), 'S/C potential', 0);
legend(h(6), 'Angle between Sun and B-field', 0);

clear command theta_xy theta_x theta B_ds E_ds N_e E_pp E_pp_EDI filter ...
start_time date ph E_12 E_34 SC_p LAT R;
```

A.3 erik_angle

```
function [theta] = erik_angle(B_ds, str)
%
% function [theta] = erik_angle(B_ds, str)
%
% Input:  B-field in despun coordinates, str = what angle
% Output: Angle between spinplane and B-field if str = "xy"
%         Angle between B-field in xy-plane and x-axis if str = "x"
%
%   All references are to Parallel Electric Fields in Space
%   thesis paper by Erik Bergman, 2003


% Angle between B-field and xy-plane, see Eq. (4.4)
if str == 'xy'
  B = av_abs(B_ds); % B is B_ds with an added column 5 that has values of |B_ds|
  theta = [B(:,1) asin(B(:,4)./B(:,5))*180/pi];

% Angle between B-field in xy-plane and x-axis, see Eq. (4.5)
elseif str == 'x'
  theta = [B_ds(:,1) atan(B_ds(:,3)./B_ds(:,2))*180/pi];
else
  theta = [Nan NaN];
  disp('Error in str in erik_angle(B_ds, str): not valid string');
end
```

Appendix B

Plots

B.1 Selected

B.1.1 2002-01-10

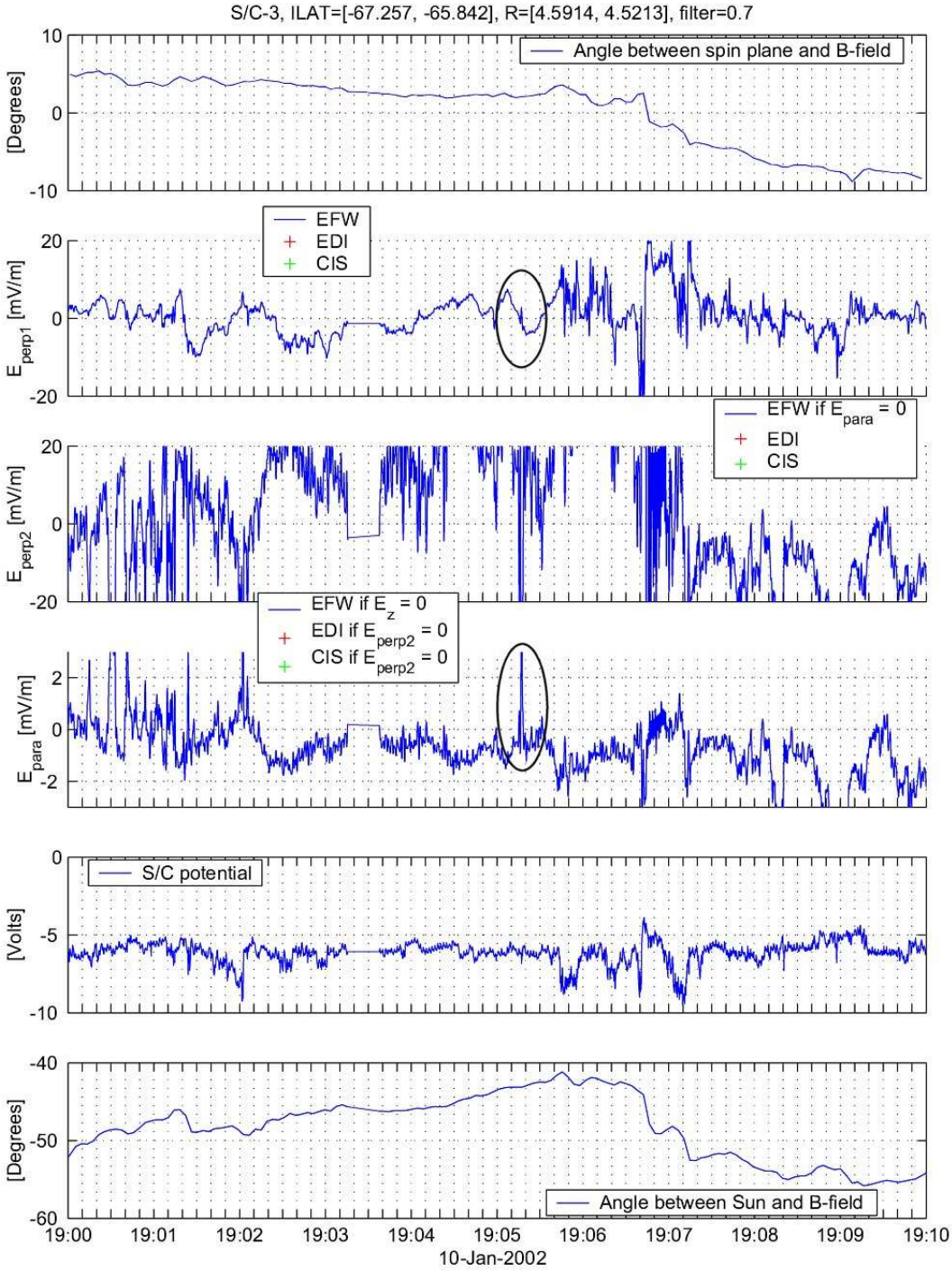

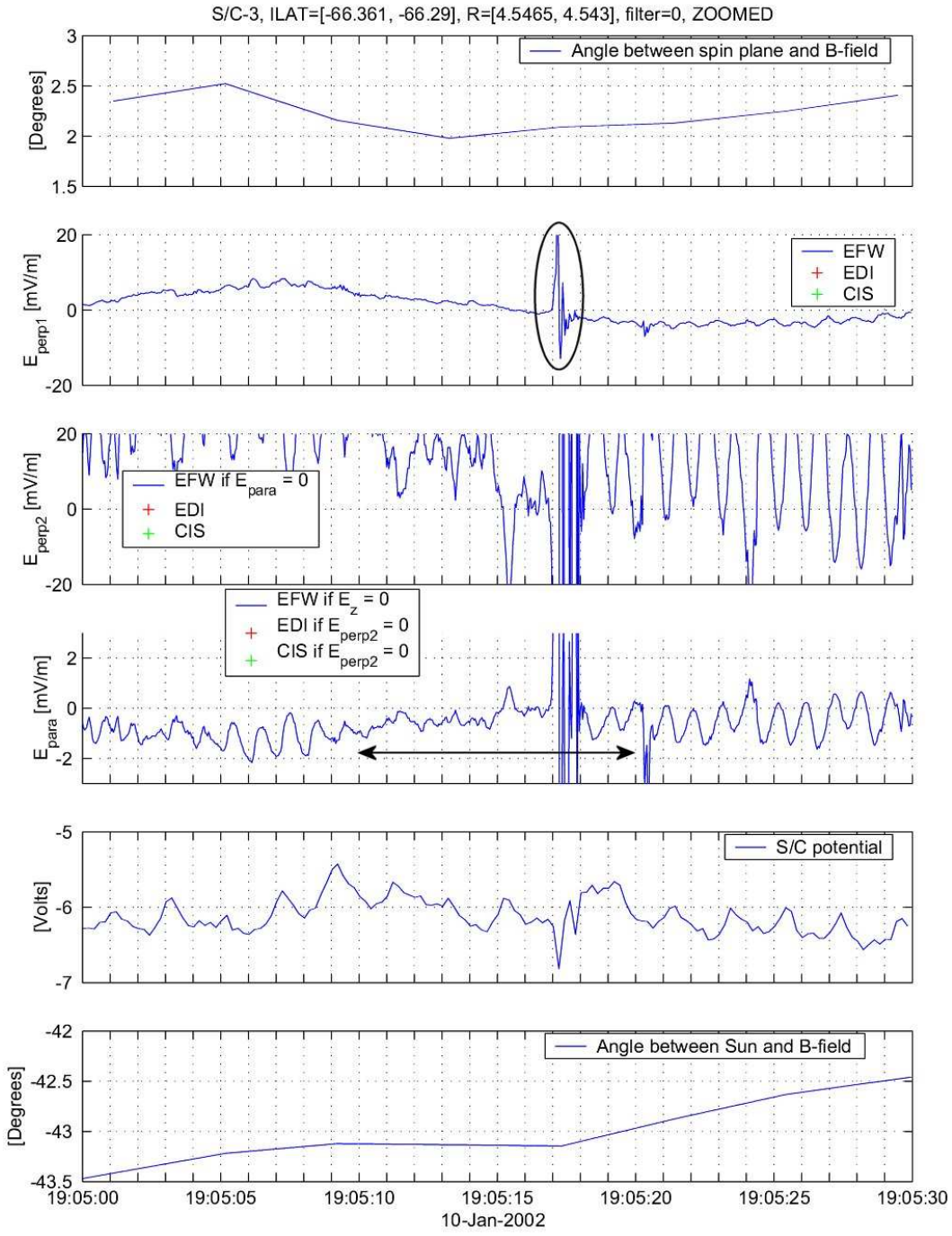
S/C-3, ILAT=[-66.361, -66.29], R=[4.5465, 4.543], filter=0, ZOOMED
Angle between spin plane and B-field
[Degrees]
EFW
EDI
CIS
E perp1 [mV/m]
EFW if E para = 0
EDI
CIS
E perp2 [mV/m]
EFW if E z = 0
EDI if E perp2 = 0
CIS if E perp2 = 0
E para [mV/m]
S/C potential
[Volts]
Angle between Sun and B-field
[Degrees]
19:05:00
19:05:05
19:05:10
19:05:15
19:05:20
19:05:25
19:05:30
10-Jan-2002

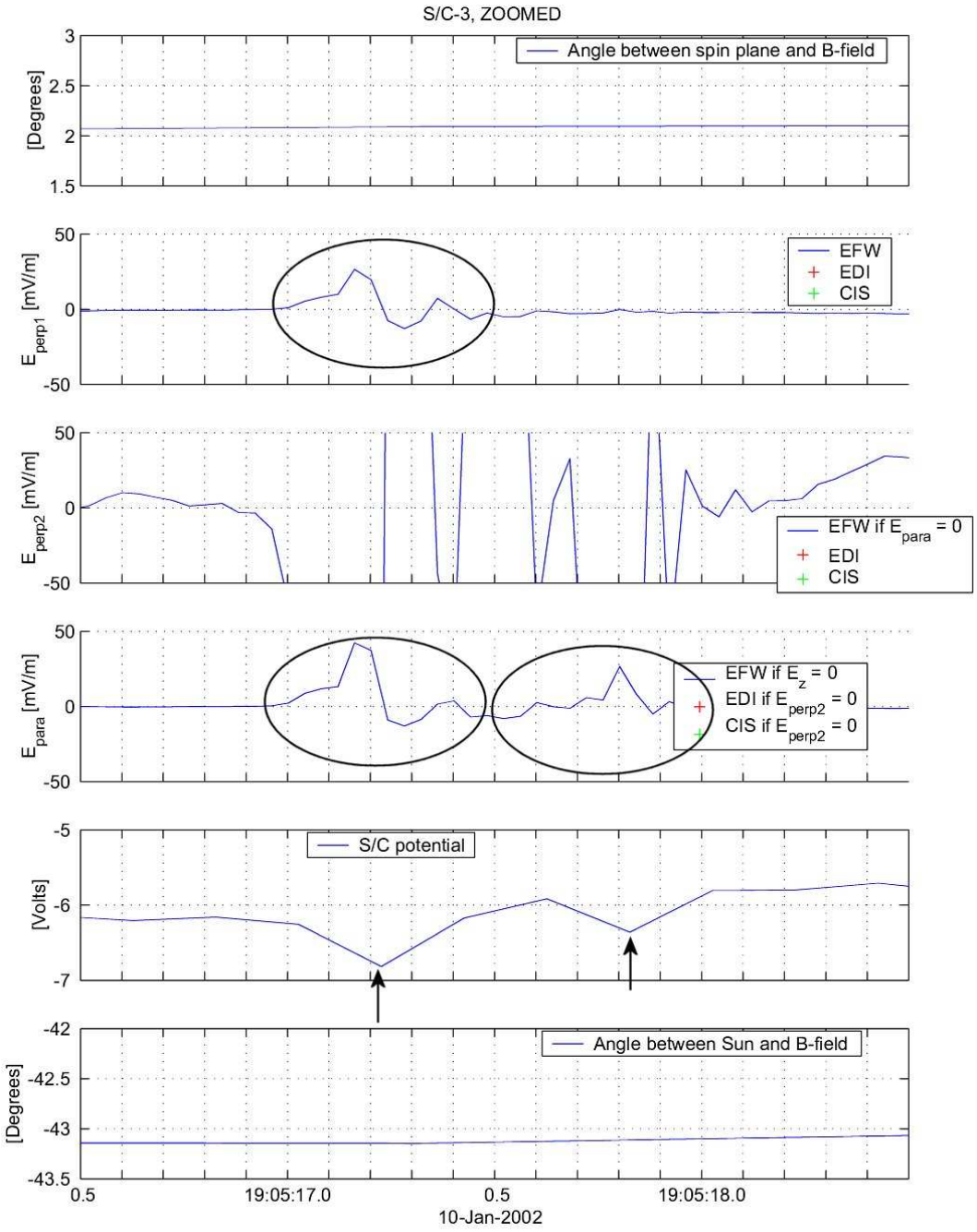
S/C-3, ZOOMED
Angle between spin plane and B-field
[Degrees]
3
2.5
2
1.5
EFW
EDI
CIS
E_{perp1} [mV/m]
50
0
-50
E_{perp2} [mV/m]
EFW if E_{para} = 0
EDI
CIS
E_{para} [mV/m]
EFW if E_z = 0
EDI if E_{perp2} = 0
CIS if E_{perp2} = 0
S/C potential
[Volts]
-5
-6
-7
Angle between Sun and B-field
[Degrees]
-42
-42.5
-43
-43.5
0.5
19:05:17.0
0.5
19:05:18.0
10-Jan-2002

B.1.2 2002-02-06

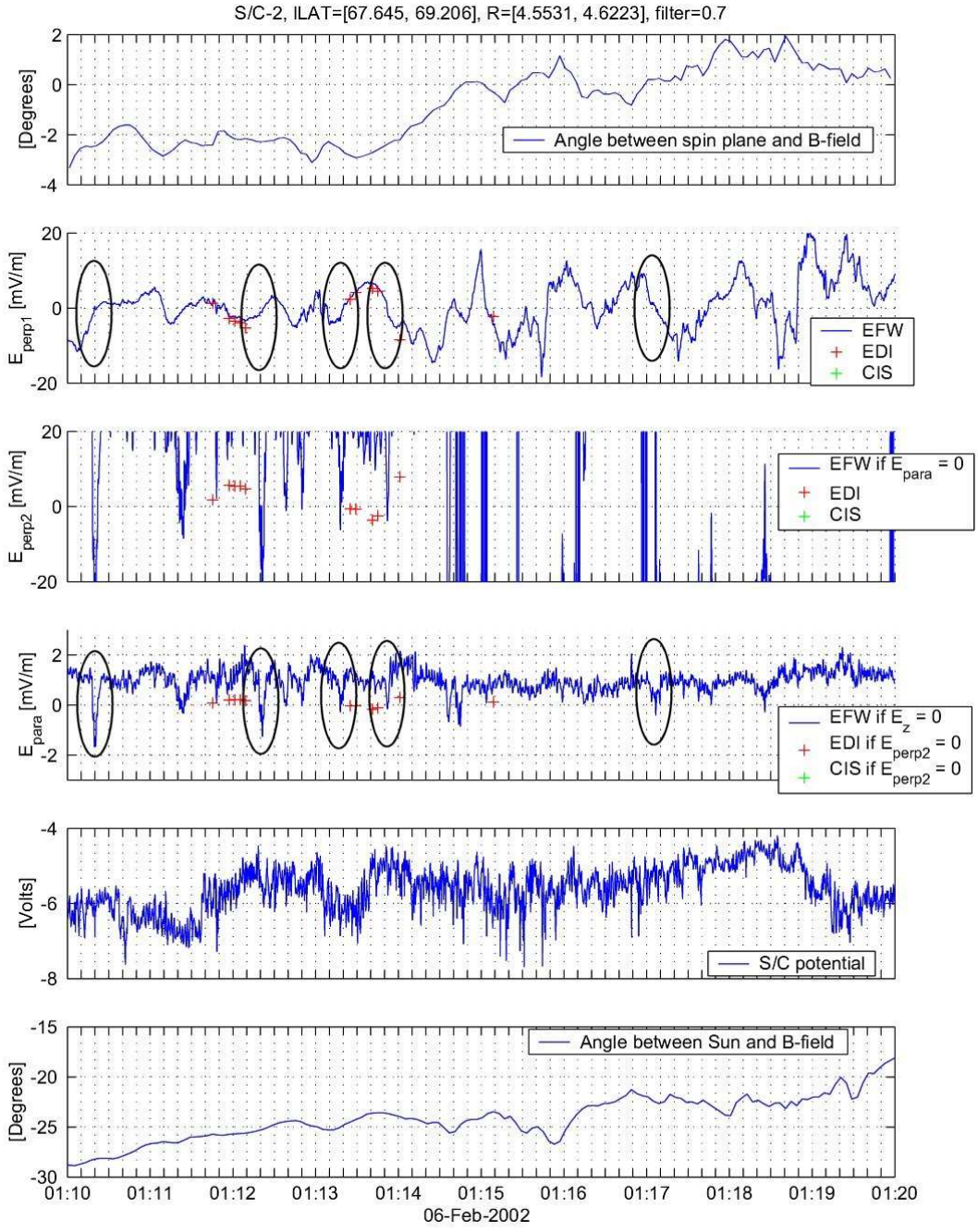

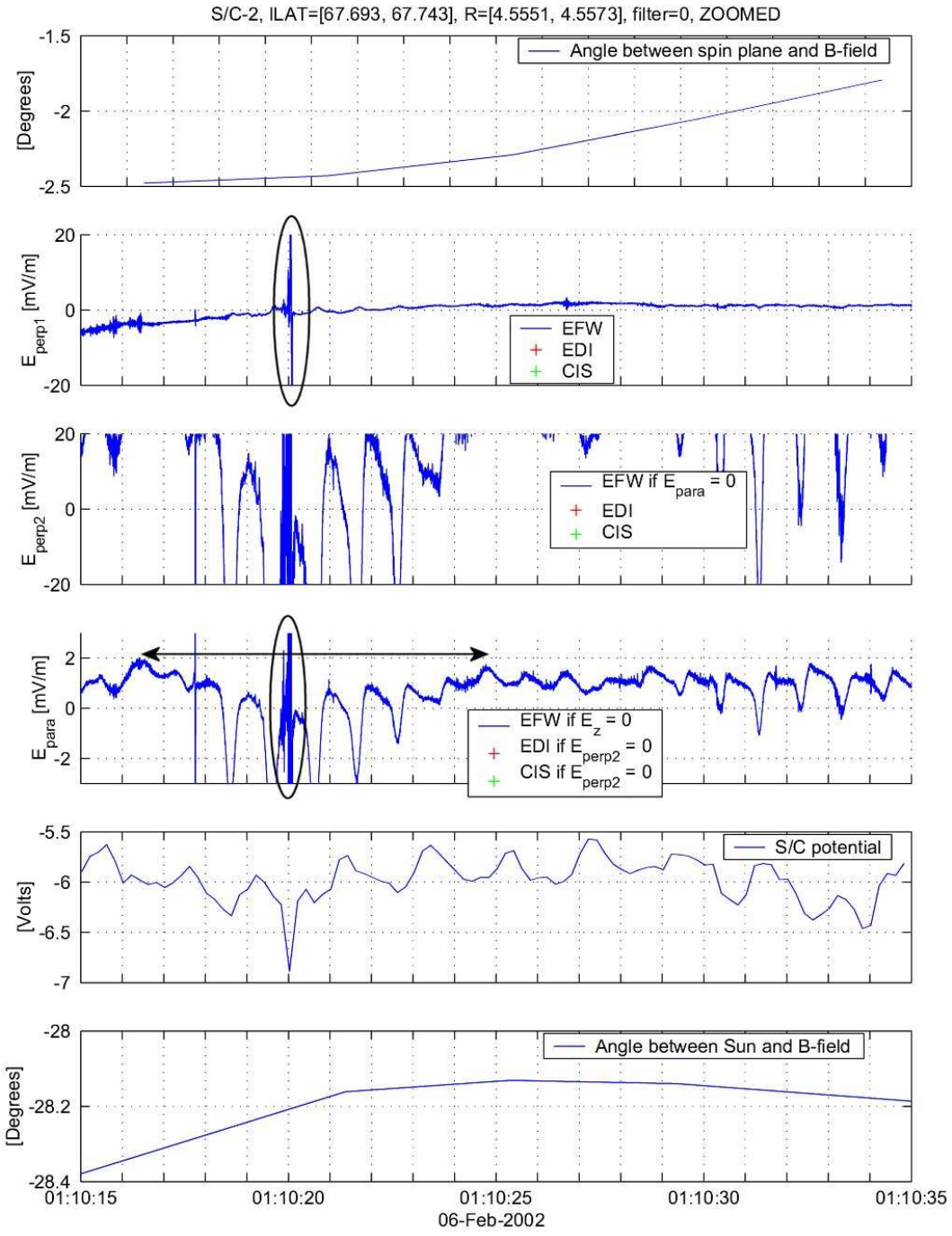
S/C-2, ILAT=[67.693, 67.743], R=[4.5551, 4.5573], filter=0, ZOOMED
Angle between spin plane and B-field
[Degrees]
-1.5
-2
-2.5
E perp1 [mV/m]
20
0
-20
EFW
EDI
CIS
E perp2 [mV/m]
EFW if E para = 0
EDI
CIS
E para [mV/m]
2
0
-2
EFW if E z = 0
EDI if E perp2 = 0
CIS if E perp2 = 0
[Volts]
-5.5
-6
-6.5
-7
S/C potential
[Degrees]
-28
-28.2
-28.4
Angle between Sun and B-field
01:10:15
01:10:20
01:10:25
01:10:30
01:10:35
06-Feb-2002

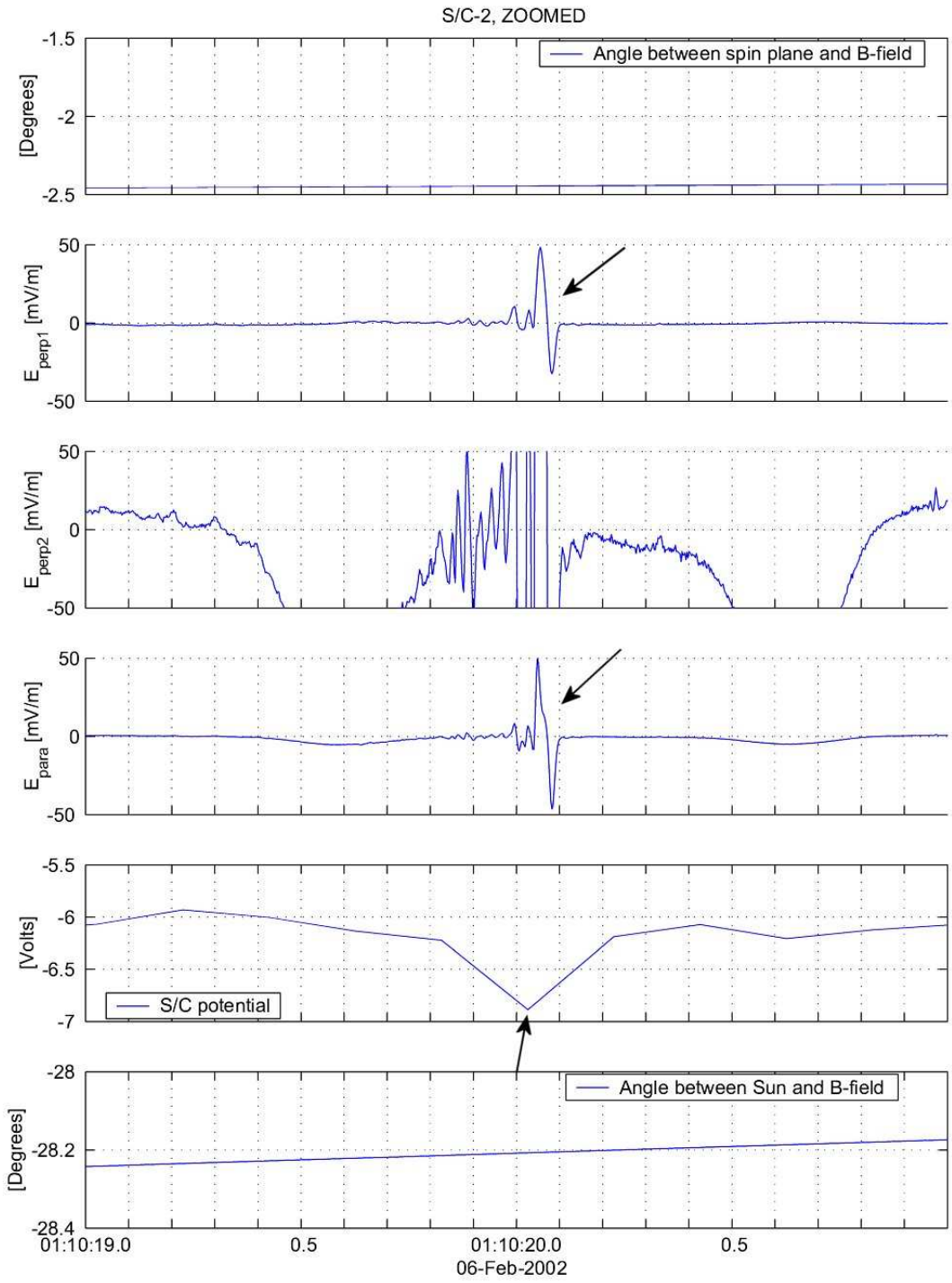
S/C-2, ZOOMED
Angle between spin plane and B-field
[Degrees]
-1.5
-2
-2.5
E_{perp1} [mV/m]
E_{perp2} [mV/m]
E_{para} [mV/m]
50
0
-50
[Volts]
-5.5
-6
-6.5
-7
S/C potential
Angle between Sun and B-field
-28
-28.2
-28.4
01:10:19.0
0.5
01:10:20.0
0.5
06-Feb-2002

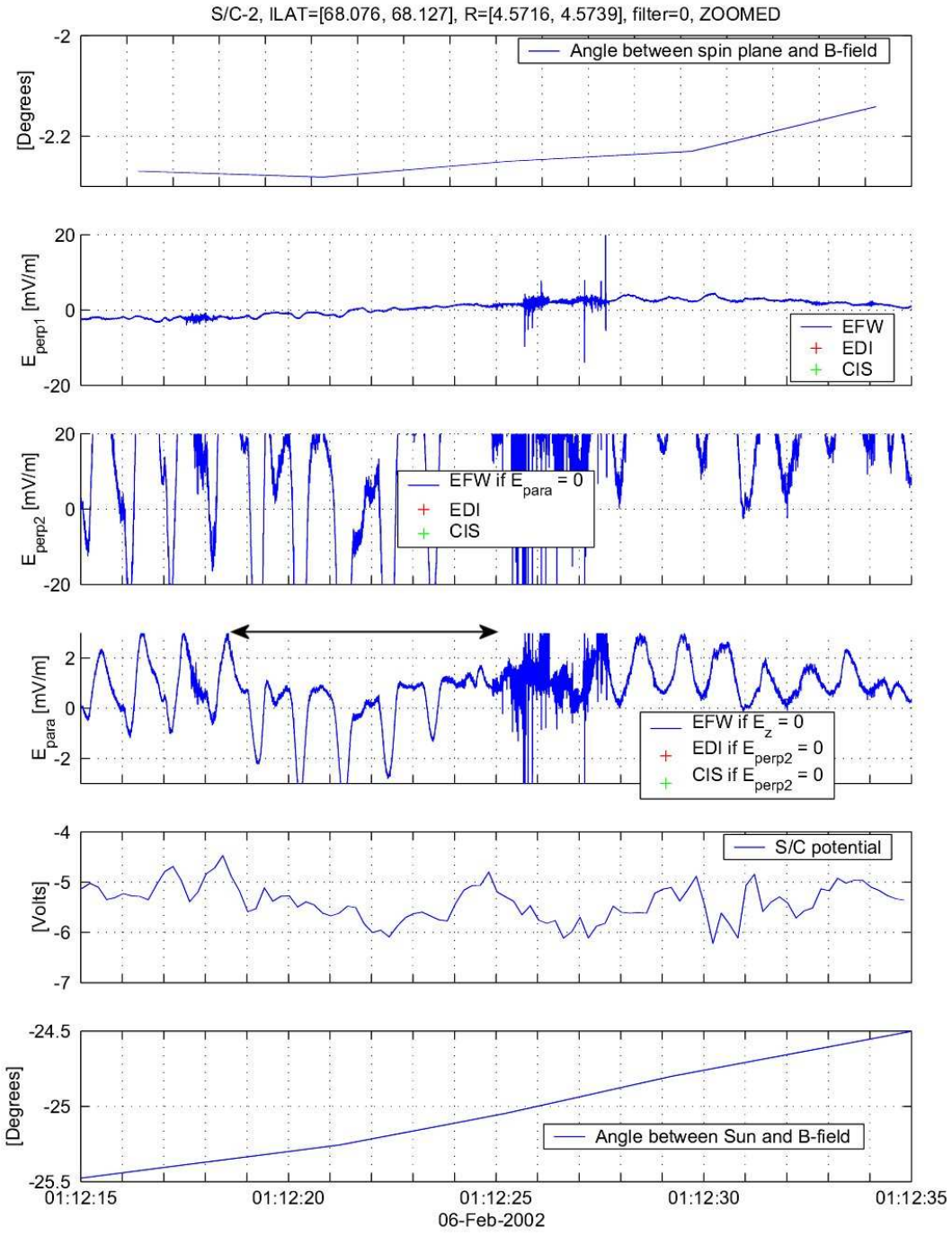
S/C-2, ILAT=[68.076, 68.127], R=[4.5716, 4.5739], filter=0, ZOOMED
Angle between spin plane and B-field
[Degrees]
-2
-2.2
E perp1 [mV/m]
20
0
-20
EFW
EDI
CIS
E perp2 [mV/m]
EFW if E para = 0
EDI
CIS
E para [mV/m]
2
0
-2
EFW if E z = 0
EDI if E perp2 = 0
CIS if E perp2 = 0
S/C potential
[Volts]
-4
-5
-6
-7
[Degrees]
-24.5
-25
-25.5
Angle between Sun and B-field
01:12:15
01:12:20
01:12:25
01:12:30
01:12:35
06-Feb-2002

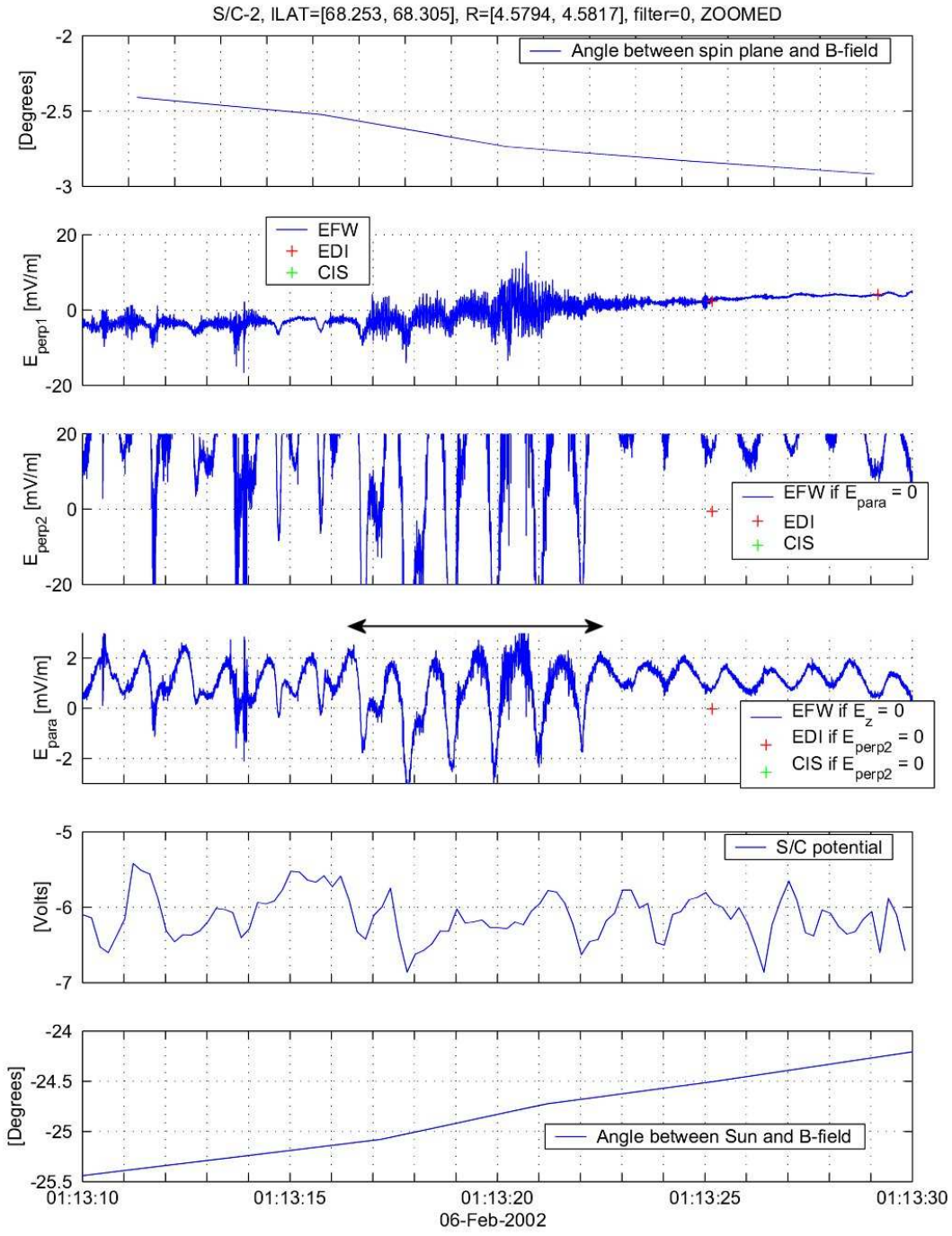
S/C-2, ILAT=[68.253, 68.305], R=[4.5794, 4.5817], filter=0, ZOOMED
Angle between spin plane and B-field
[Degrees]
-2
-2.5
-3
EFW
EDI
CIS
E perp1 [mV/m]
20
0
-20
E perp2 [mV/m]
EFW if E para = 0
EDI
CIS
E para [mV/m]
2
0
-2
EFW if E z = 0
EDI if E perp2 = 0
CIS if E perp2 = 0
S/C potential
[Volts]
-5
-6
-7
Angle between Sun and B-field
[Degrees]
-24
-24.5
-25
-25.5
01:13:10
01:13:15
01:13:20
01:13:25
01:13:30
06-Feb-2002

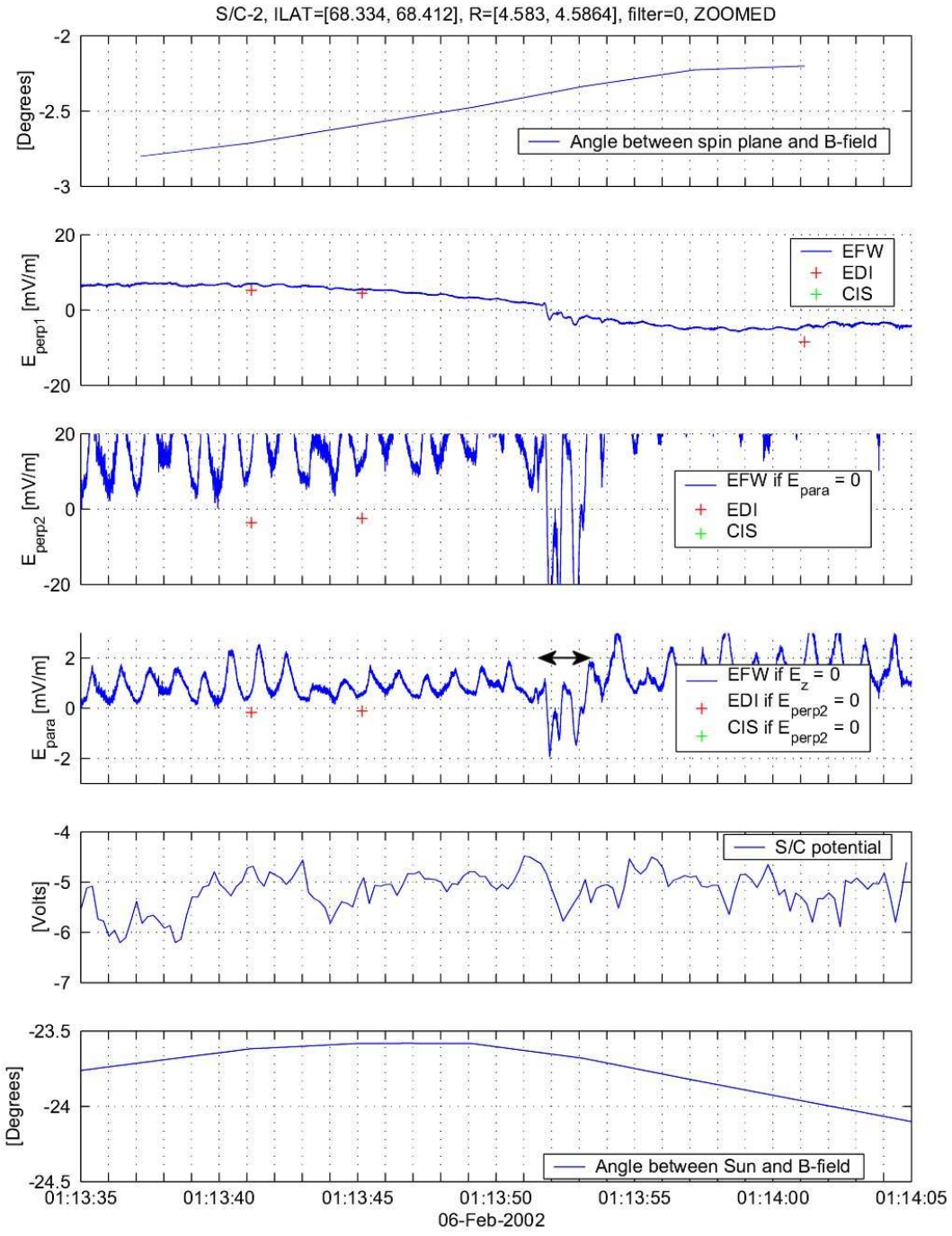
S/C-2, ILAT=[68.334, 68.412], R=[4.583, 4.5864], filter=0, ZOOMED
[Degrees]
Angle between spin plane and B-field
E perp1 [mV/m]
EFW
EDI
CIS
E perp2 [mV/m]
EFW if E para = 0
EDI
CIS
E para [mV/m]
EFW if E z = 0
EDI if E perp2 = 0
CIS if E perp2 = 0
[Volts]
S/C potential
[Degrees]
Angle between Sun and B-field
01:13:35
01:13:40
01:13:45
01:13:50
01:13:55
01:14:00
01:14:05
06-Feb-2002

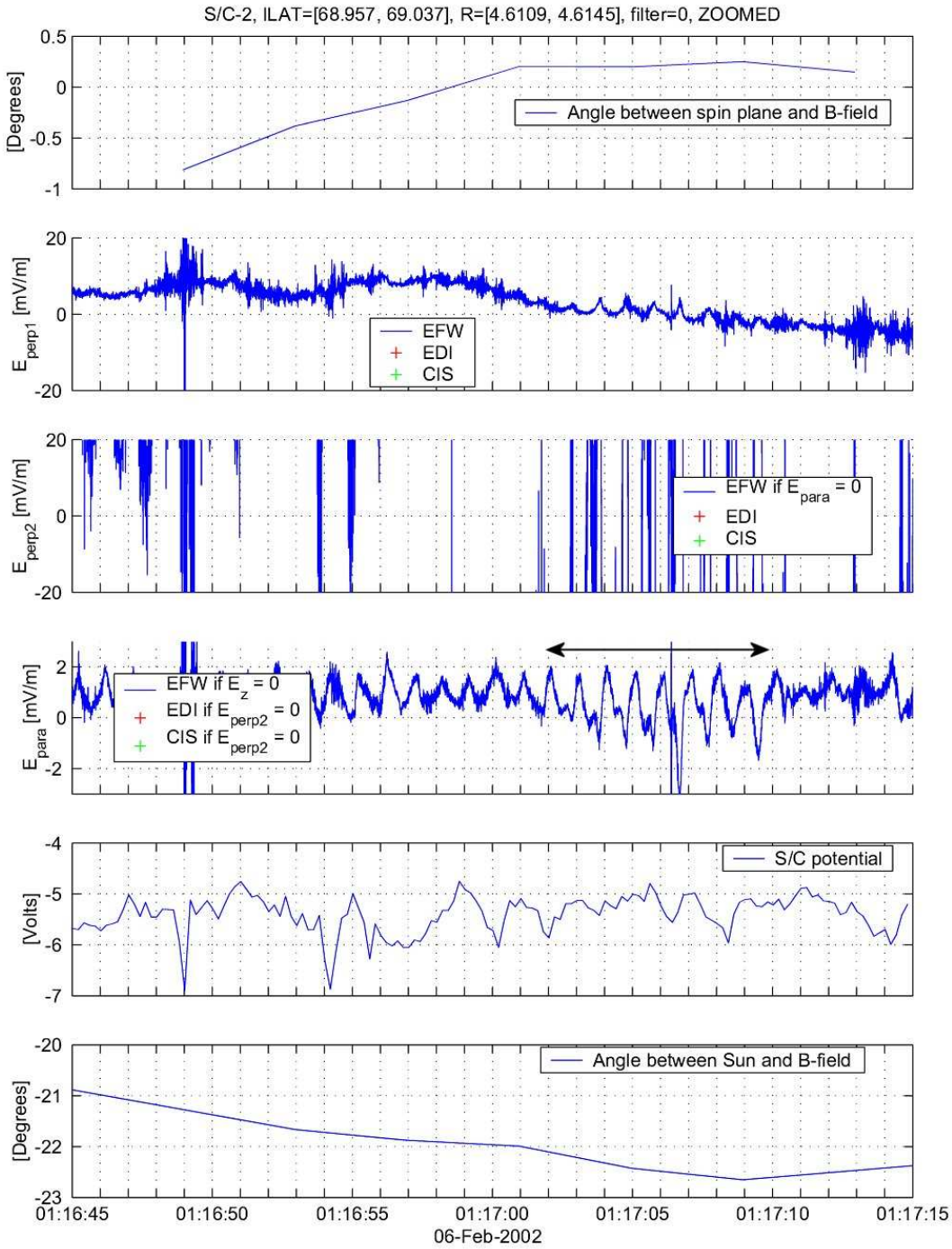
S/C-2, ILAT=[68.957, 69.037], R=[4.6109, 4.6145], filter=0, ZOOMED
[Degrees]
Angle between spin plane and B-field
E perp1 [mV/m]
EFW
EDI
CIS
E perp2 [mV/m]
EFW if E para = 0
EDI
CIS
E para [mV/m]
EFW if E z = 0
EDI if E perp2 = 0
CIS if E perp2 = 0
[Volts]
S/C potential
[Degrees]
Angle between Sun and B-field
01:16:45
01:16:50
01:16:55
01:17:00
01:17:05
01:17:10
01:17:15
06-Feb-2002

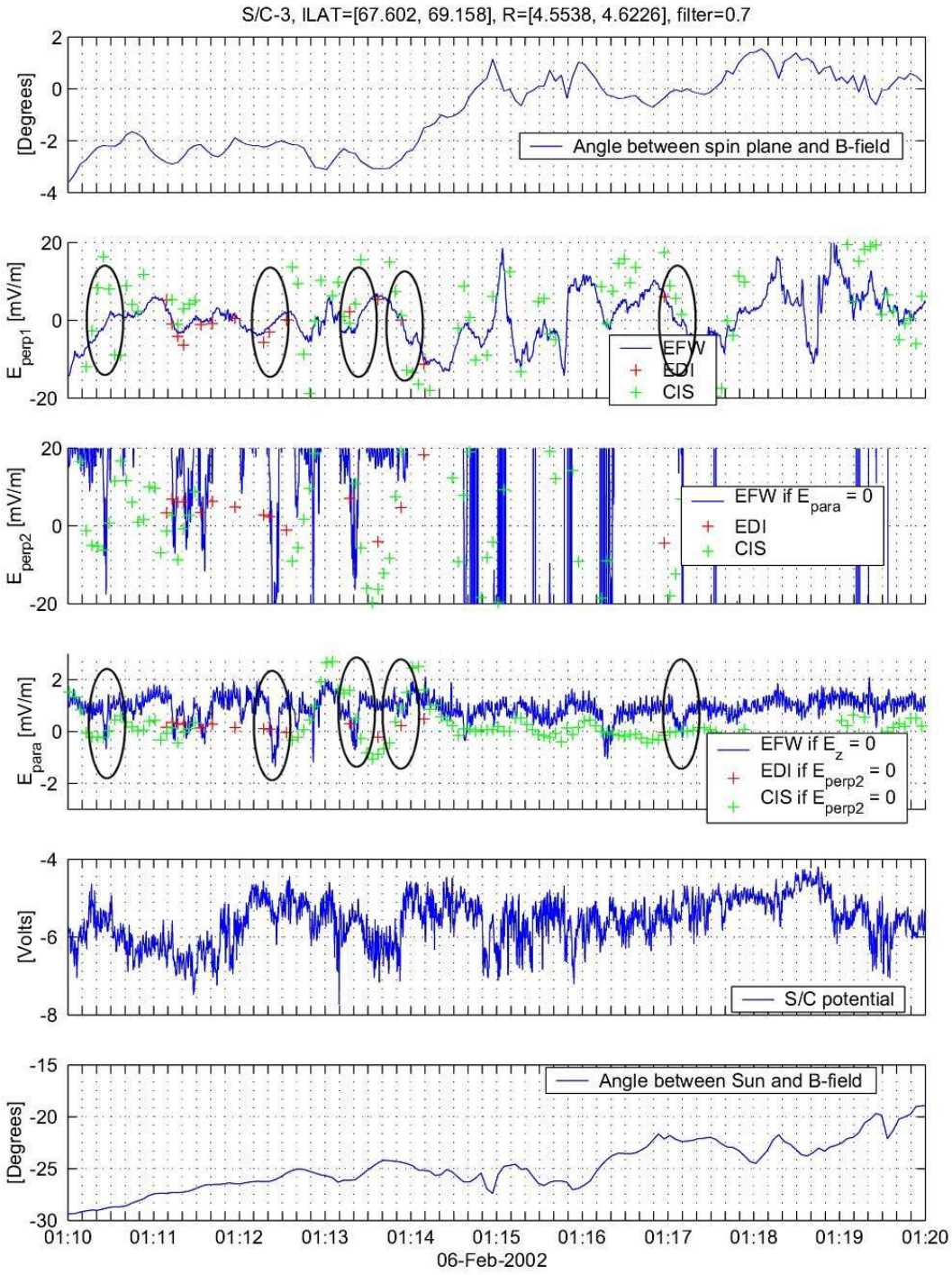
S/C-3, ILAT=[67.602, 69.158], R=[4.5538, 4.6226], filter=0.7
[Degrees]
Angle between spin plane and B-field
E_perp1 [mV/m]
EFW
EDI
CIS
E_perp2 [mV/m]
EFW if E_para = 0
EDI
CIS
E_para [mV/m]
EFW if E_z = 0
EDI if E_perp2 = 0
CIS if E_perp2 = 0
[Volts]
S/C potential
[Degrees]
Angle between Sun and B-field
01:10
01:11
01:12
01:13
01:14
01:15
01:16
01:17
01:18
01:19
01:20
06-Feb-2002

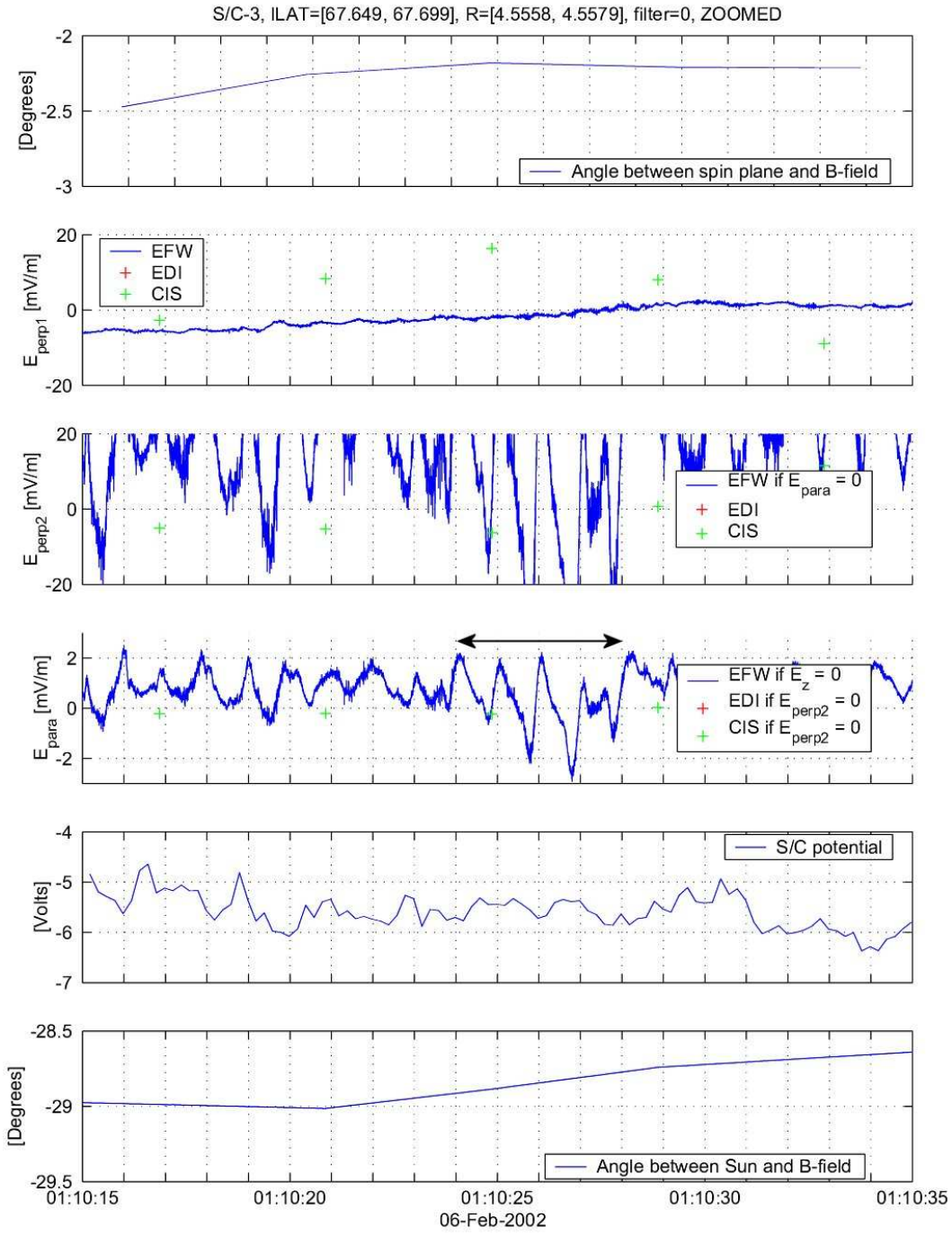
S/C-3, ILAT=[67.649, 67.699], R=[4.5558, 4.5579], filter=0, ZOOMED
[Degrees]
Angle between spin plane and B-field
E perp1 [mV/m]
EFW
EDI
CIS
E perp2 [mV/m]
EFW if E para = 0
EDI
CIS
E para [mV/m]
EFW if E z = 0
EDI if E perp2 = 0
CIS if E perp2 = 0
[Volts]
S/C potential
[Degrees]
Angle between Sun and B-field
01:10:15
01:10:20
01:10:25
01:10:30
01:10:35
06-Feb-2002

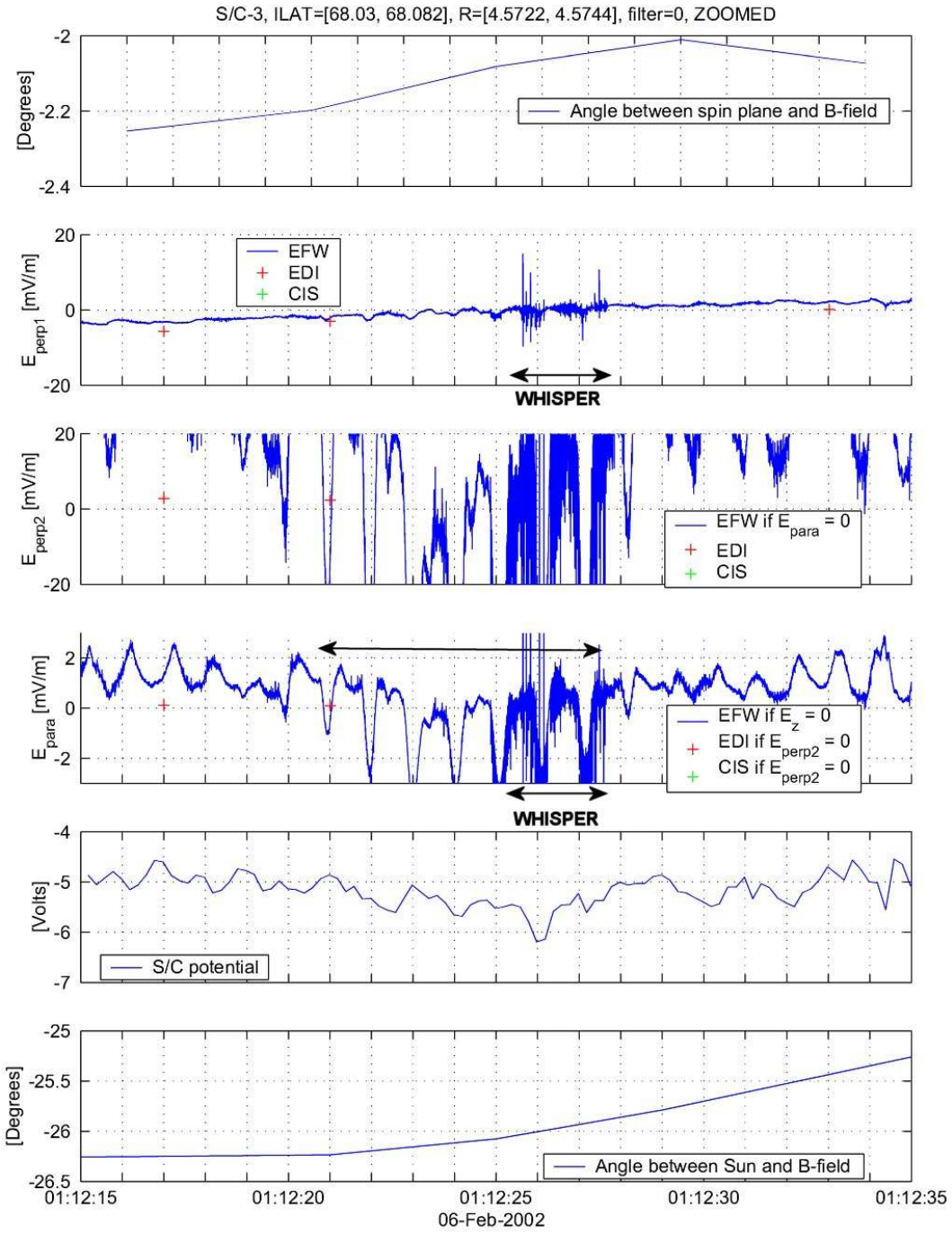
S/C-3, ILAT=[68.03, 68.082], R=[4.5722, 4.5744], filter=0, ZOOMED
[Degrees]
Angle between spin plane and B-field
E_perp1 [mV/m]
EFW
EDI
CIS
WHISPER
E_perp2 [mV/m]
EFW if E_para = 0
EDI
CIS
E_para [mV/m]
EFW if E_z = 0
EDI if E_perp2 = 0
CIS if E_perp2 = 0
WHISPER
[Volts]
S/C potential
[Degrees]
Angle between Sun and B-field
01:12:15
01:12:20
01:12:25
01:12:30
01:12:35
06-Feb-2002

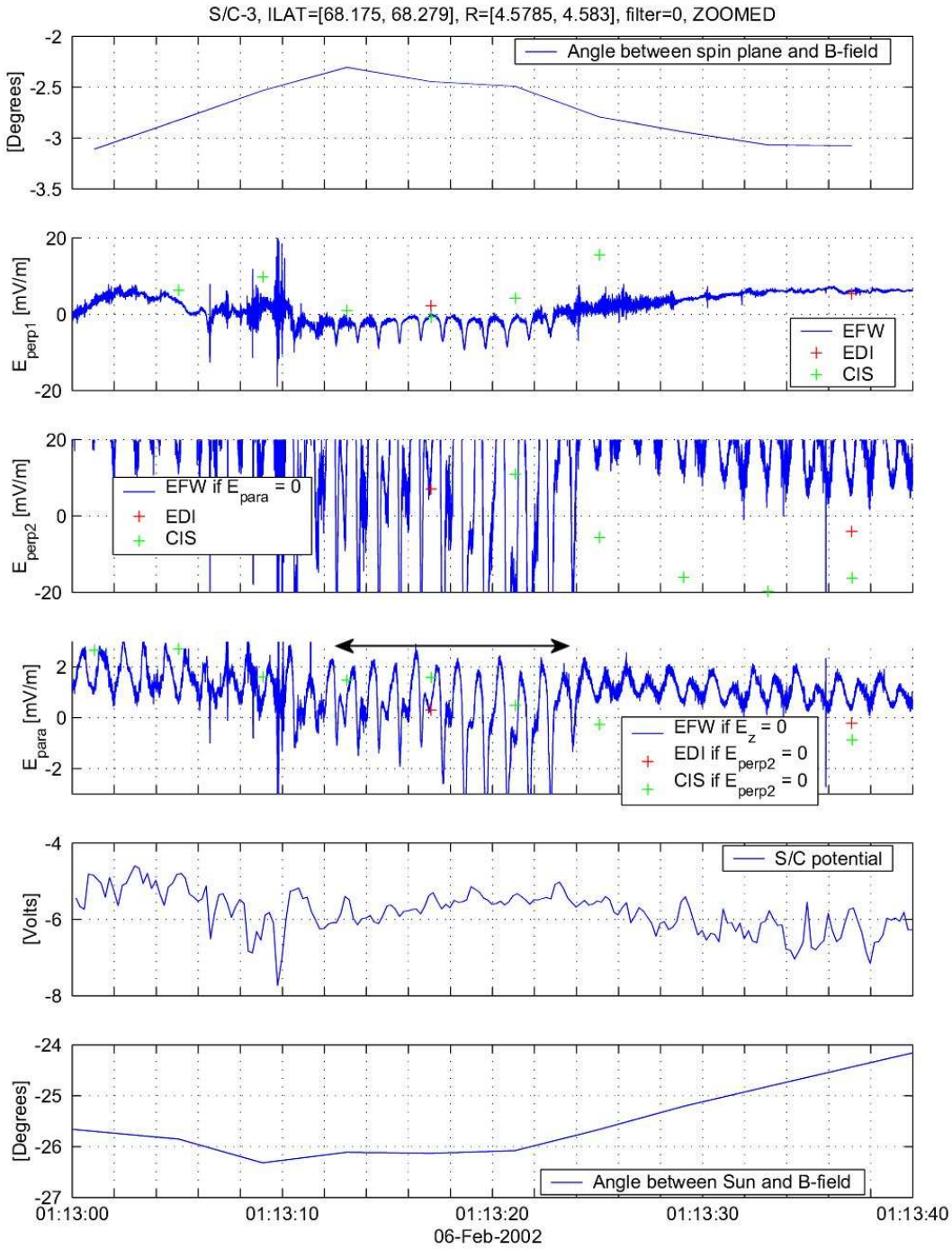
S/C-3, ILAT=[68.175, 68.279], R=[4.5785, 4.583], filter=0, ZOOMED
Angle between spin plane and B-field
[Degrees]
-2
-2.5
-3
-3.5
E_perp1 [mV/m]
20
0
-20
EFW
EDI
CIS
E_perp2 [mV/m]
EFW if E_para = 0
EDI
CIS
E_para [mV/m]
2
0
-2
EFW if E_z = 0
EDI if E_perp2 = 0
CIS if E_perp2 = 0
[Volts]
-4
-6
-8
S/C potential
[Degrees]
-24
-25
-26
-27
Angle between Sun and B-field
01:13:00
01:13:10
01:13:20
01:13:30
01:13:40
06-Feb-2002

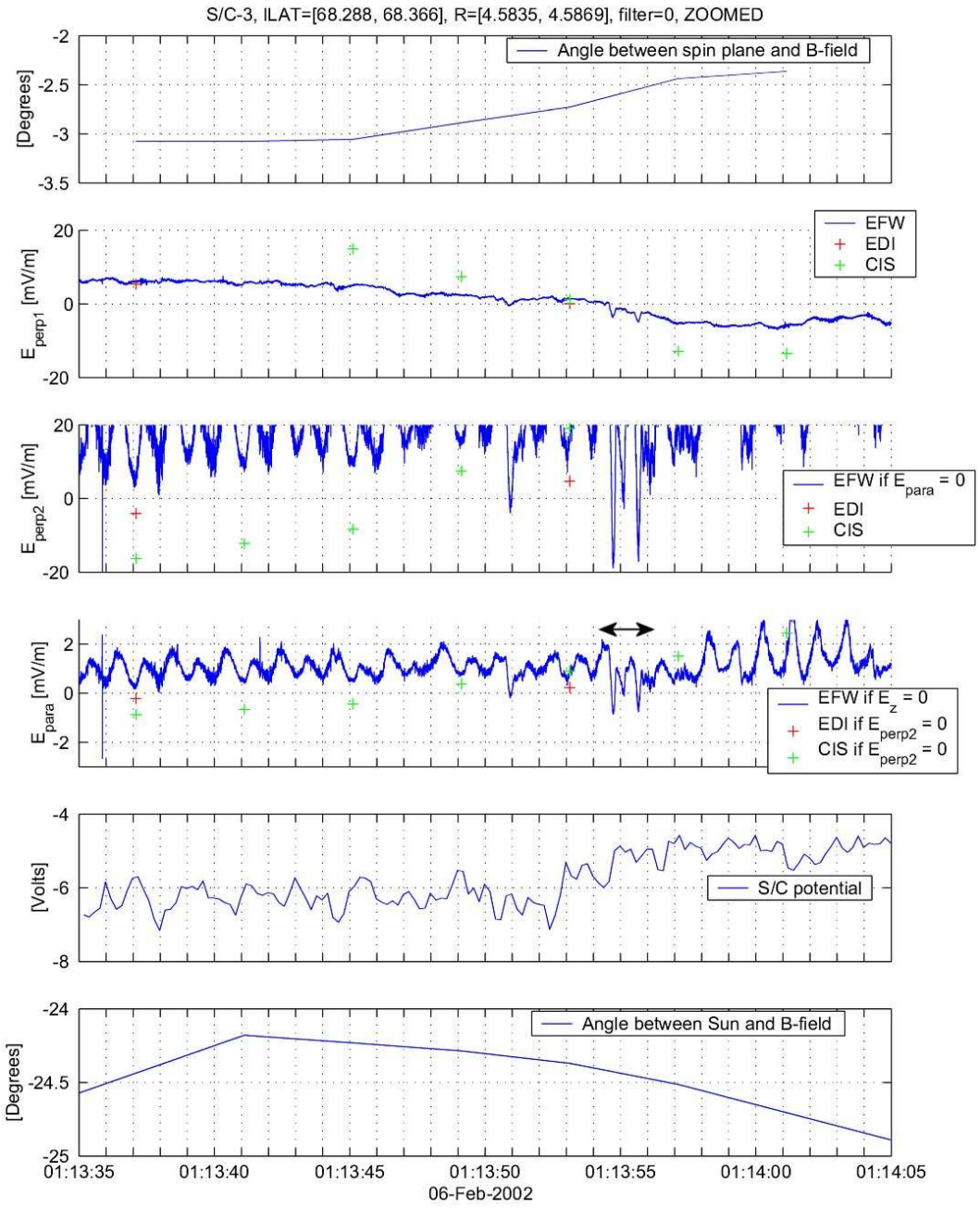
S/C-3, ILAT=[68.288, 68.366], R=[4.5835, 4.5869], filter=0, ZOOMED
Angle between spin plane and B-field
[Degrees]
EFW
EDI
CIS
E perp1 [mV/m]
EFW if E para = 0
EDI
CIS
E perp2 [mV/m]
EFW if E z = 0
EDI if E perp2 = 0
CIS if E perp2 = 0
E para [mV/m]
S/C potential
[Volts]
Angle between Sun and B-field
[Degrees]
01:13:35
01:13:40
01:13:45
01:13:50
01:13:55
01:14:00
01:14:05
06-Feb-2002

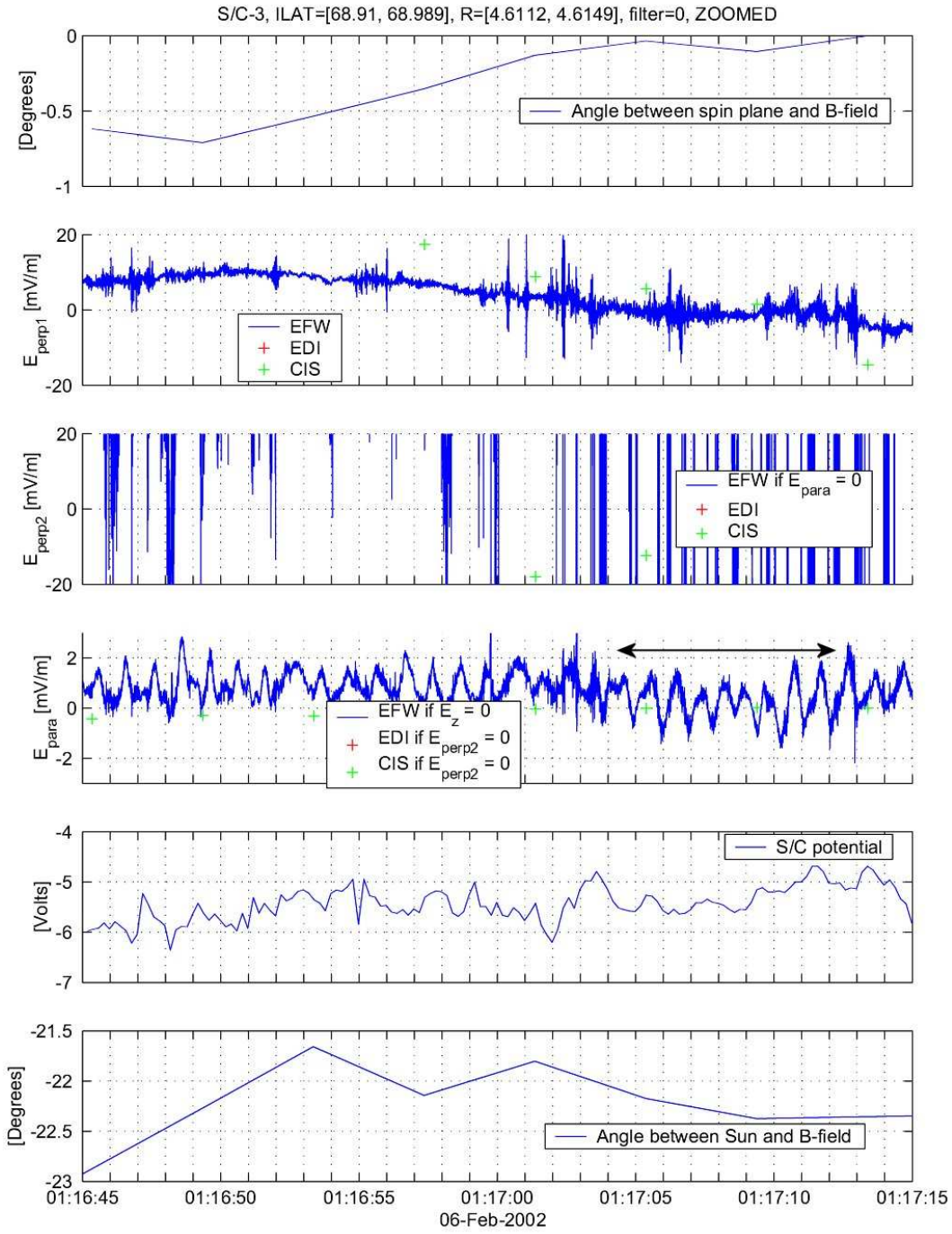
S/C-3, ILAT=[68.91, 68.989], R=[4.6112, 4.6149], filter=0, ZOOMED
[Degrees]
Angle between spin plane and B-field
E perp1 [mV/m]
EFW
EDI
CIS
E perp2 [mV/m]
EFW if E para = 0
EDI
CIS
E para [mV/m]
EFW if E z = 0
EDI if E perp2 = 0
CIS if E perp2 = 0
[Volts]
S/C potential
[Degrees]
Angle between Sun and B-field
01:16:45
01:16:50
01:16:55
01:17:00
01:17:05
01:17:10
01:17:15
06-Feb-2002

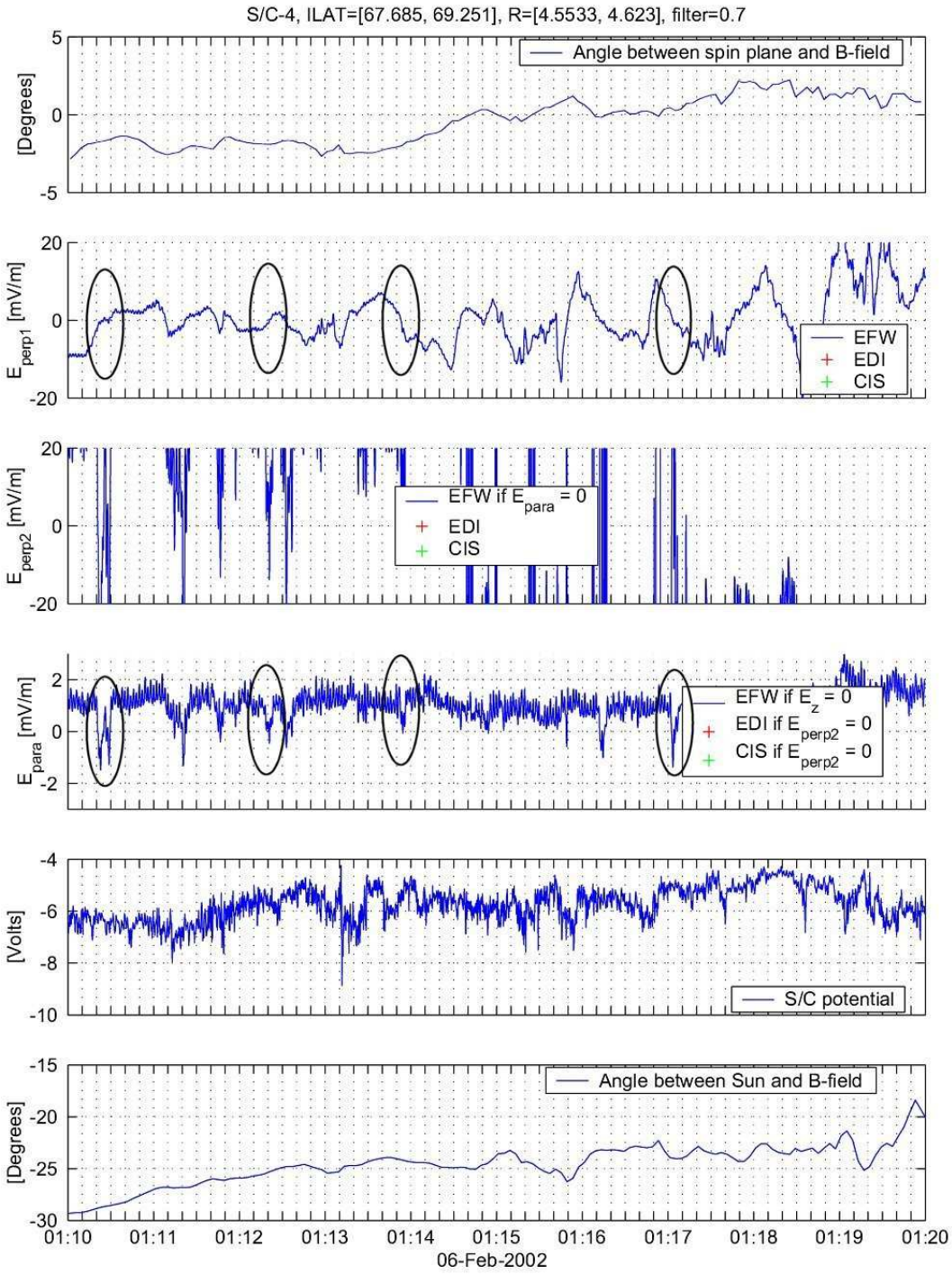
S/C-4, ILAT=[67.685, 69.251], R=[4.5533, 4.623], filter=0.7
Angle between spin plane and B-field
[Degrees]
5
0
-5
E perp1 [mV/m]
20
0
-20
EFW
EDI
CIS
E perp2 [mV/m]
EFW if E para = 0
EDI
CIS
E para [mV/m]
2
0
-2
EFW if E z = 0
EDI if E perp2 = 0
CIS if E perp2 = 0
[Volts]
-4
-6
-8
-10
S/C potential
[Degrees]
-15
-20
-25
-30
Angle between Sun and B-field
01:10
01:11
01:12
01:13
01:14
01:15
01:16
01:17
01:18
01:19
01:20
06-Feb-2002

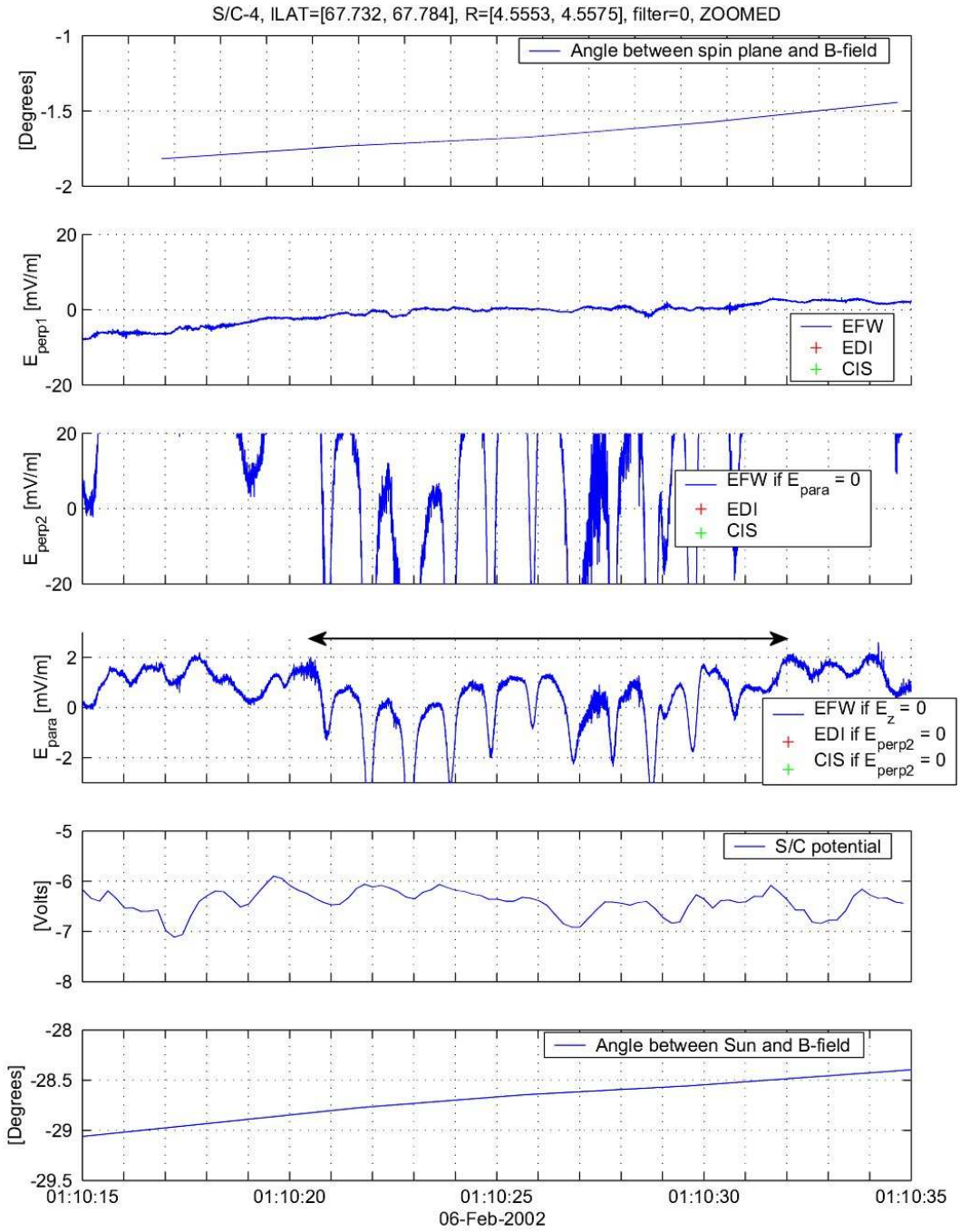
S/C-4, ILAT=[67.732, 67.784], R=[4.5553, 4.5575], filter=0, ZOOMED
Angle between spin plane and B-field
[Degrees]
-1
-1.5
-2
E_perp1 [mV/m]
20
0
-20
EFW
EDI
CIS
E_perp2 [mV/m]
EFW if E_para = 0
EDI
CIS
E_para [mV/m]
2
0
-2
EFW if E_z = 0
EDI if E_perp2 = 0
CIS if E_perp2 = 0
[Volts]
-5
-6
-7
-8
S/C potential
[Degrees]
-28
-28.5
-29
-29.5
Angle between Sun and B-field
01:10:15
01:10:20
01:10:25
01:10:30
01:10:35
06-Feb-2002

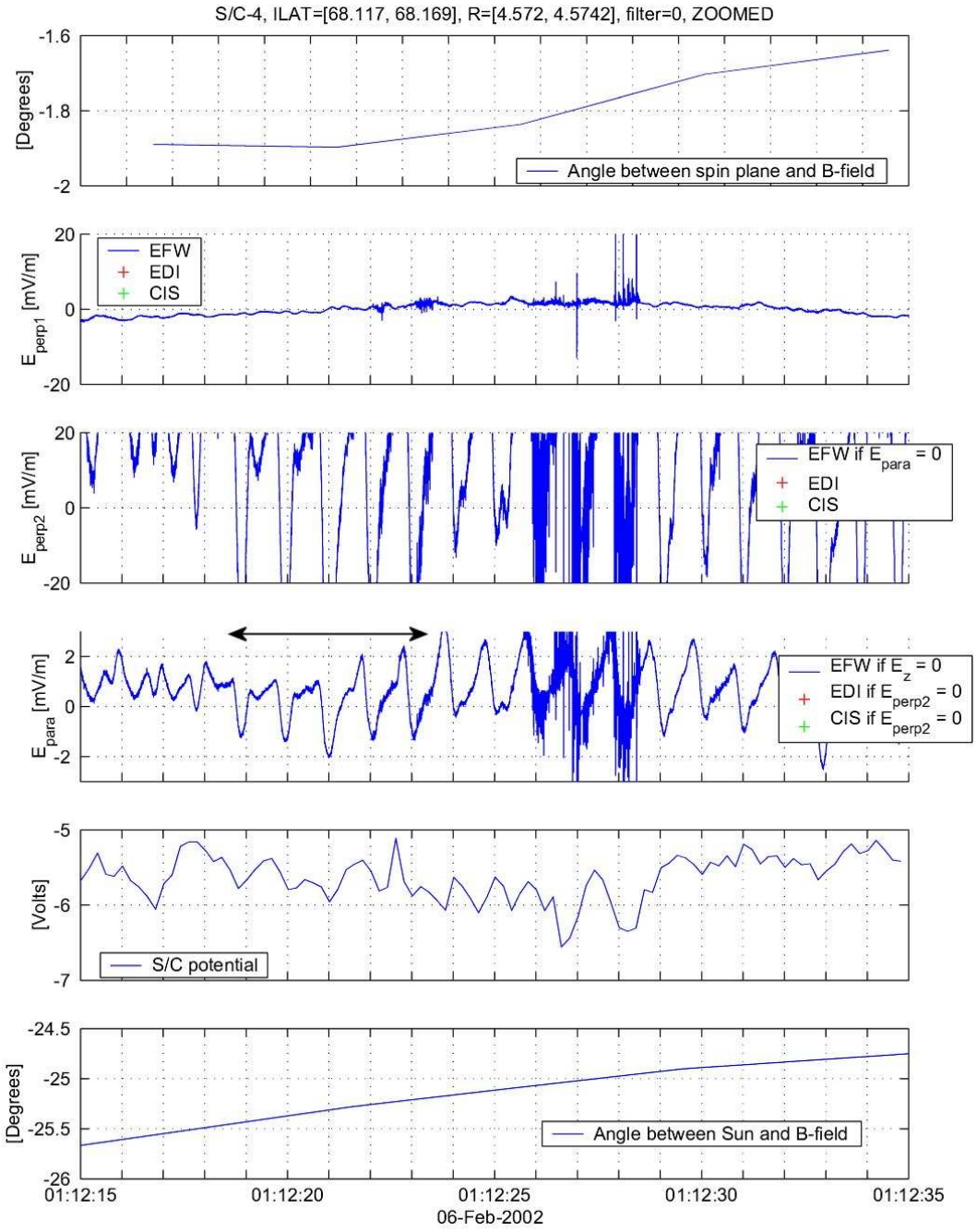
S/C-4, ILAT=[68.117, 68.169], R=[4.572, 4.5742], filter=0, ZOOMED
[Degrees]
-1.6
-1.8
-2
Angle between spin plane and B-field
E perp1 [mV/m]
20
0
-20
EFW
EDI
CIS
E perp2 [mV/m]
EFW if E para = 0
EDI
CIS
E para [mV/m]
2
0
-2
EFW if E z = 0
EDI if E perp2 = 0
CIS if E perp2 = 0
[Volts]
-5
-6
-7
S/C potential
[Degrees]
-24.5
-25
-25.5
-26
Angle between Sun and B-field
01:12:15
01:12:20
01:12:25
01:12:30
01:12:35
06-Feb-2002

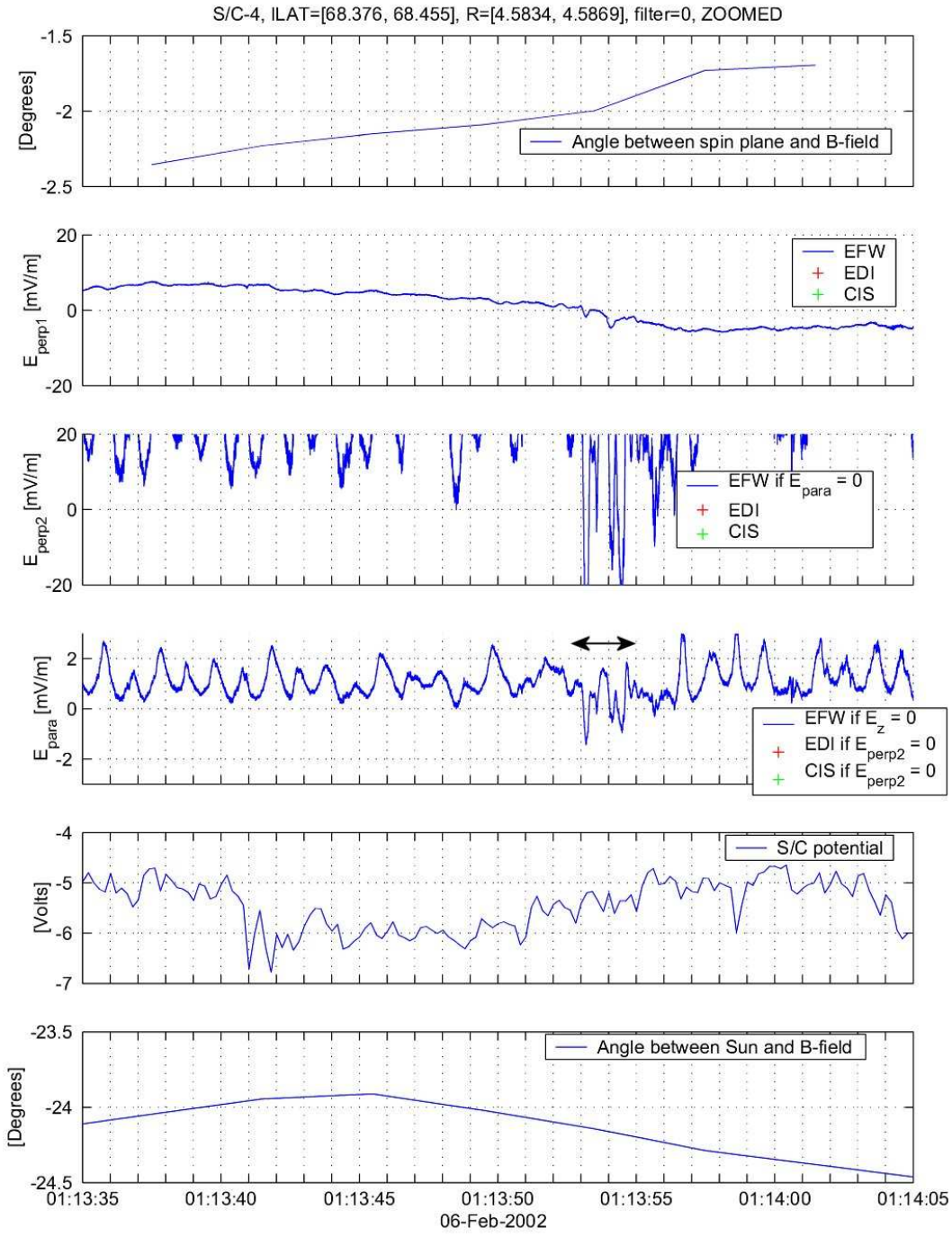
S/C-4, ILAT=[68.376, 68.455], R=[4.5834, 4.5869], filter=0, ZOOMED
[Degrees]
Angle between spin plane and B-field
E_perp1 [mV/m]
EFW
EDI
CIS
E_perp2 [mV/m]
EFW if E_para = 0
EDI
CIS
E_para [mV/m]
EFW if E_z = 0
EDI if E_perp2 = 0
CIS if E_perp2 = 0
[Volts]
S/C potential
[Degrees]
Angle between Sun and B-field
01:13:35
01:13:40
01:13:45
01:13:50
01:13:55
01:14:00
01:14:05
06-Feb-2002

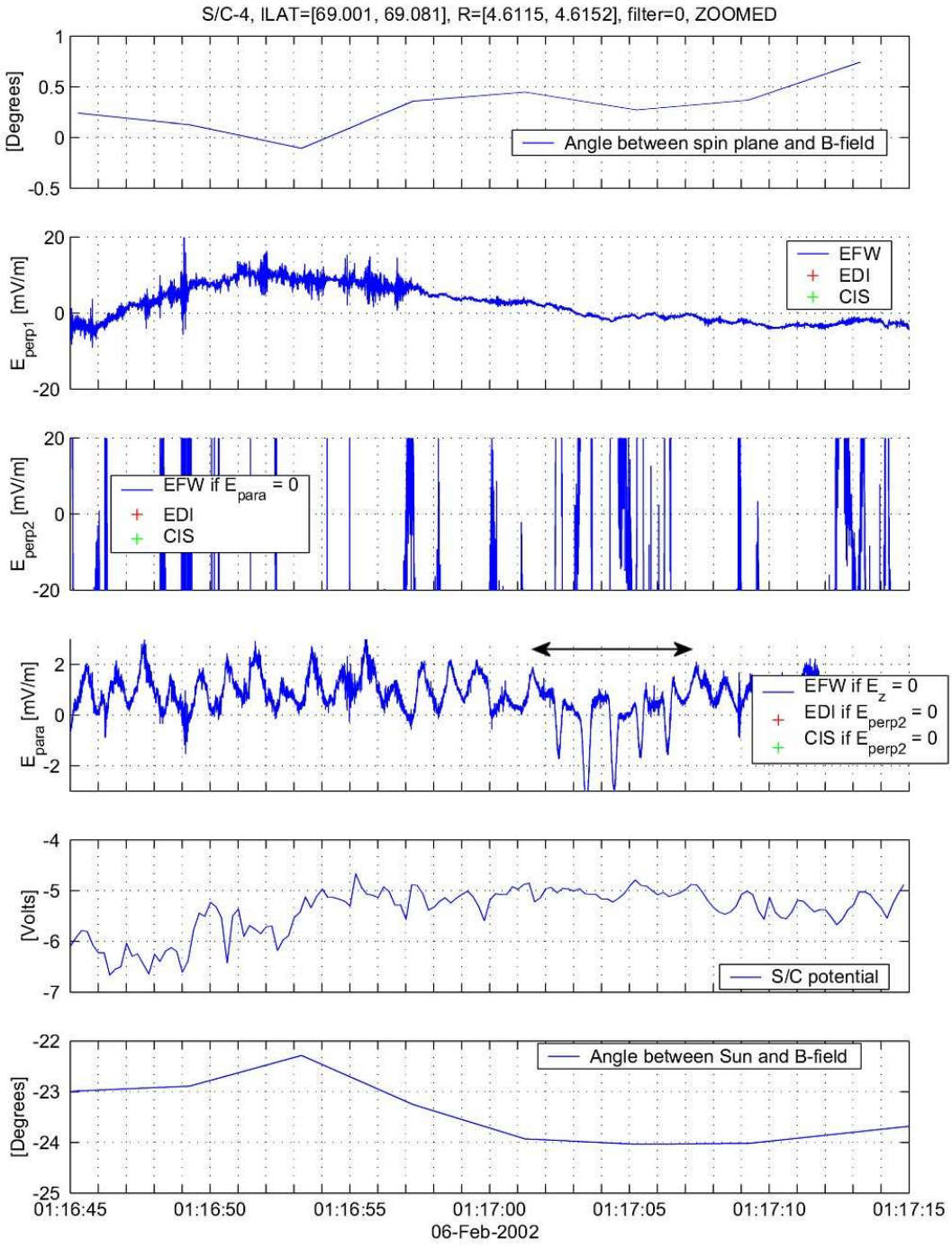
S/C-4, ILAT=[69.001, 69.081], R=[4.6115, 4.6152], filter=0, ZOOMED
[Degrees]
Angle between spin plane and B-field
E perp1 [mV/m]
EFW
EDI
CIS
E perp2 [mV/m]
EFW if E para = 0
EDI
CIS
E para [mV/m]
EFW if E z = 0
EDI if E perp2 = 0
CIS if E perp2 = 0
[Volts]
S/C potential
[Degrees]
Angle between Sun and B-field
01:16:45
01:16:50
01:16:55
01:17:00
01:17:05
01:17:10
01:17:15
06-Feb-2002

B.1.3 2002-02-17

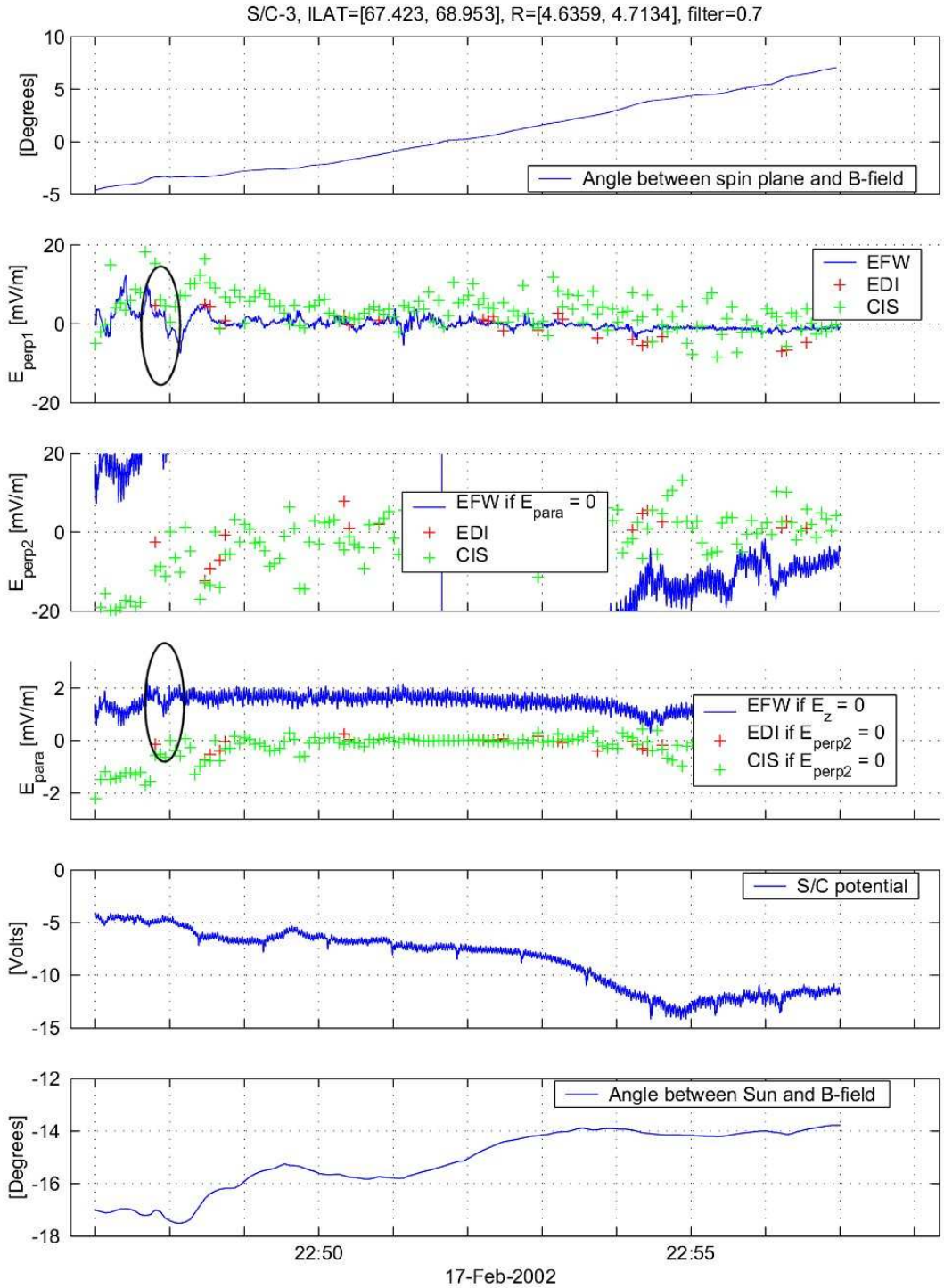

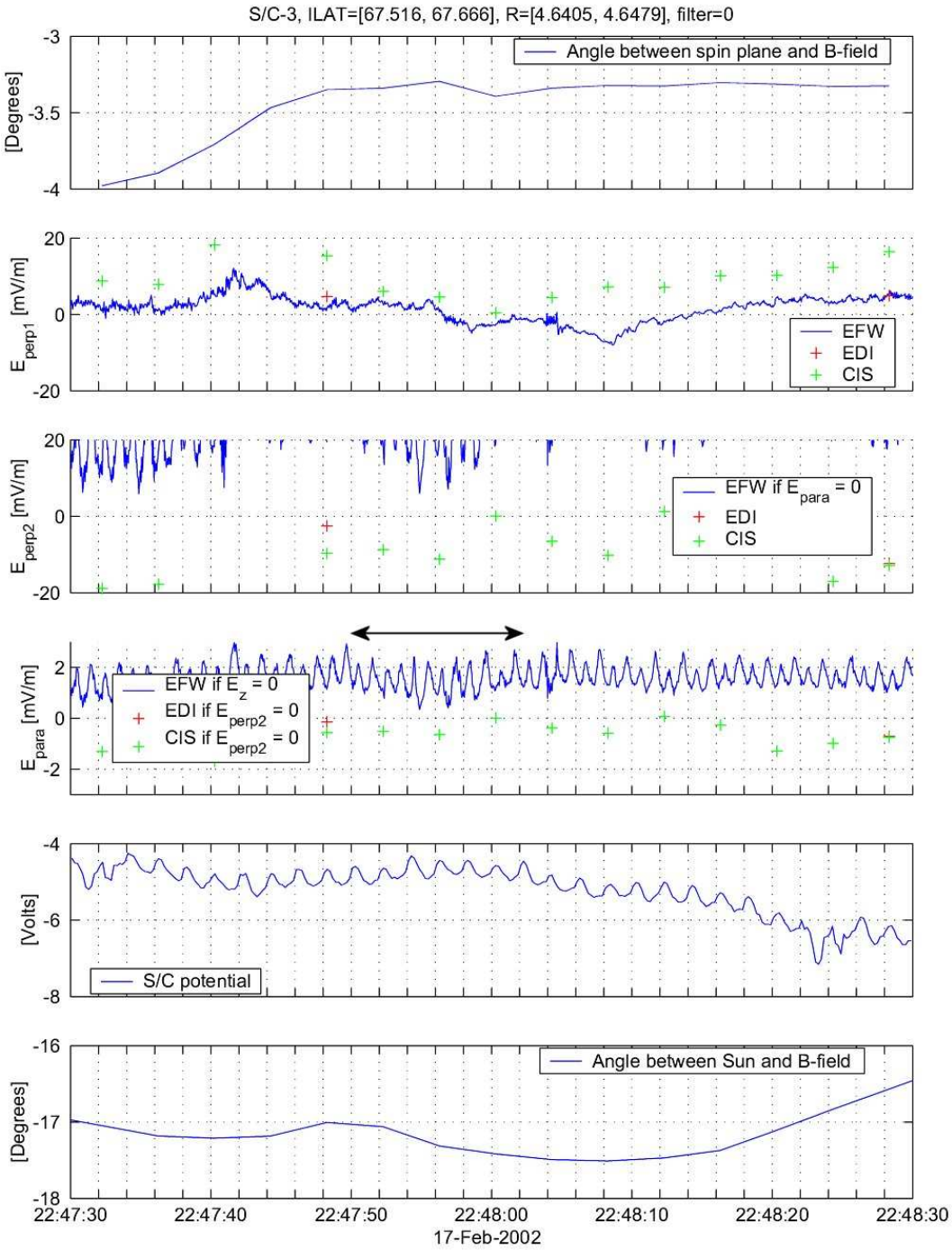
S/C-3, ILAT=[67.516, 67.666], R=[4.6405, 4.6479], filter=0
Angle between spin plane and B-field
[Degrees]
-3
-3.5
-4
E_perp1 [mV/m]
20
0
-20
EFW
EDI
CIS
E_perp2 [mV/m]
EFW if E_para = 0
EDI
CIS
E_para [mV/m]
2
0
-2
EFW if E_z = 0
EDI if E_perp2 = 0
CIS if E_perp2 = 0
[Volts]
-4
-6
-8
S/C potential
[Degrees]
-16
-17
-18
Angle between Sun and B-field
22:47:30
22:47:40
22:47:50
22:48:00
22:48:10
22:48:20
22:48:30
17-Feb-2002

B.1.4 2002-03-06

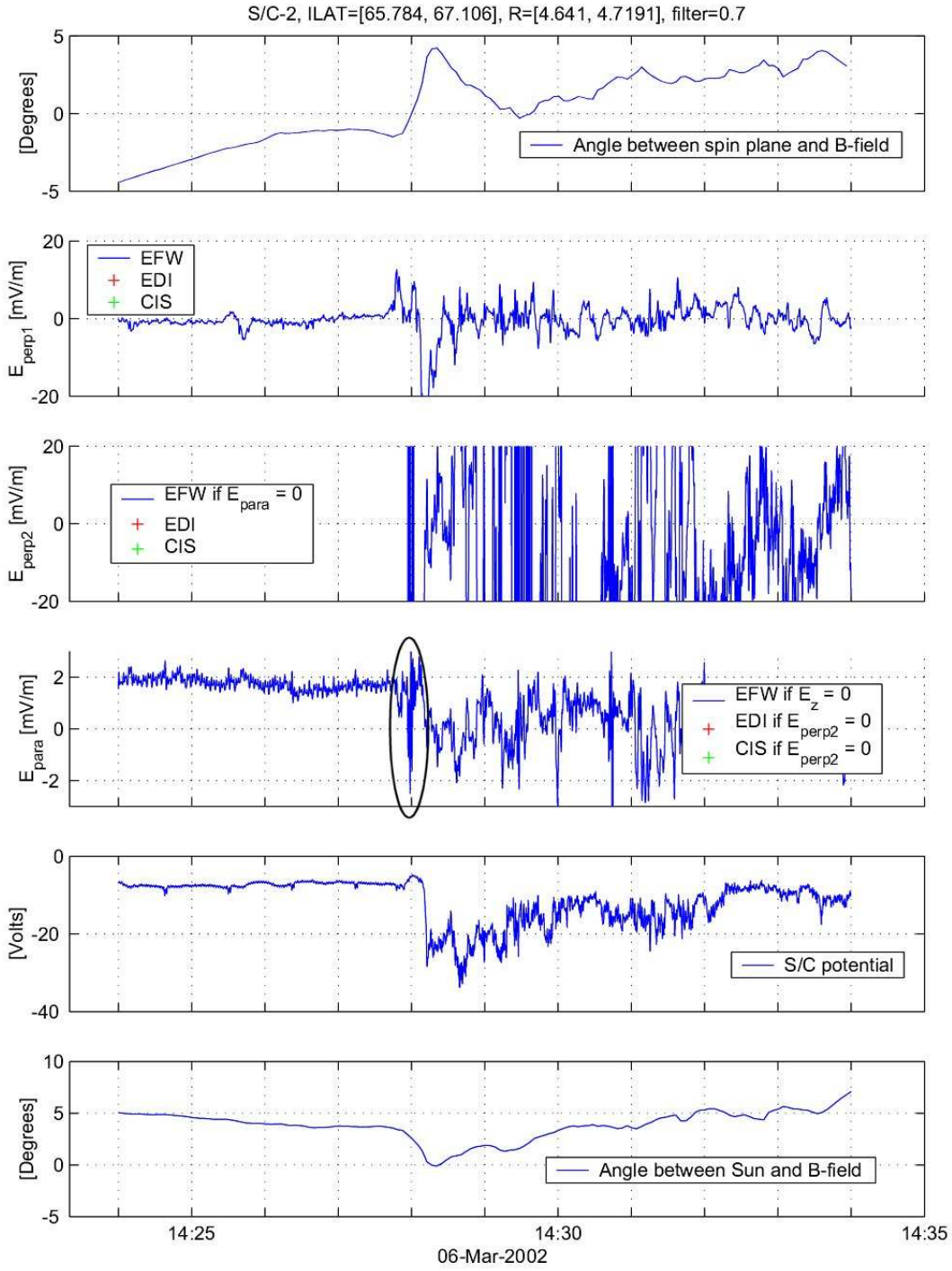

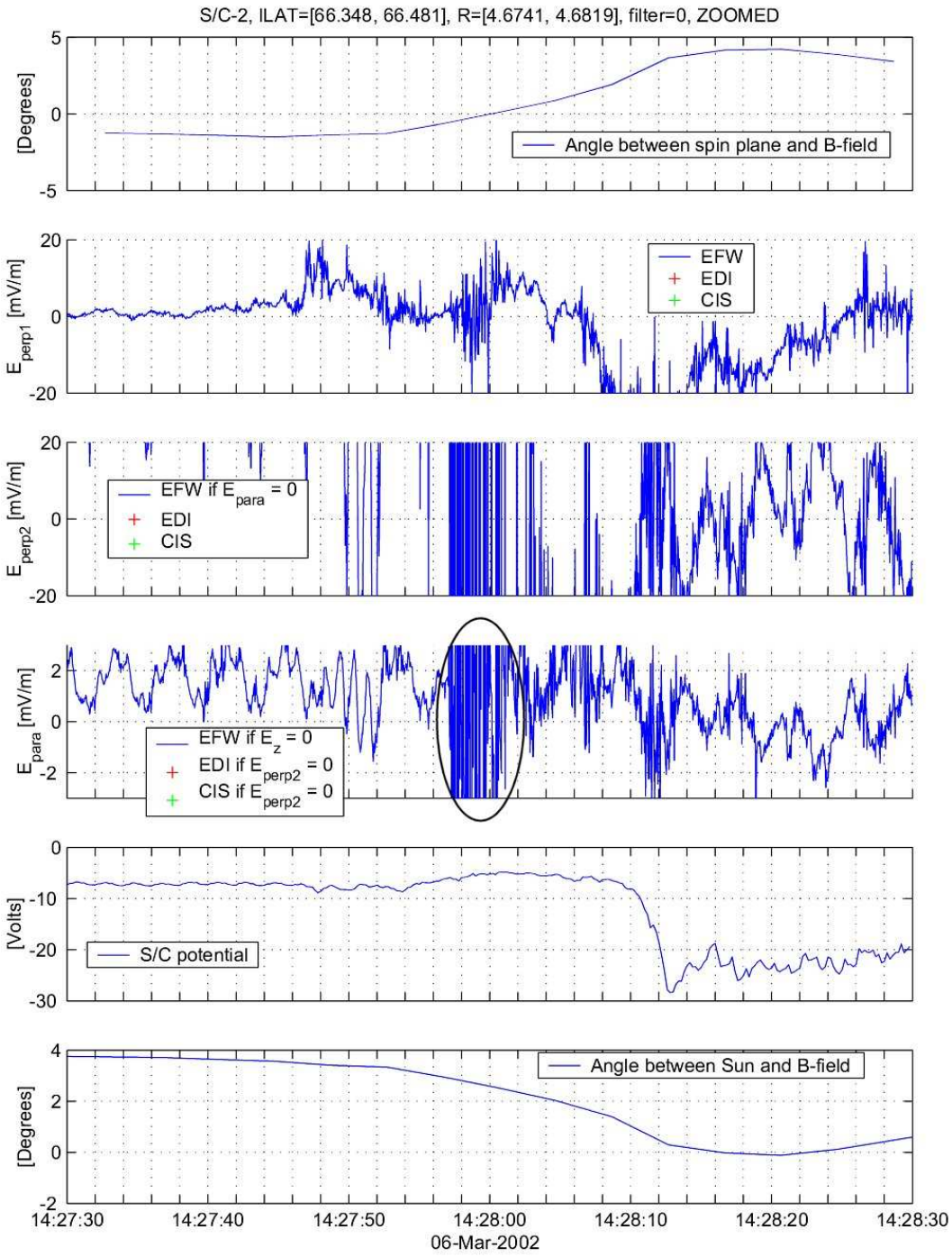
S/C-2, ILAT=[66.348, 66.481], R=[4.6741, 4.6819], filter=0, ZOOMED
[Degrees]
Angle between spin plane and B-field
E perp1 [mV/m]
EFW
EDI
CIS
E perp2 [mV/m]
EFW if E para = 0
EDI
CIS
E para [mV/m]
EFW if E z = 0
EDI if E perp2 = 0
CIS if E perp2 = 0
[Volts]
S/C potential
[Degrees]
Angle between Sun and B-field
14:27:30
14:27:40
14:27:50
14:28:00
14:28:10
14:28:20
14:28:30
06-Mar-2002

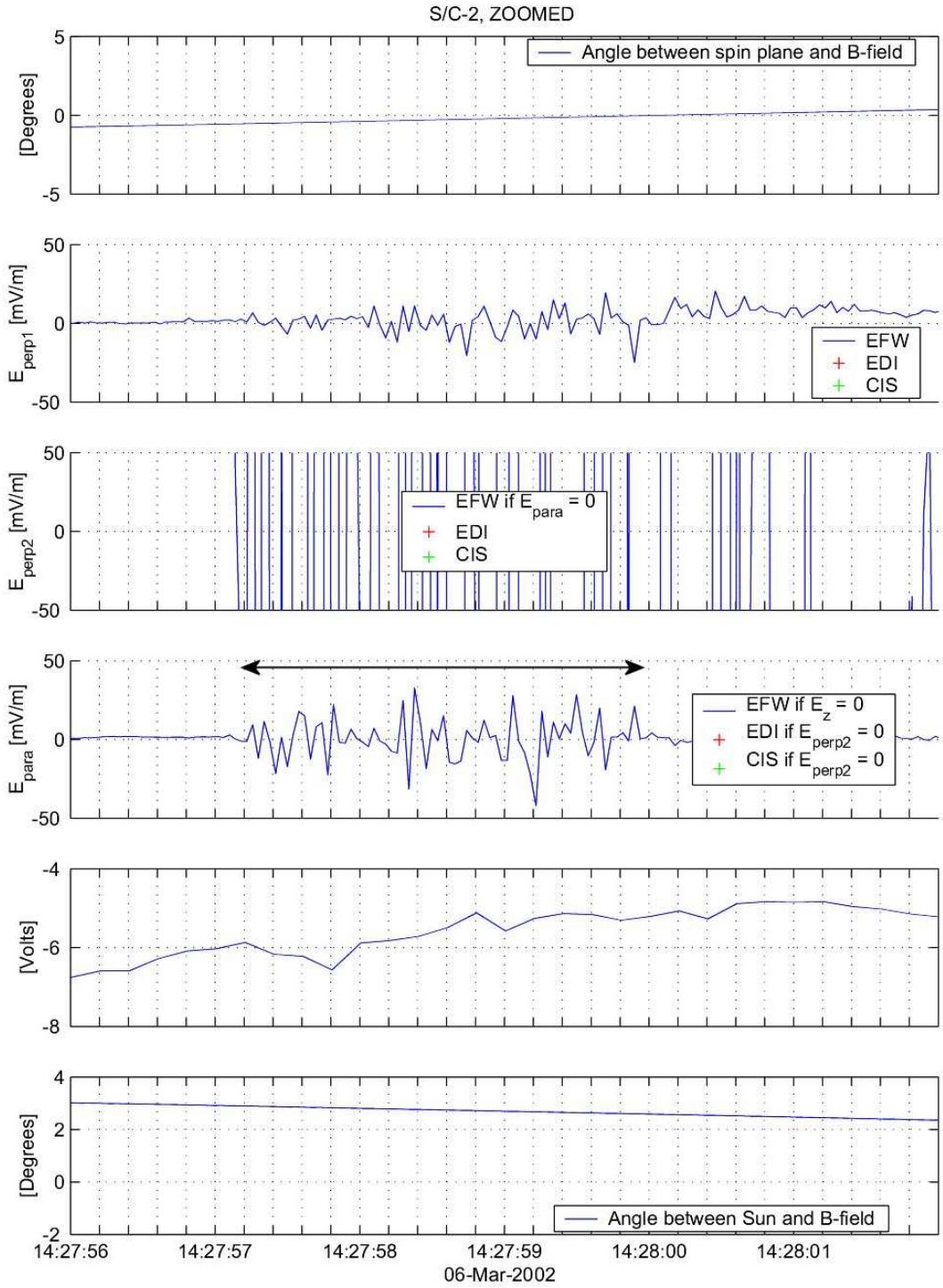
S/C-2, ZOOMED
Angle between spin plane and B-field
[Degrees]
5
0
-5
E_{perp1} [mV/m]
50
0
-50
EFW
EDI
CIS
E_{perp2} [mV/m]
EFW if E_{para} = 0
EDI
CIS
E_{para} [mV/m]
EFW if E_z = 0
EDI if E_{perp2} = 0
CIS if E_{perp2} = 0
[Volts]
-4
-6
-8
[Degrees]
4
2
0
-2
Angle between Sun and B-field
14:27:56
14:27:57
14:27:58
14:27:59
14:28:00
14:28:01
06-Mar-2002

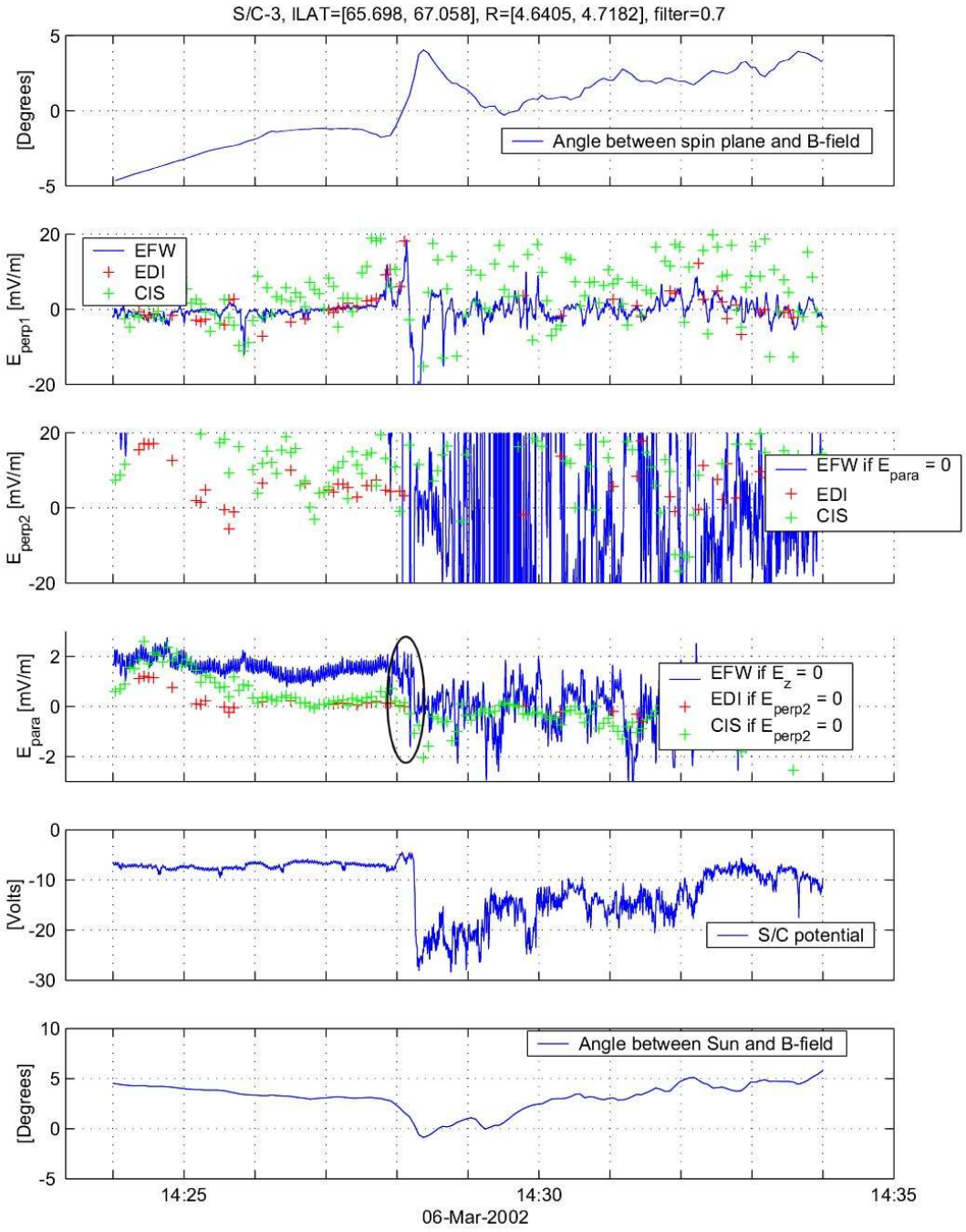
S/C-3, ILAT=[65.698, 67.058], R=[4.6405, 4.7182], filter=0.7
[Degrees]
Angle between spin plane and B-field
E perp1 [mV/m]
EFW
EDI
CIS
E perp2 [mV/m]
EFW if E para = 0
EDI
CIS
E para [mV/m]
EFW if E z = 0
EDI if E perp2 = 0
CIS if E perp2 = 0
[Volts]
S/C potential
[Degrees]
Angle between Sun and B-field
14:25
14:30
14:35
06-Mar-2002

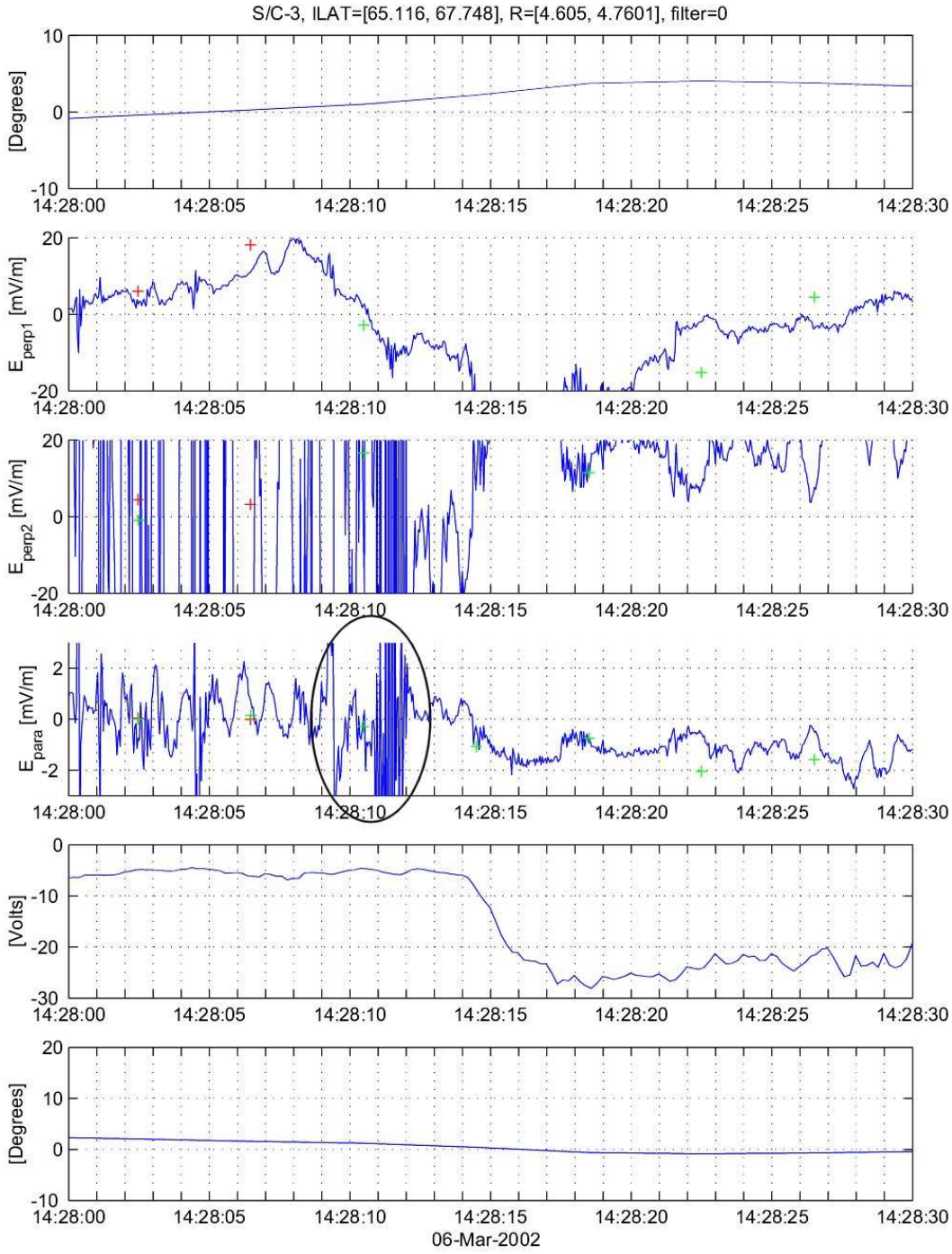
S/C-3, ILAT=[65.116, 67.748], R=[4.605, 4.7601], filter=0
[Degrees]
E perp1 [mV/m]
E perp2 [mV/m]
E para [mV/m]
[Volts]
[Degrees]
14:28:00
14:28:05
14:28:10
14:28:15
14:28:20
14:28:25
14:28:30
06-Mar-2002

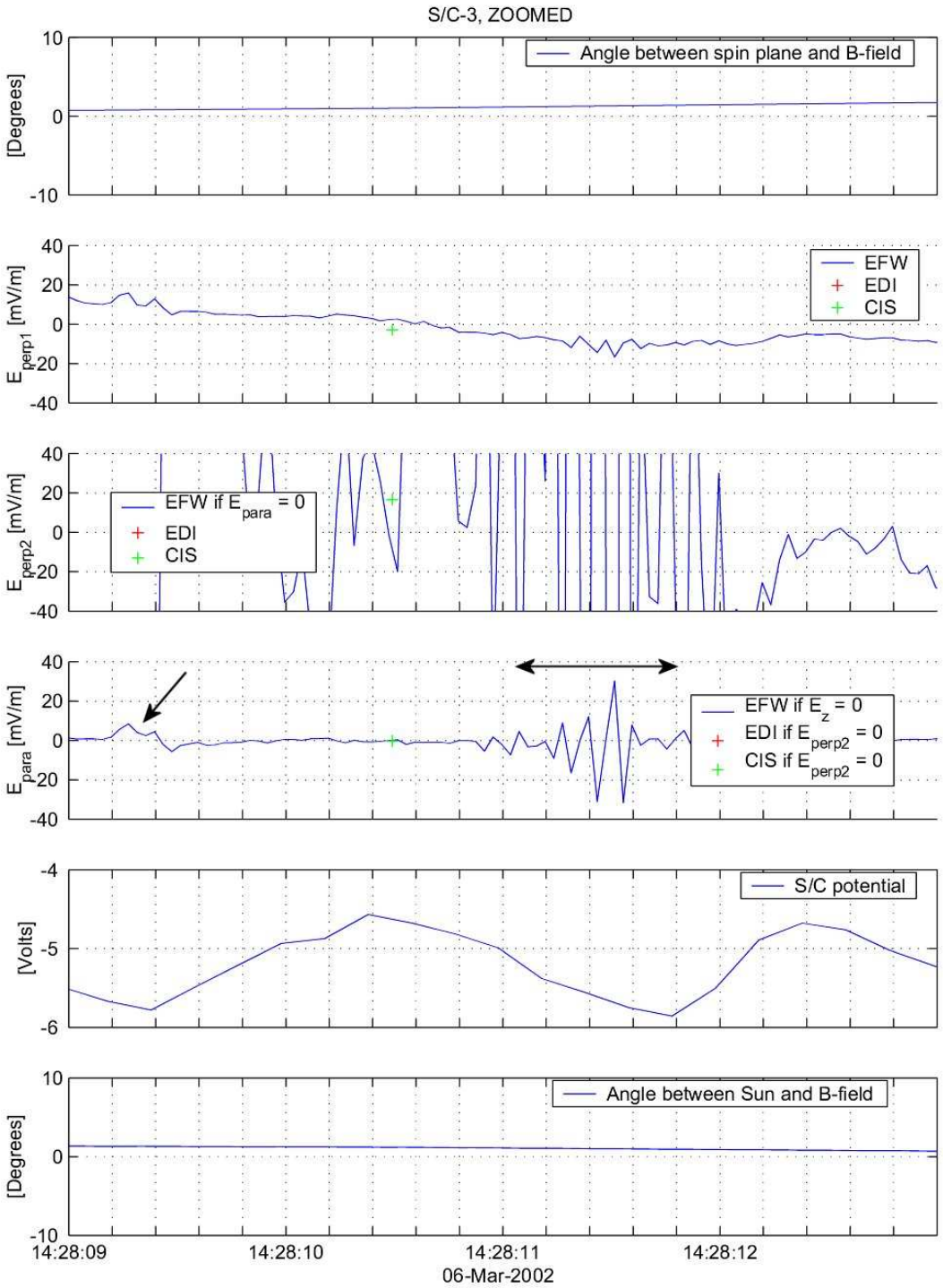
S/C-3, ZOOMED
Angle between spin plane and B-field
[Degrees]
EFW
EDI
CIS
E perp1 [mV/m]
EFW if E para = 0
EDI
CIS
E perp2 [mV/m]
EFW if E z = 0
EDI if E perp2 = 0
CIS if E perp2 = 0
E para [mV/m]
S/C potential
[Volts]
Angle between Sun and B-field
[Degrees]
14:28:09
14:28:10
14:28:11
14:28:12
06-Mar-2002

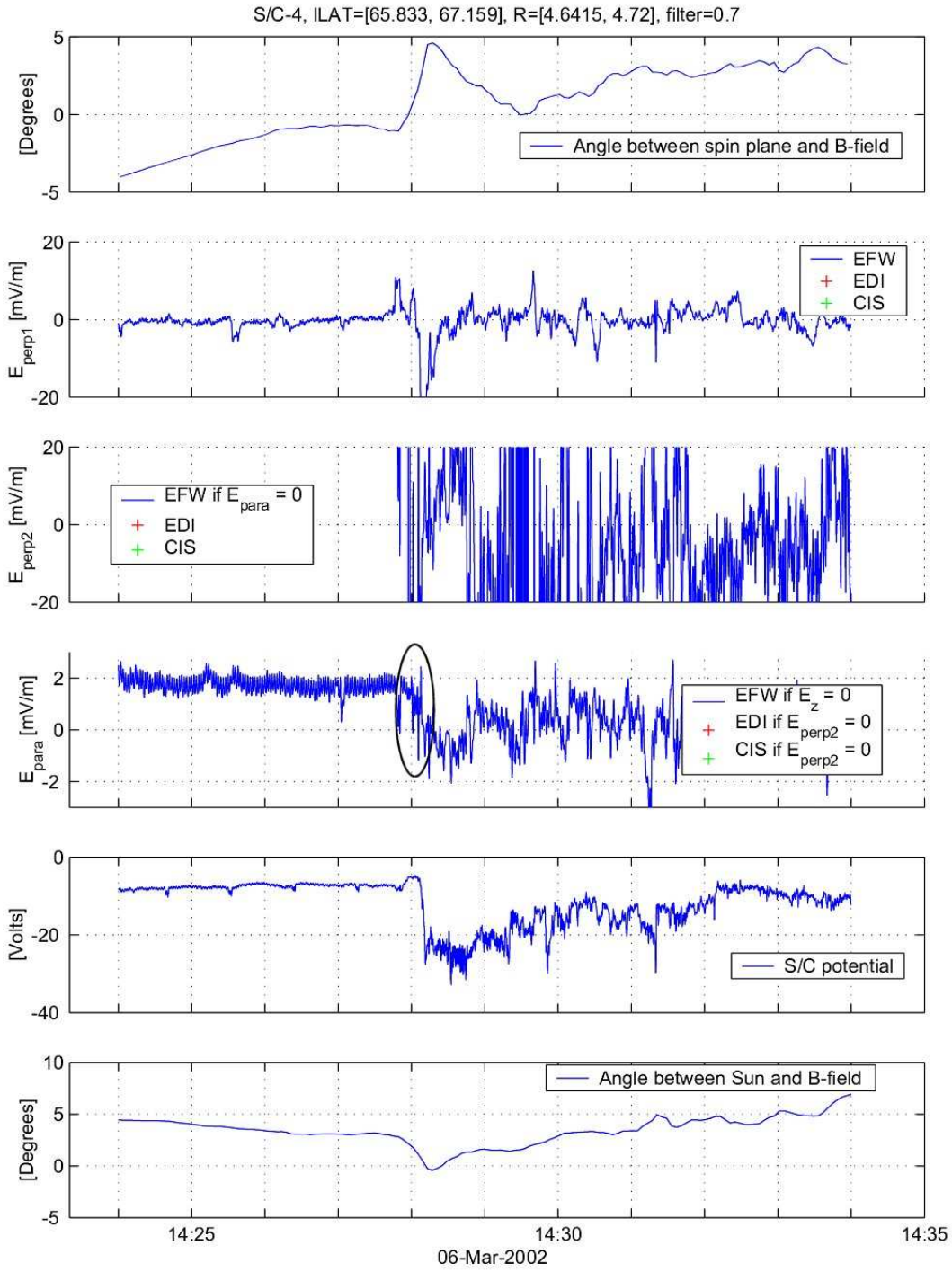
S/C-4, ILAT=[65.833, 67.159], R=[4.6415, 4.72], filter=0.7
[Degrees]
Angle between spin plane and B-field
E_perp1 [mV/m]
EFW
EDI
CIS
E_perp2 [mV/m]
EFW if E_para = 0
EDI
CIS
E_para [mV/m]
EFW if E_z = 0
EDI if E_perp2 = 0
CIS if E_perp2 = 0
[Volts]
S/C potential
[Degrees]
Angle between Sun and B-field
14:25
14:30
14:35
06-Mar-2002

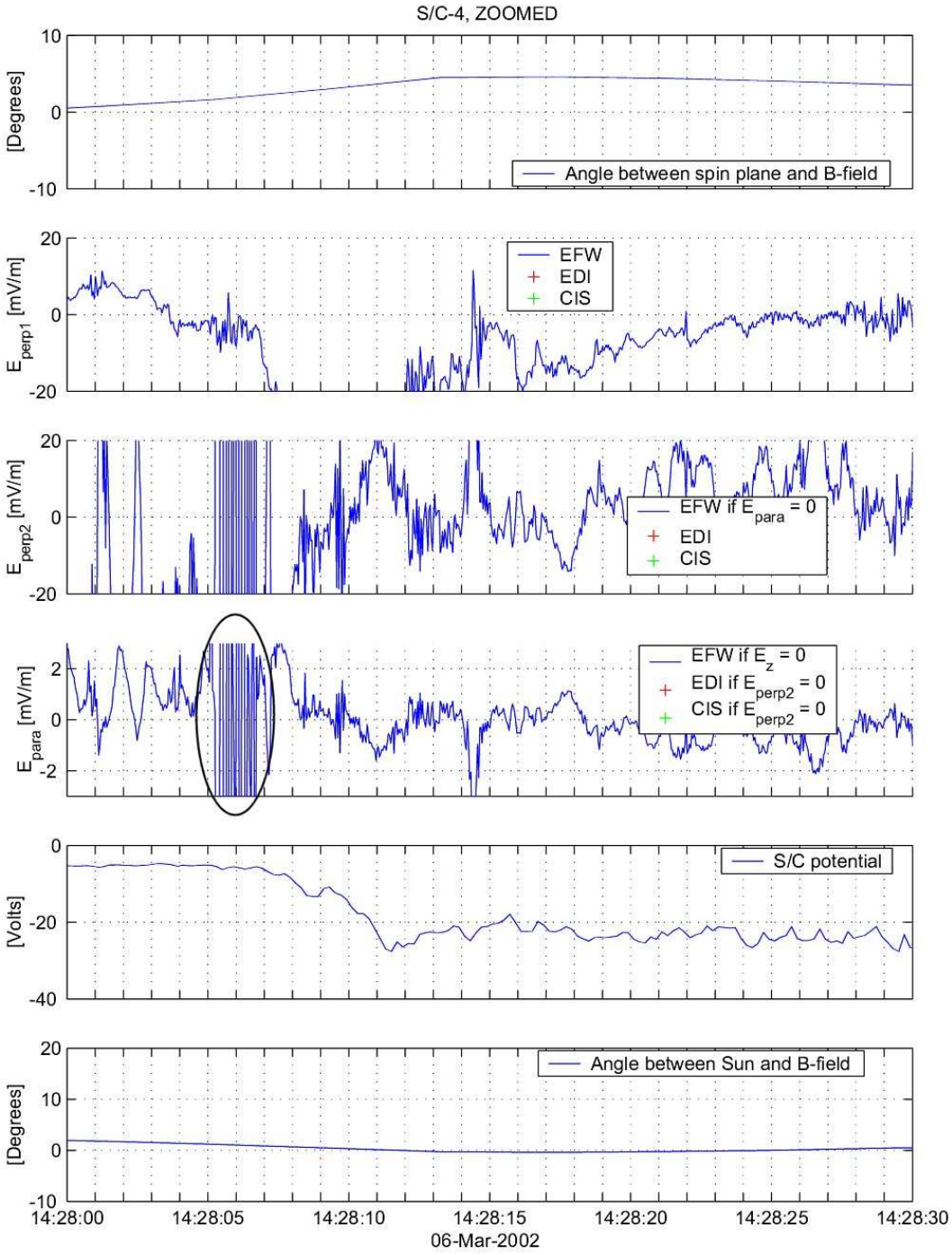
S/C-4, ZOOMED
[Degrees]
Angle between spin plane and B-field
E perp1 [mV/m]
EFW
EDI
CIS
E perp2 [mV/m]
EFW if E para = 0
EDI
CIS
E para [mV/m]
EFW if E z = 0
EDI if E perp2 = 0
CIS if E perp2 = 0
[Volts]
S/C potential
[Degrees]
Angle between Sun and B-field
14:28:00
14:28:05
14:28:10
14:28:15
14:28:20
14:28:25
14:28:30
06-Mar-2002

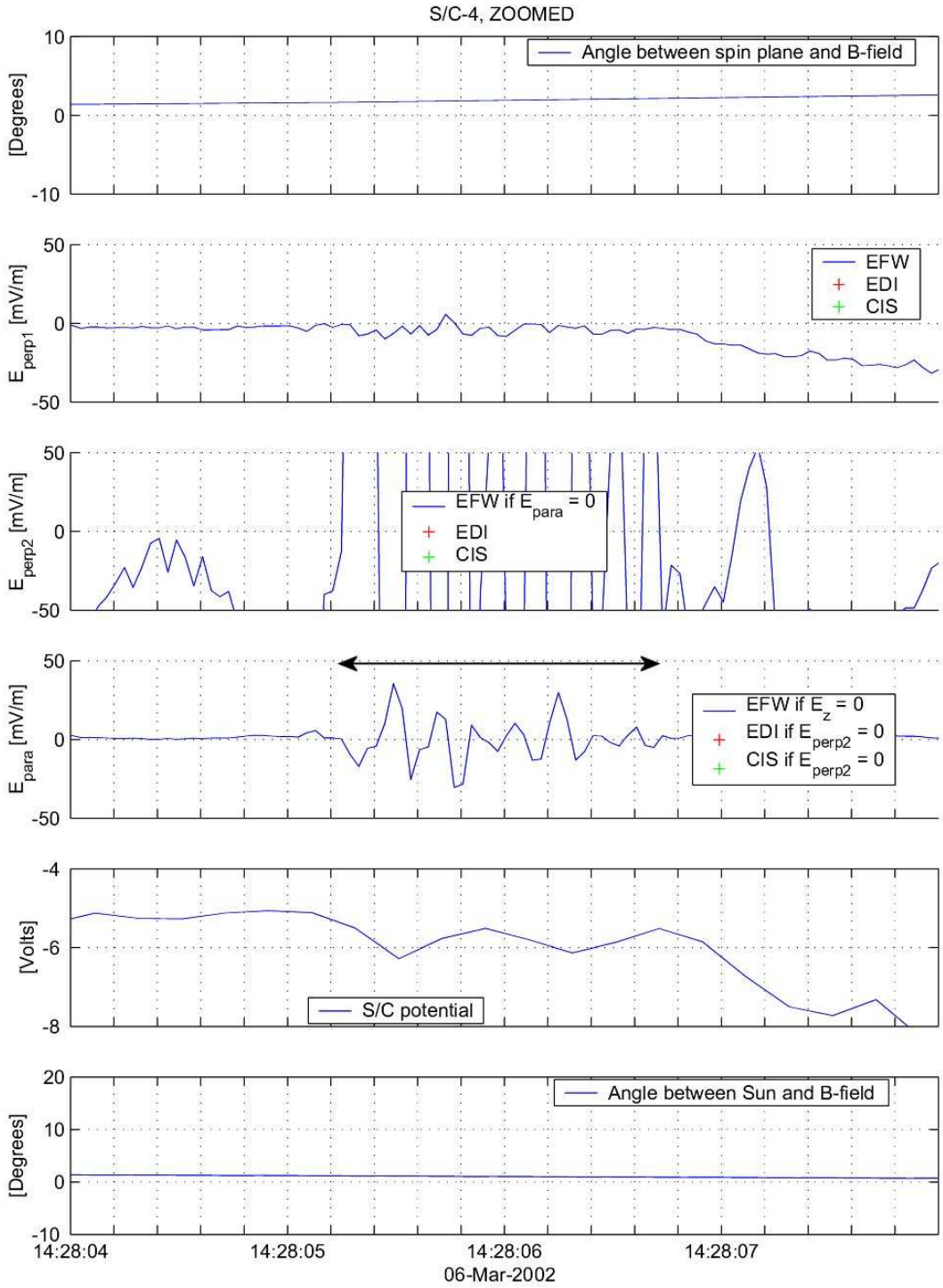
S/C-4, ZOOMED
Angle between spin plane and B-field
[Degrees]
10
0
-10
EFW
EDI
CIS
E_{perp1} [mV/m]
50
0
-50
EFW if E_{para} = 0
EDI
CIS
E_{perp2} [mV/m]
EFW if E_z = 0
EDI if E_{perp2} = 0
CIS if E_{perp2} = 0
E_{para} [mV/m]
S/C potential
[Volts]
-4
-6
-8
Angle between Sun and B-field
20
14:28:04
14:28:05
14:28:06
14:28:07
06-Mar-2002

B.1.5 2002-03-18

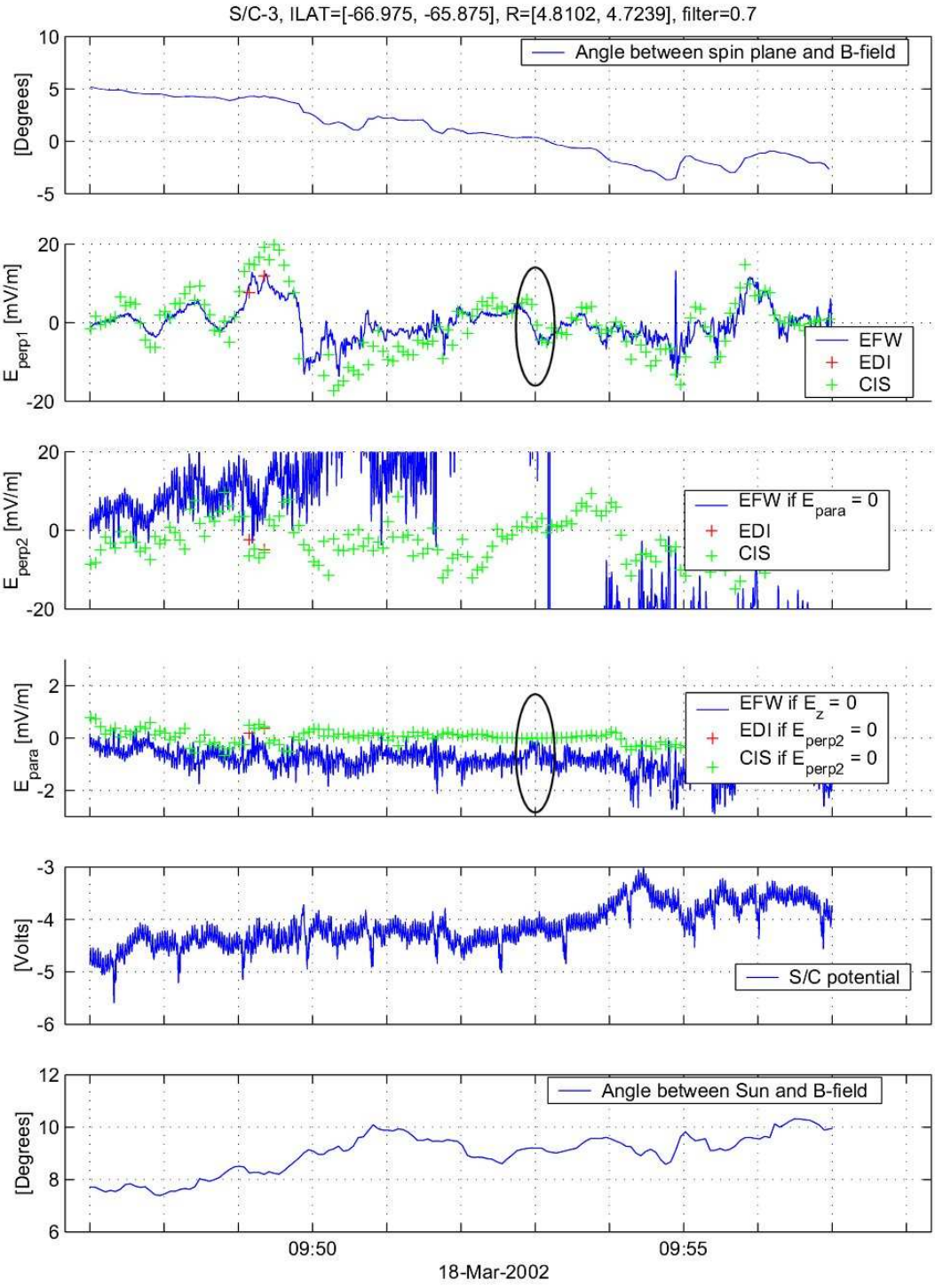

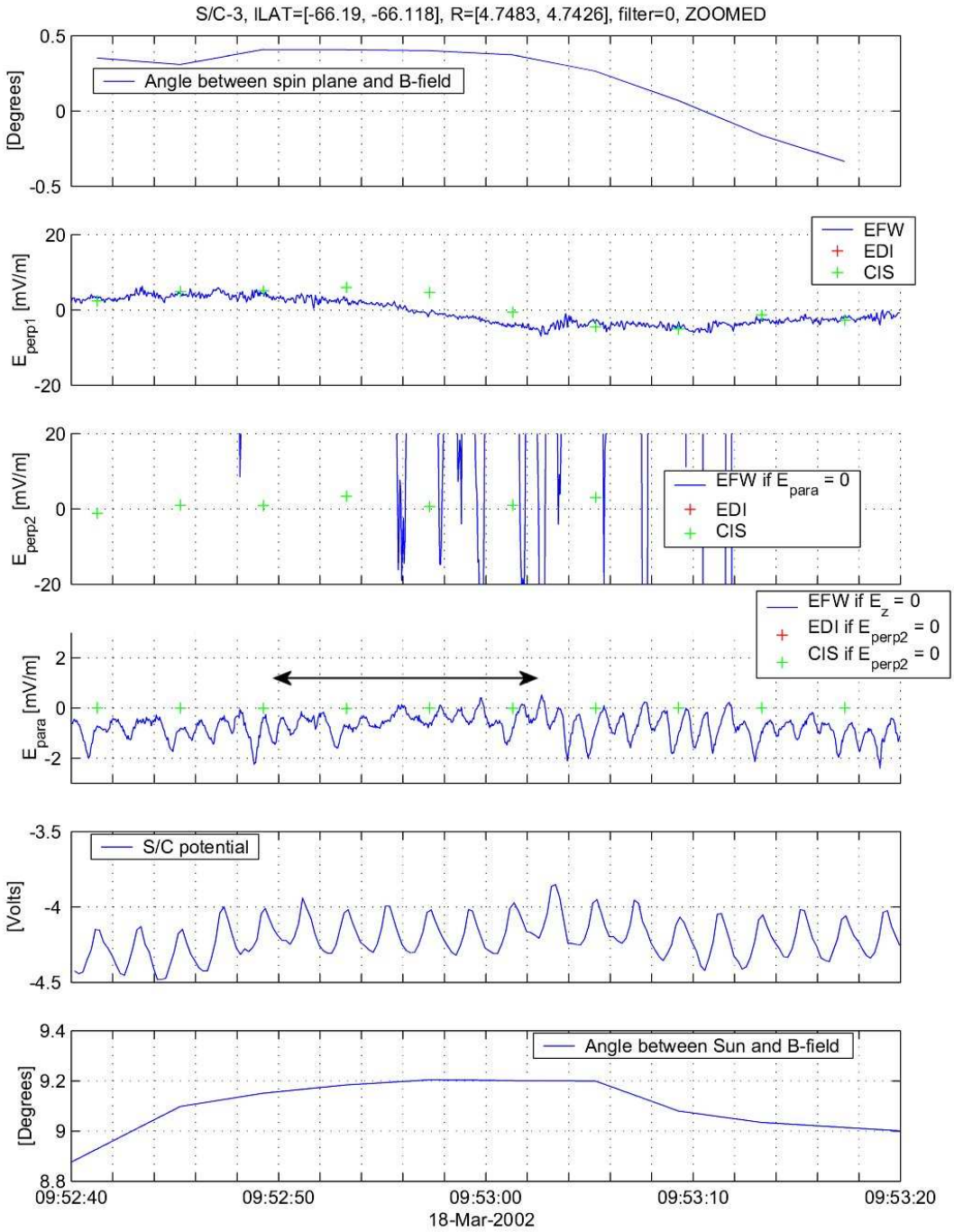
S/C-3, ILAT=[-66.19, -66.118], R=[4.7483, 4.7426], filter=0, ZOOMED
[Degrees]
Angle between spin plane and B-field
E_perp1 [mV/m]
EFW
EDI
CIS
E_perp2 [mV/m]
EFW if E_para = 0
EDI
CIS
E_para [mV/m]
EFW if E_z = 0
EDI if E_perp2 = 0
CIS if E_perp2 = 0
[Volts]
S/C potential
[Degrees]
Angle between Sun and B-field
09:52:40
09:52:50
09:53:00
09:53:10
09:53:20
18-Mar-2002

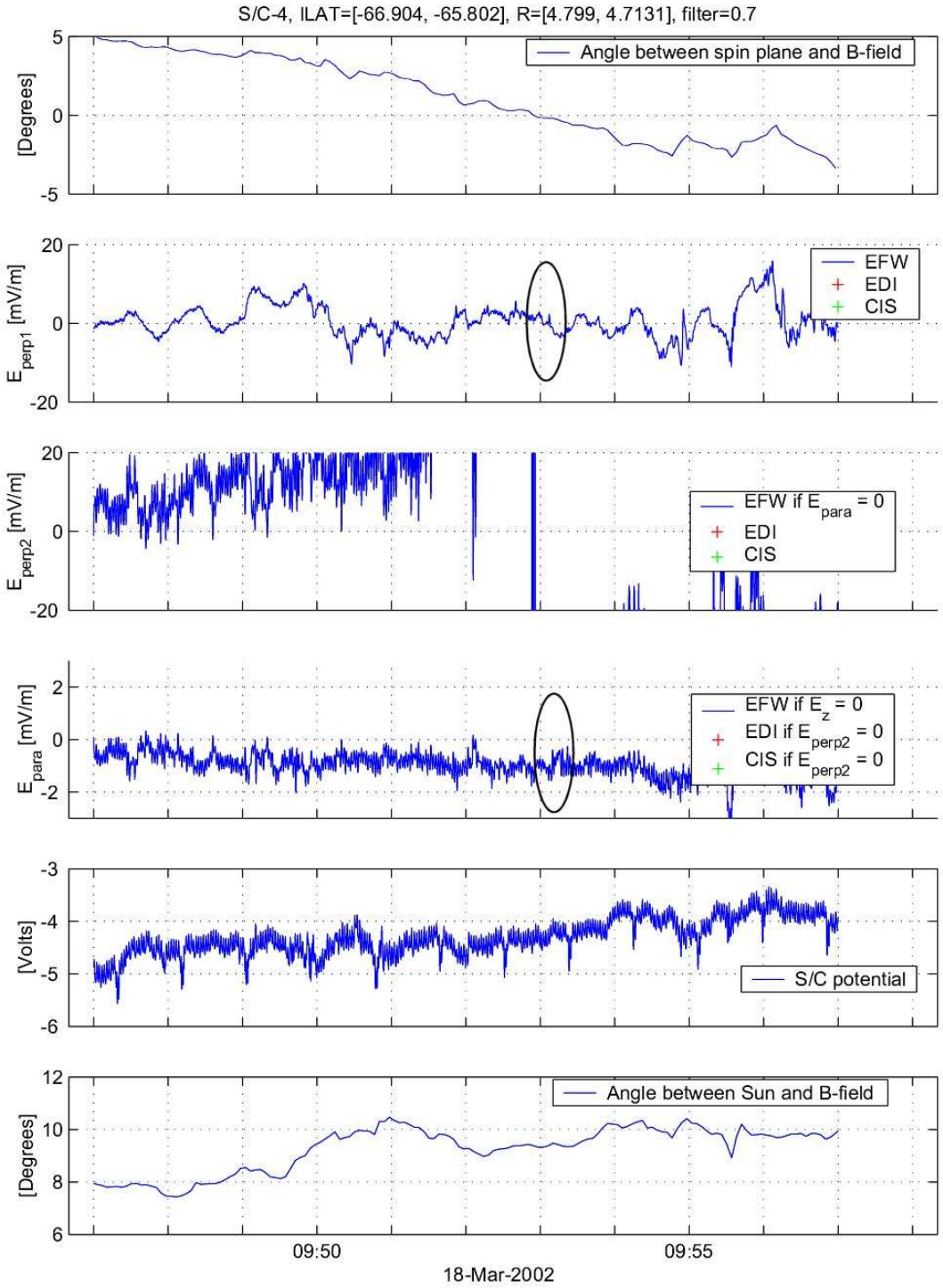
S/C-4, ILAT=[-66.904, -65.802], R=[4.799, 4.7131], filter=0.7
Angle between spin plane and B-field
[Degrees]
EFW
EDI
CIS
E perp1 [mV/m]
EFW if E para = 0
EDI
CIS
E perp2 [mV/m]
EFW if E z = 0
EDI if E perp2 = 0
CIS if E perp2 = 0
E para [mV/m]
S/C potential
[Volts]
Angle between Sun and B-field
[Degrees]
09:50
09:55
18-Mar-2002

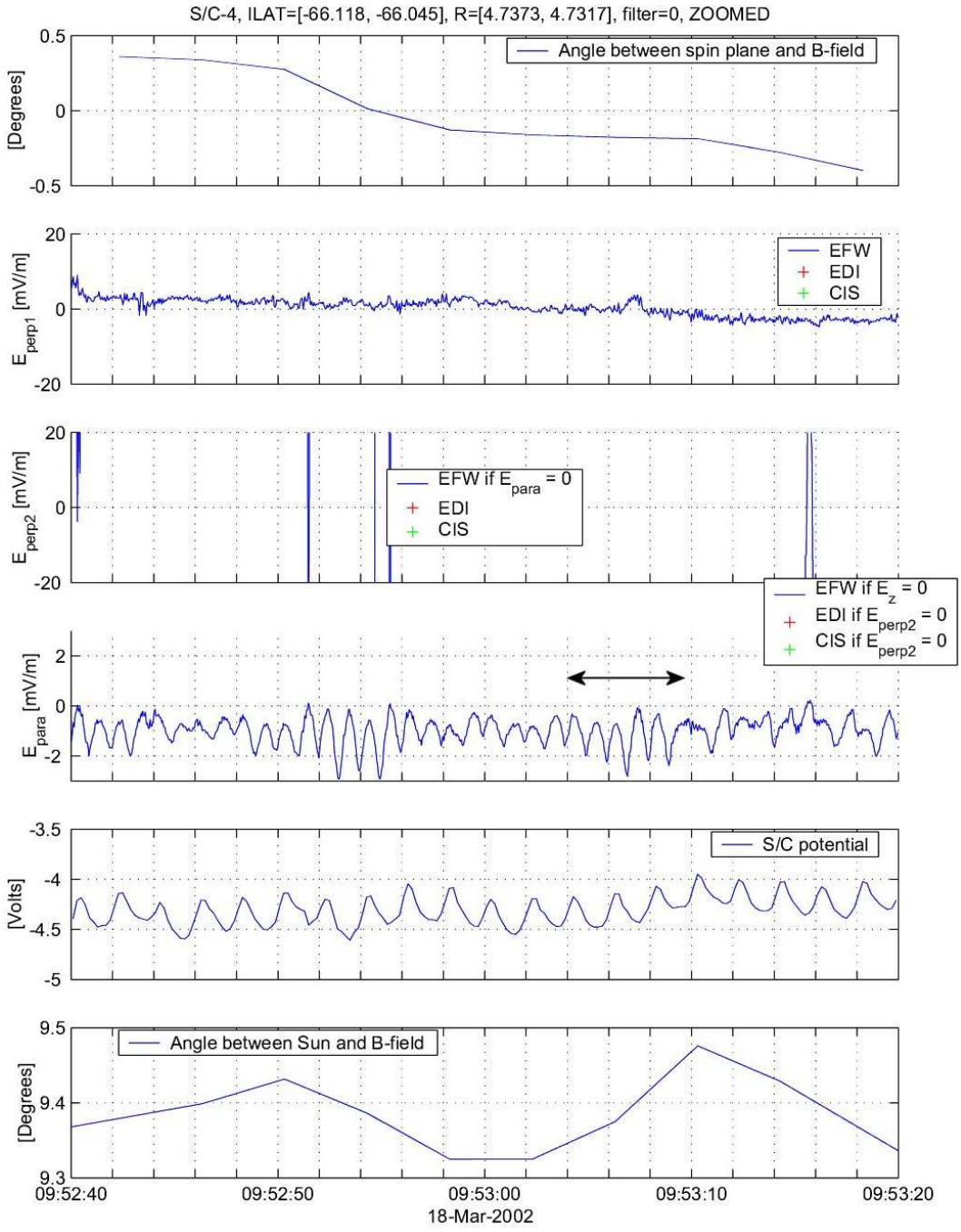
S/C-4, ILAT=[-66.118, -66.045], R=[4.7373, 4.7317], filter=0, ZOOMED
Angle between spin plane and B-field
[Degrees]
0.5
0
-0.5
EFW
EDI
CIS
E_perp1 [mV/m]
20
0
-20
EFW if E_para = 0
EDI
CIS
E_perp2 [mV/m]
20
0
-20
EFW if E_z = 0
EDI if E_perp2 = 0
CIS if E_perp2 = 0
E_para [mV/m]
2
0
-2
S/C potential
[Volts]
-3.5
-4
-4.5
-5
Angle between Sun and B-field
[Degrees]
9.5
9.4
9.3
09:52:40
09:52:50
09:53:00
09:53:10
09:53:20
18-Mar-2002

B.2 Good

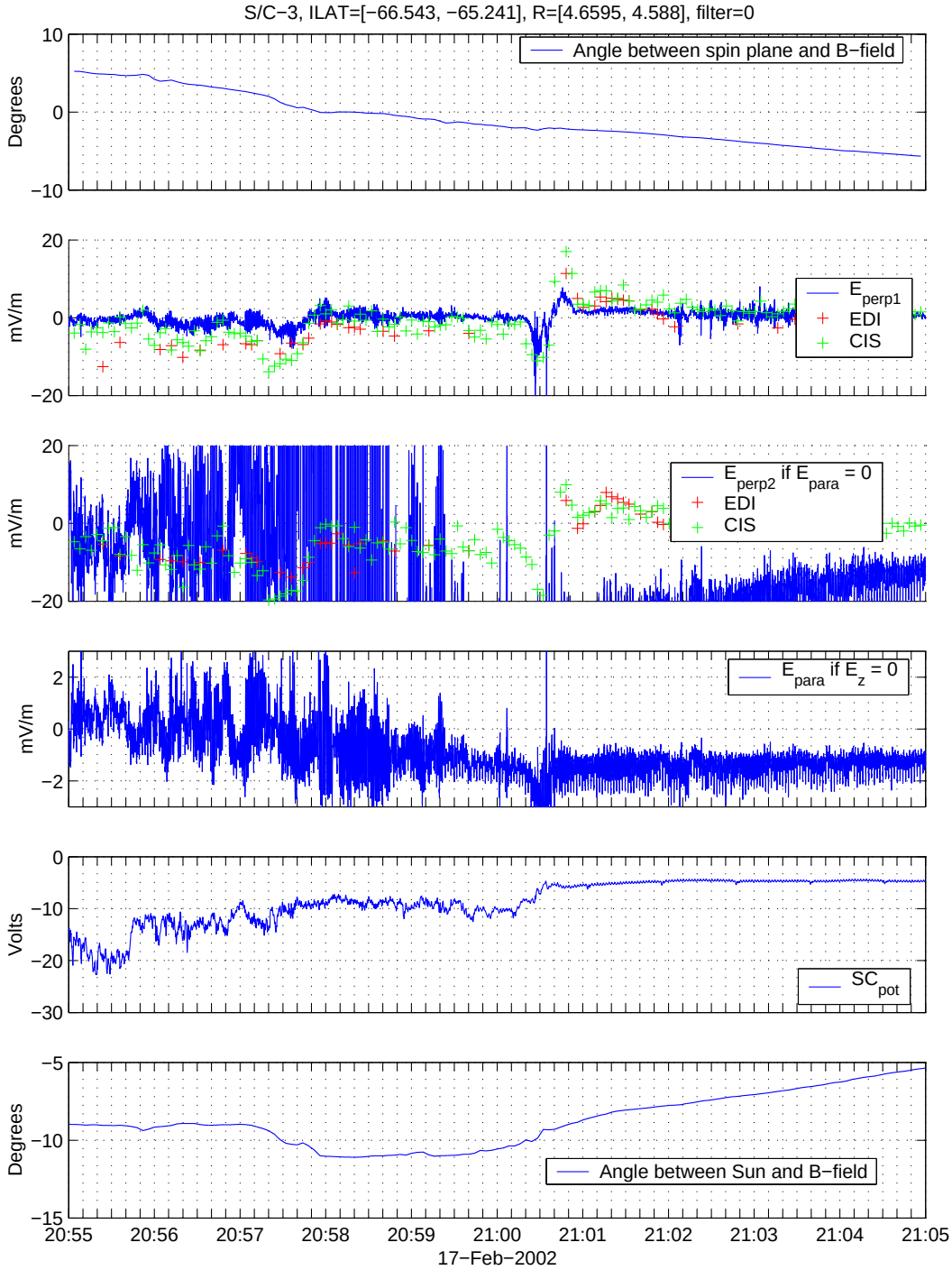
S/C−3, ILAT=[−66.543, −65.241], R=[4.6595, 4.588], filter=0
Angle between spin plane and B−field
Degrees
E perp1
EDI
CIS
mV/m
E perp2 if E para = 0
EDI
CIS
mV/m
E para if E z = 0
mV/m
SC pot
Volts
Angle between Sun and B−field
Degrees
20:55
20:56
20:57
20:58
20:59
21:00
21:01
21:02
21:03
21:04
21:05
17−Feb−2002

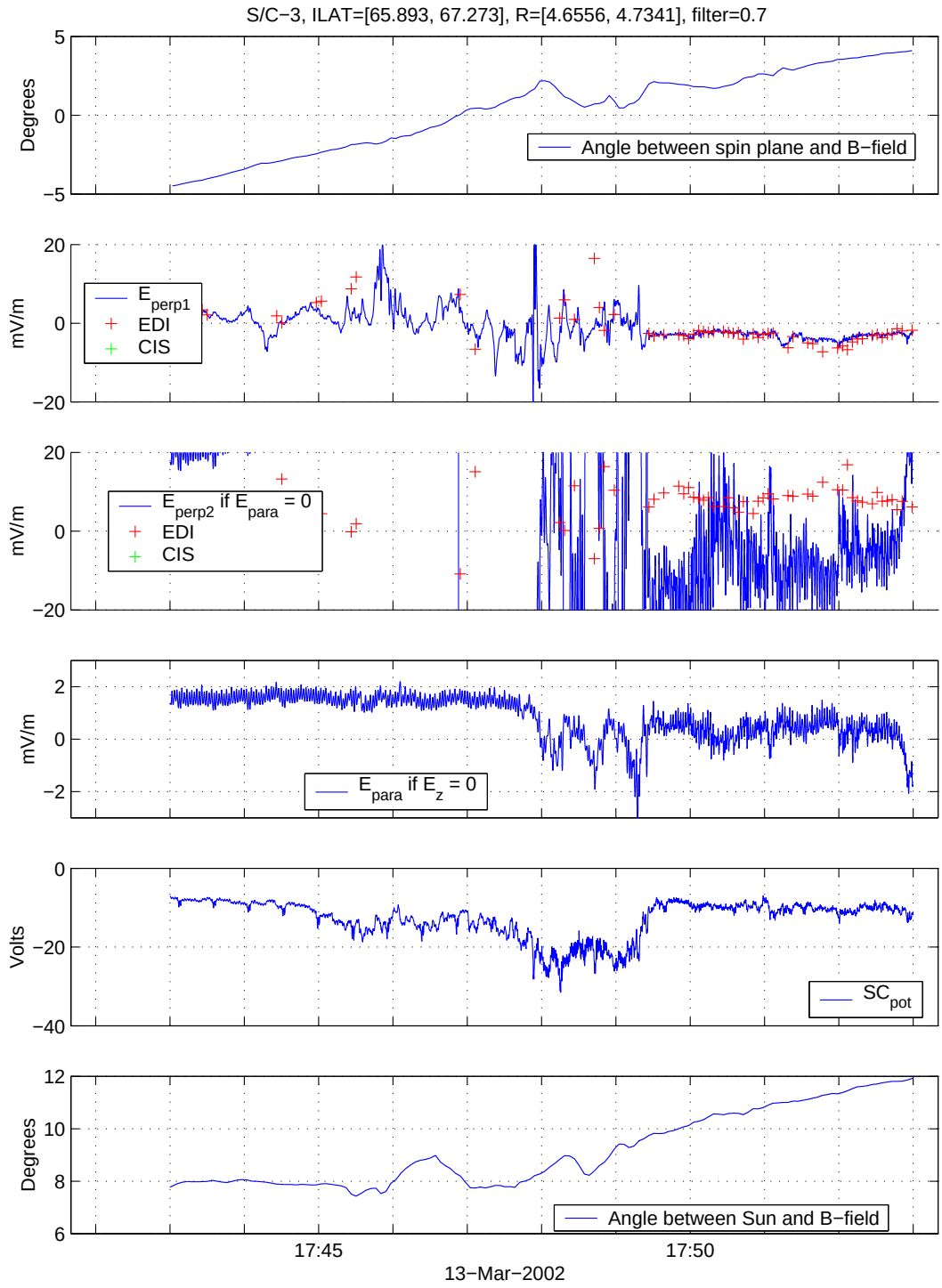
S/C−3, ILAT=[65.893, 67.273], R=[4.6556, 4.7341], filter=0.7
Degrees
Angle between spin plane and B−field
mV/m
E perp1
EDI
CIS
E perp2 if E para = 0
E para if E z = 0
Volts
SC pot
Angle between Sun and B−field
17:45
17:50
13−Mar−2002

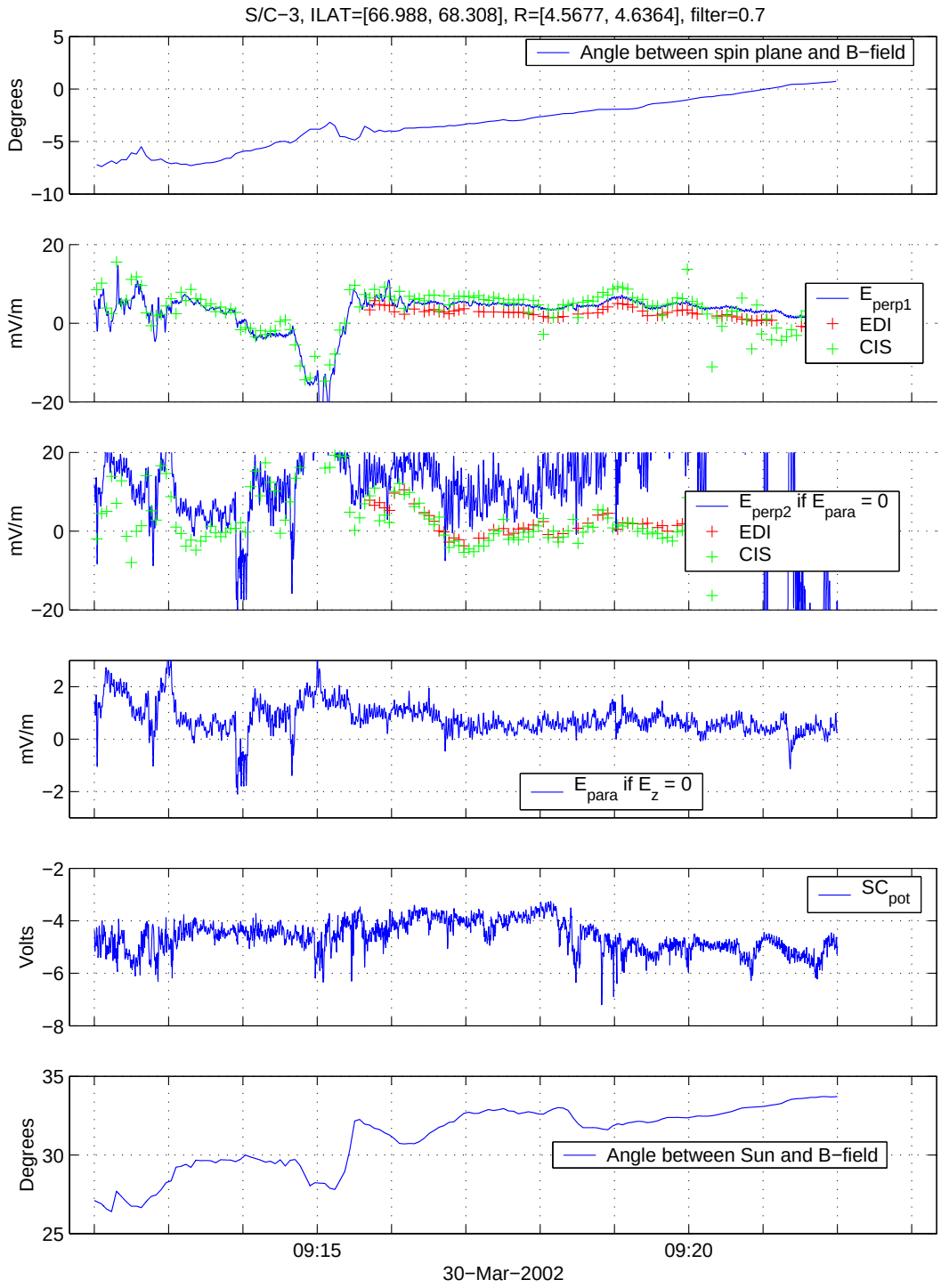
S/C−3, ILAT=[66.988, 68.308], R=[4.5677, 4.6364], filter=0.7
Angle between spin plane and B−field
Degrees
E perp1
EDI
CIS
mV/m
E perp2 if E para = 0
EDI
CIS
mV/m
E para if E z = 0
mV/m
SC pot
Volts
Angle between Sun and B−field
Degrees
09:15
09:20
30−Mar−2002

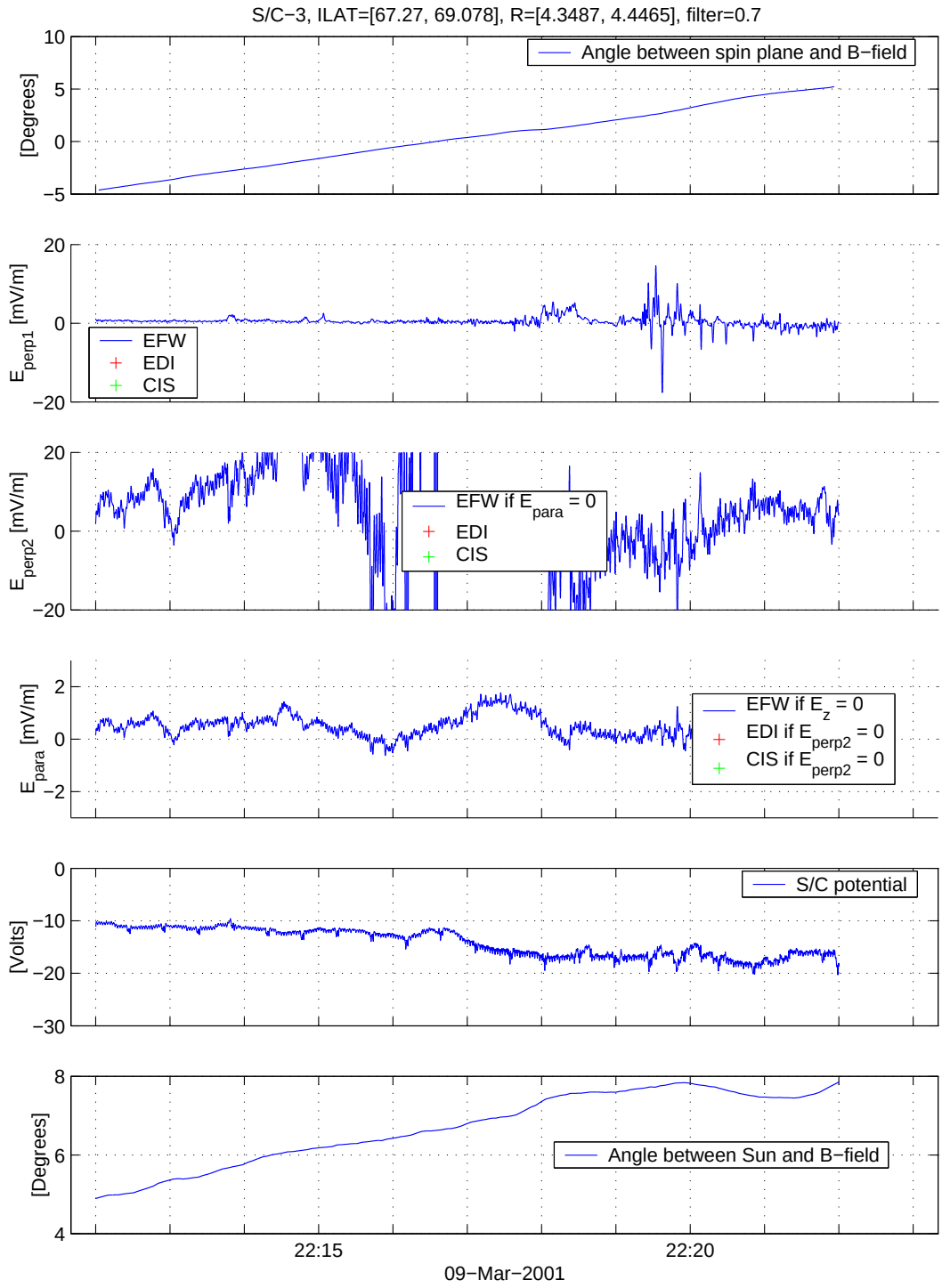
S/C−3, ILAT=[67.27, 69.078], R=[4.3487, 4.4465], filter=0.7
Angle between spin plane and B−field
[Degrees]
10
5
0
−5
E_perp1 [mV/m]
20
0
−20
EFW
EDI
CIS
E_perp2 [mV/m]
EFW if E_para = 0
EDI
CIS
E_para [mV/m]
2
0
−2
EFW if E_z = 0
EDI if E_perp2 = 0
CIS if E_perp2 = 0
[Volts]
S/C potential
−10
−20
−30
[Degrees]
8
6
4
Angle between Sun and B−field
22:15
22:20
09−Mar−2001

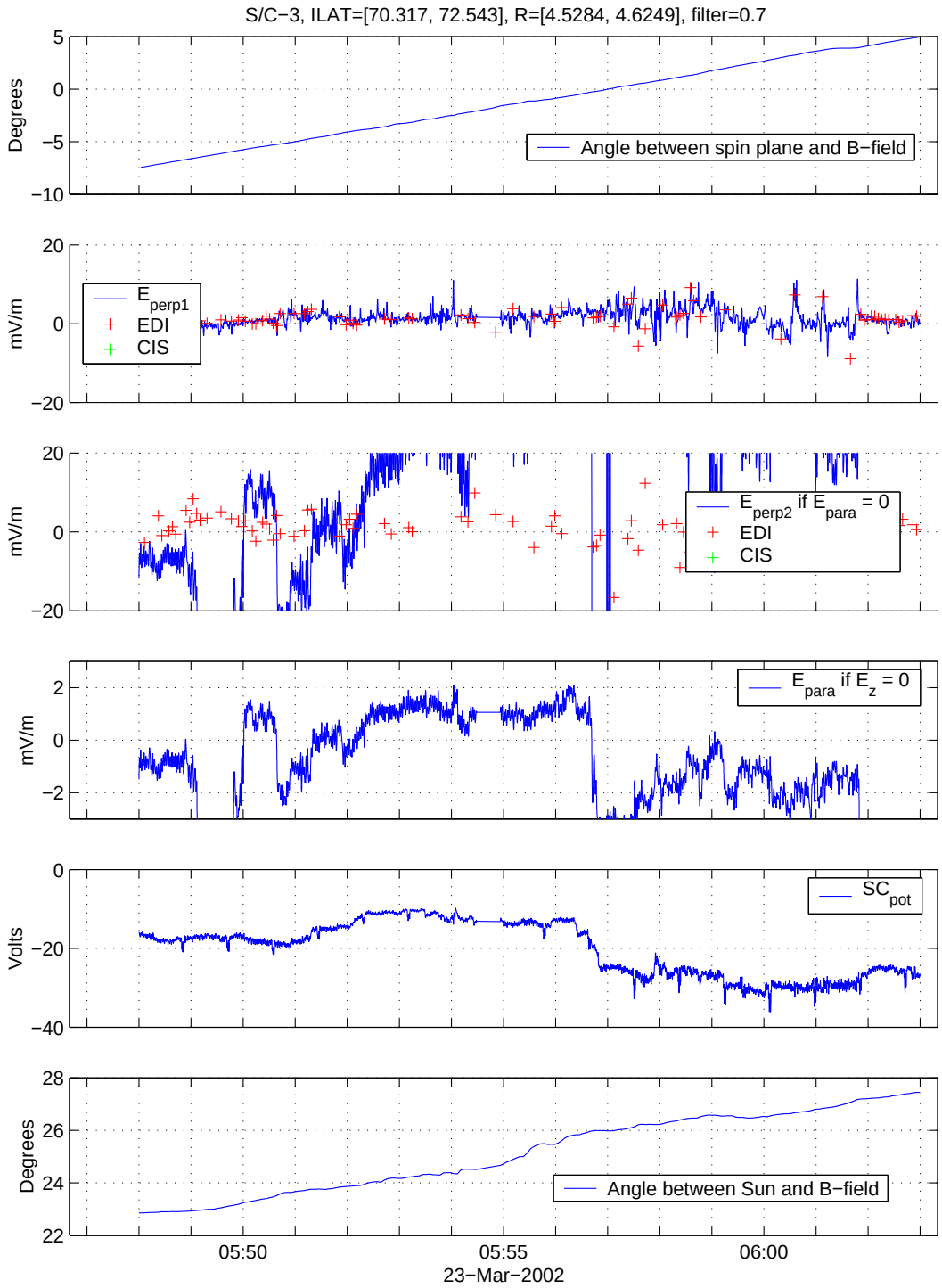
S/C−3, ILAT=[70.317, 72.543], R=[4.5284, 4.6249], filter=0.7
Degrees
Angle between spin plane and B−field
mV/m
E perp1
EDI
CIS
E perp2 if E para = 0
E para if E z = 0
Volts
SC pot
Angle between Sun and B−field
05:50
05:55
06:00
23−Mar−2002

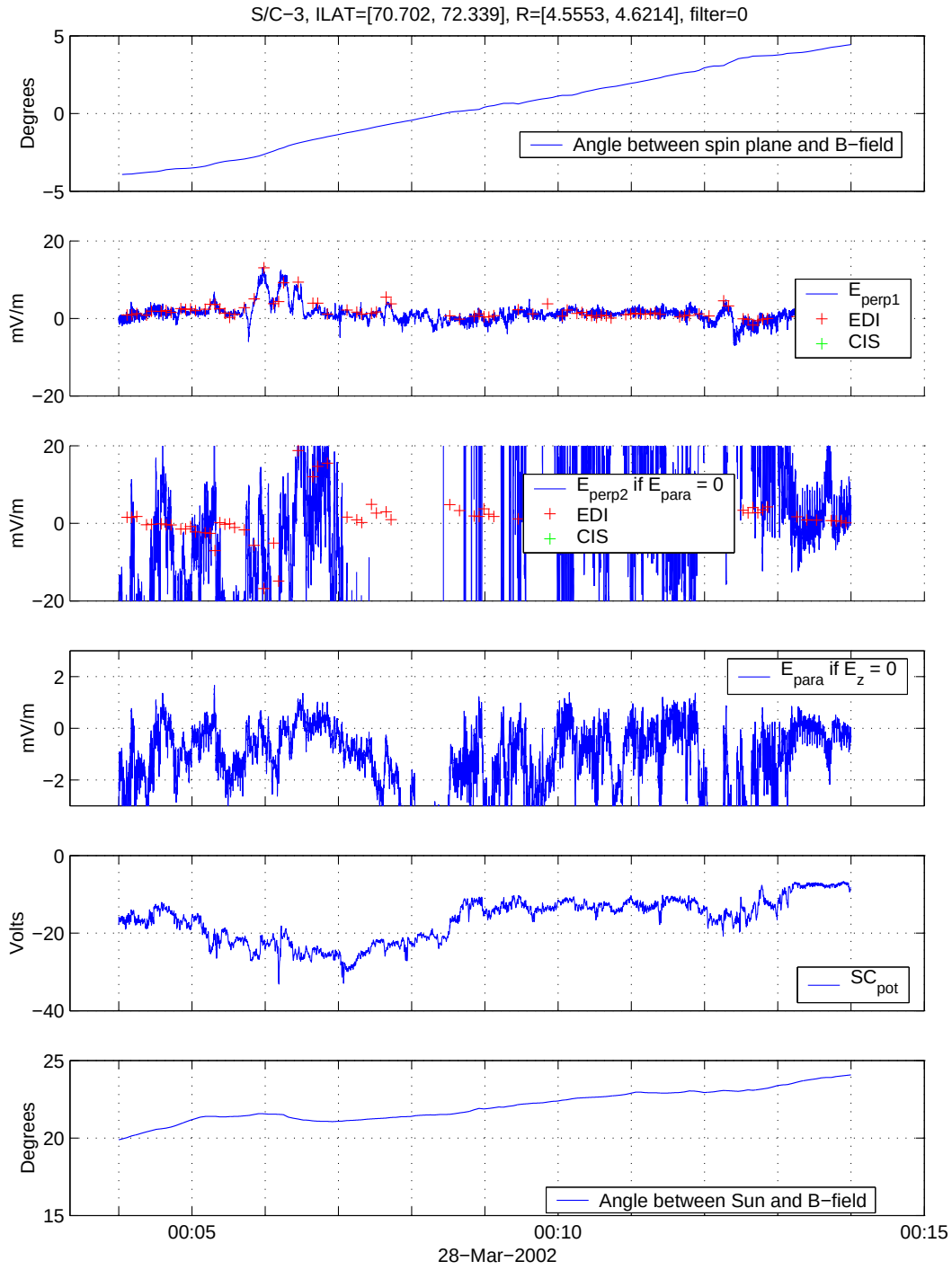
S/C−3, ILAT=[70.702, 72.339], R=[4.5553, 4.6214], filter=0
Degrees
Angle between spin plane and B−field
mV/m
E perp1
EDI
CIS
E perp2 if E para = 0
EDI
CIS
mV/m
E para if E z = 0
Volts
SC pot
Degrees
Angle between Sun and B−field
00:05
00:10
00:15
28−Mar−2002

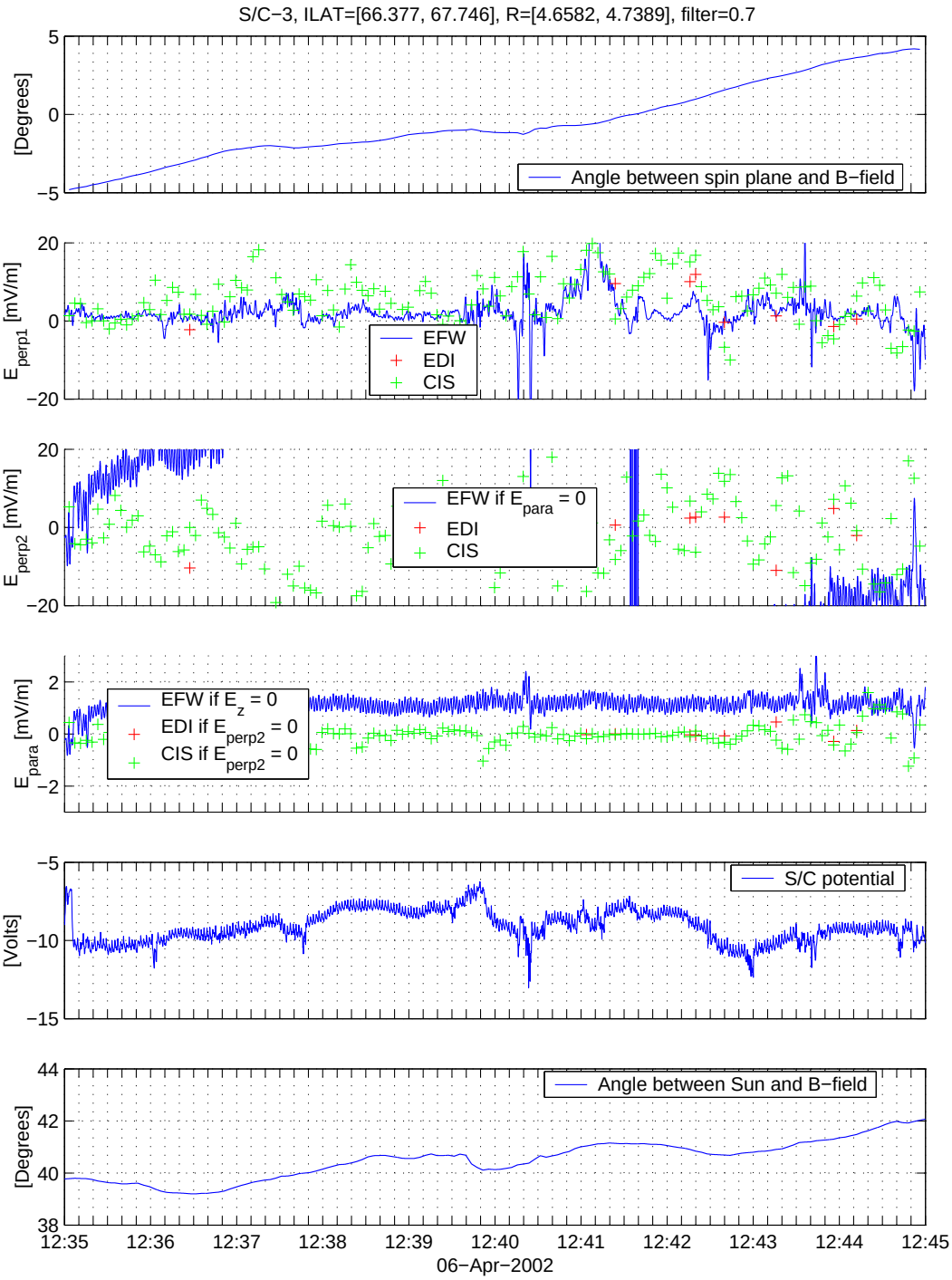
S/C−3, ILAT=[66.377, 67.746], R=[4.6582, 4.7389], filter=0.7
[Degrees]
Angle between spin plane and B−field
E_perp1 [mV/m]
EFW
EDI
CIS
E_perp2 [mV/m]
EFW if E_para = 0
EDI
CIS
E_para [mV/m]
EFW if E_z = 0
EDI if E_perp2 = 0
CIS if E_perp2 = 0
[Volts]
S/C potential
[Degrees]
Angle between Sun and B−field
12:35
12:36
12:37
12:38
12:39
12:40
12:41
12:42
12:43
12:44
12:45
06−Apr−2002

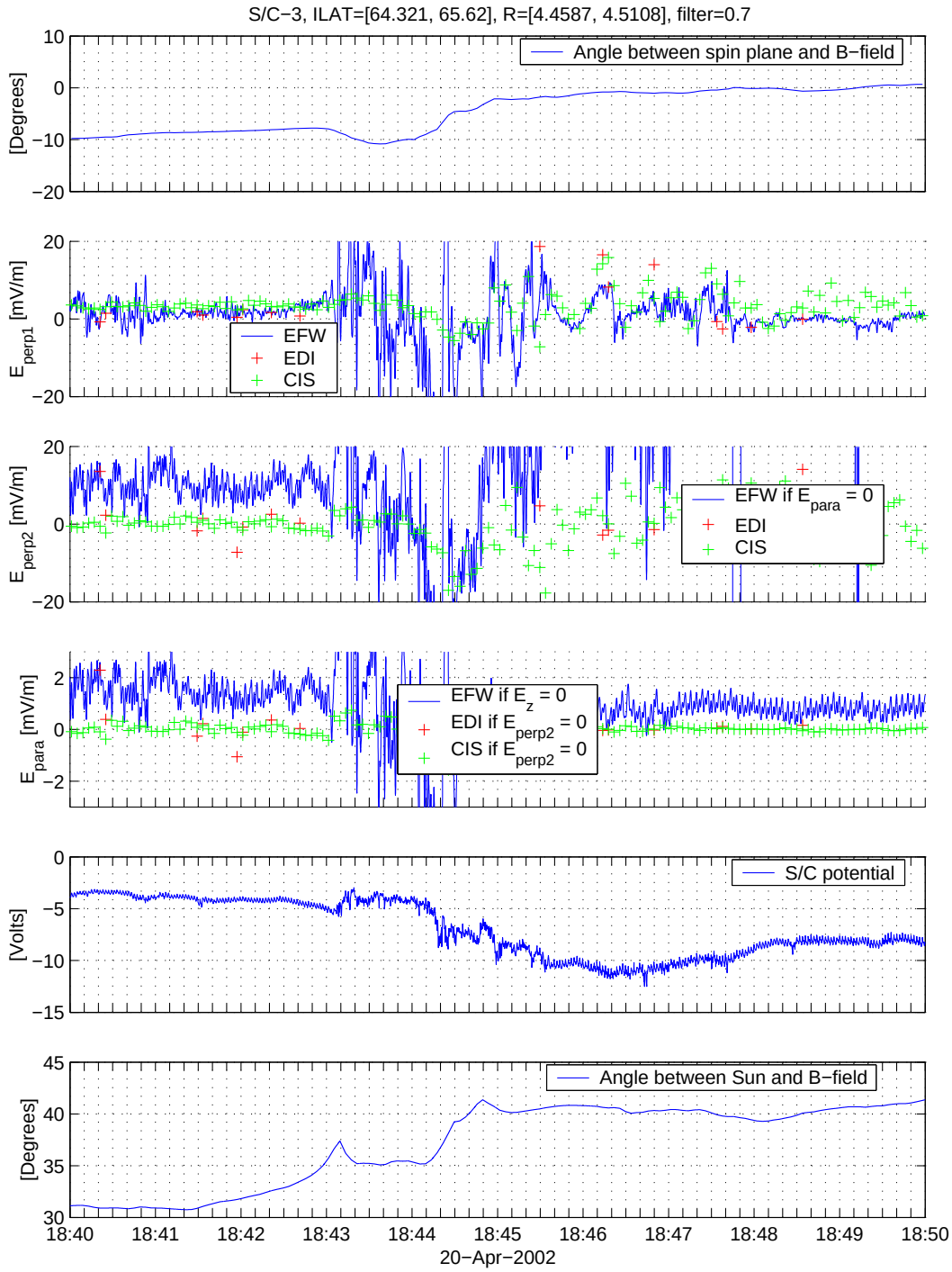
S/C−3, ILAT=[64.321, 65.62], R=[4.4587, 4.5108], filter=0.7
Angle between spin plane and B−field
[Degrees]
10
0
−10
−20
E_perp1 [mV/m]
20
0
−20
EFW
EDI
CIS
E_perp2 [mV/m]
EFW if E_para = 0
EDI
CIS
E_para [mV/m]
2
0
−2
EFW if E_z = 0
EDI if E_perp2 = 0
CIS if E_perp2 = 0
[Volts]
S/C potential
−5
−15
[Degrees]
45
40
35
30
Angle between Sun and B−field
18:40
18:41
18:42
18:43
18:44
18:45
18:46
18:47
18:48
18:49
18:50
20−Apr−2002

B.3 Too Active

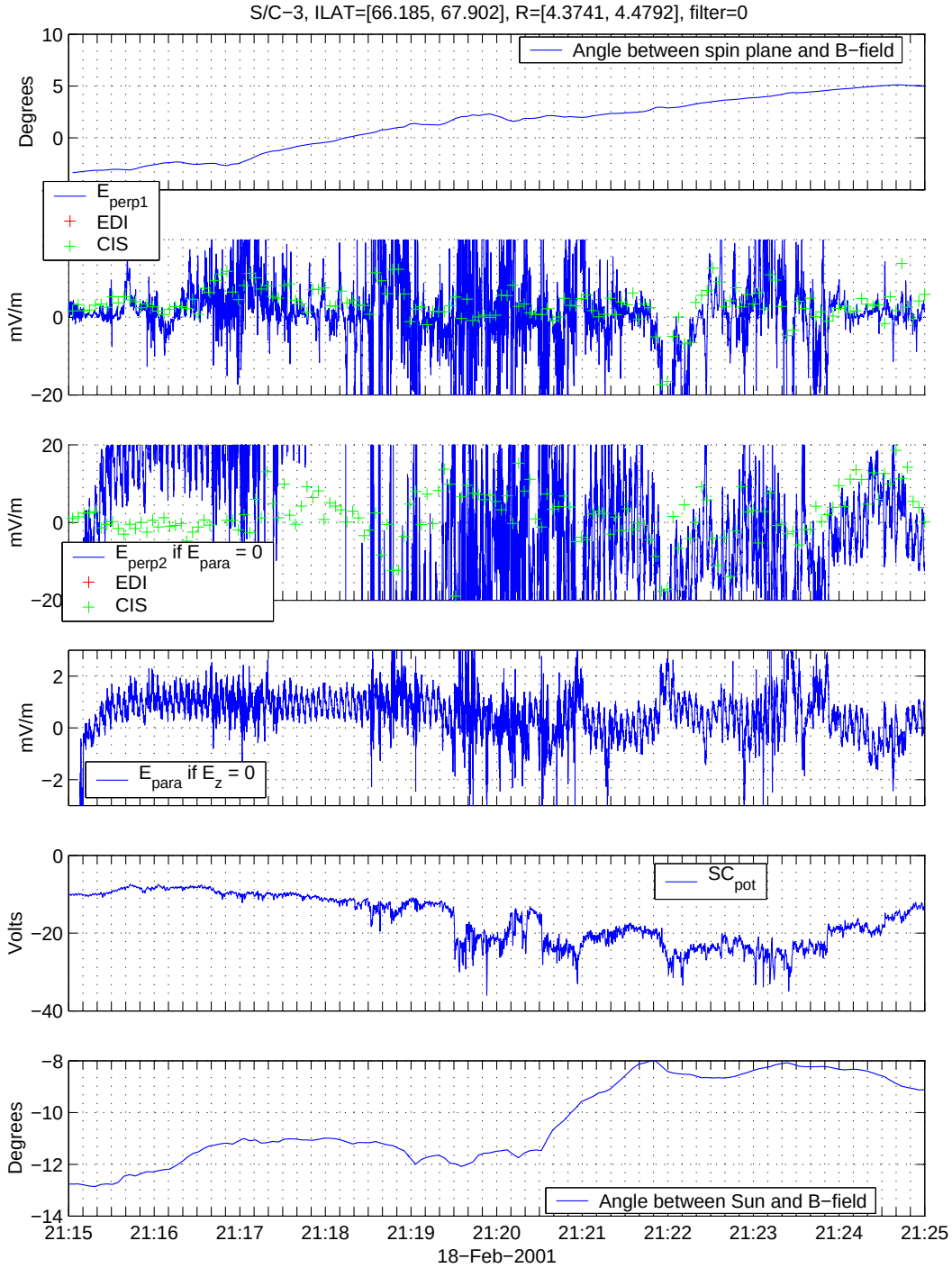

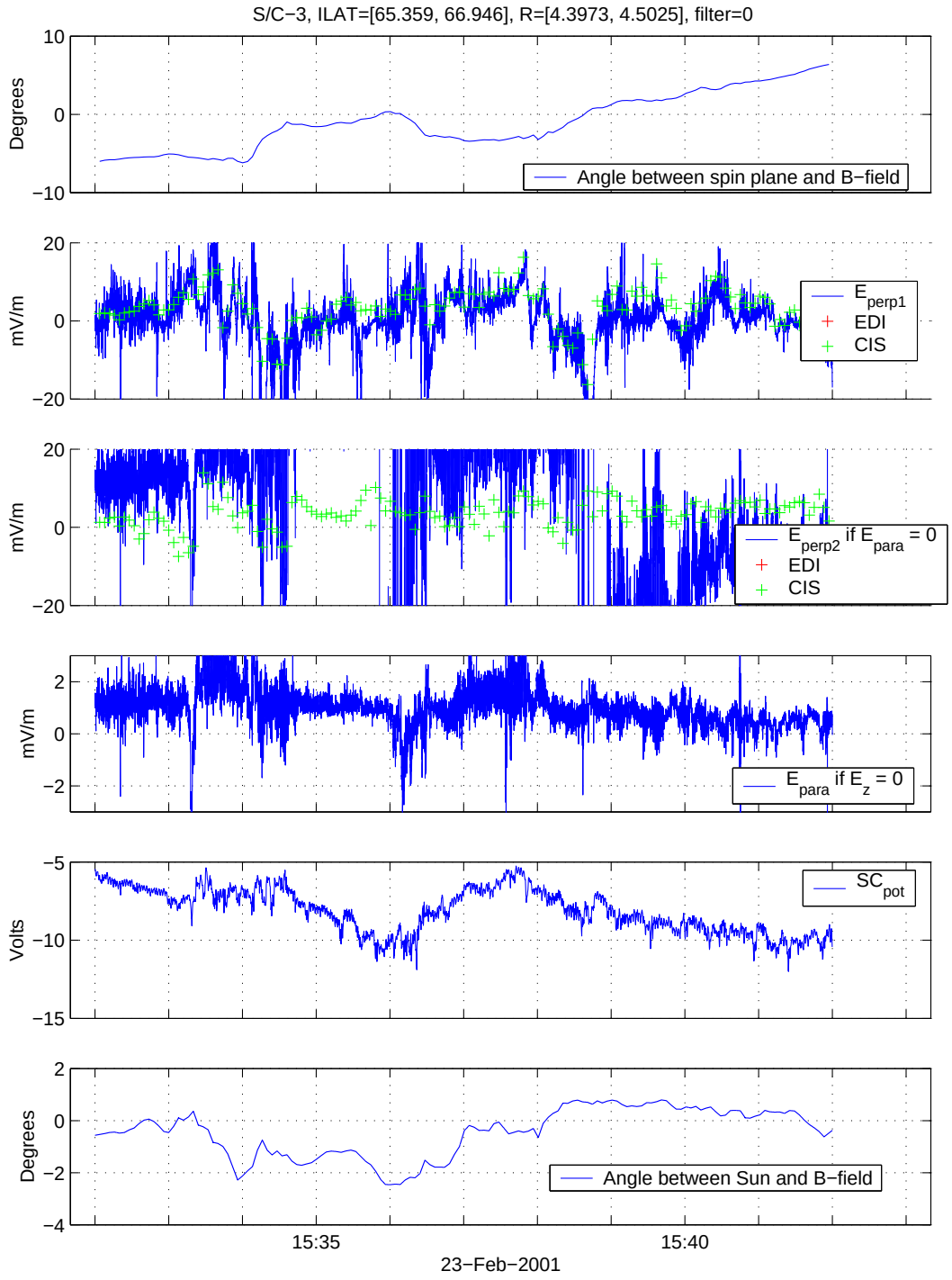
S/C−3, ILAT=[65.359, 66.946], R=[4.3973, 4.5025], filter=0
Degrees
Angle between spin plane and B−field
mV/m
E perp1
EDI
CIS
mV/m
E perp2 if E para = 0
EDI
CIS
mV/m
E para if E z = 0
Volts
SC pot
Degrees
Angle between Sun and B−field
15:35
15:40
23−Feb−2001

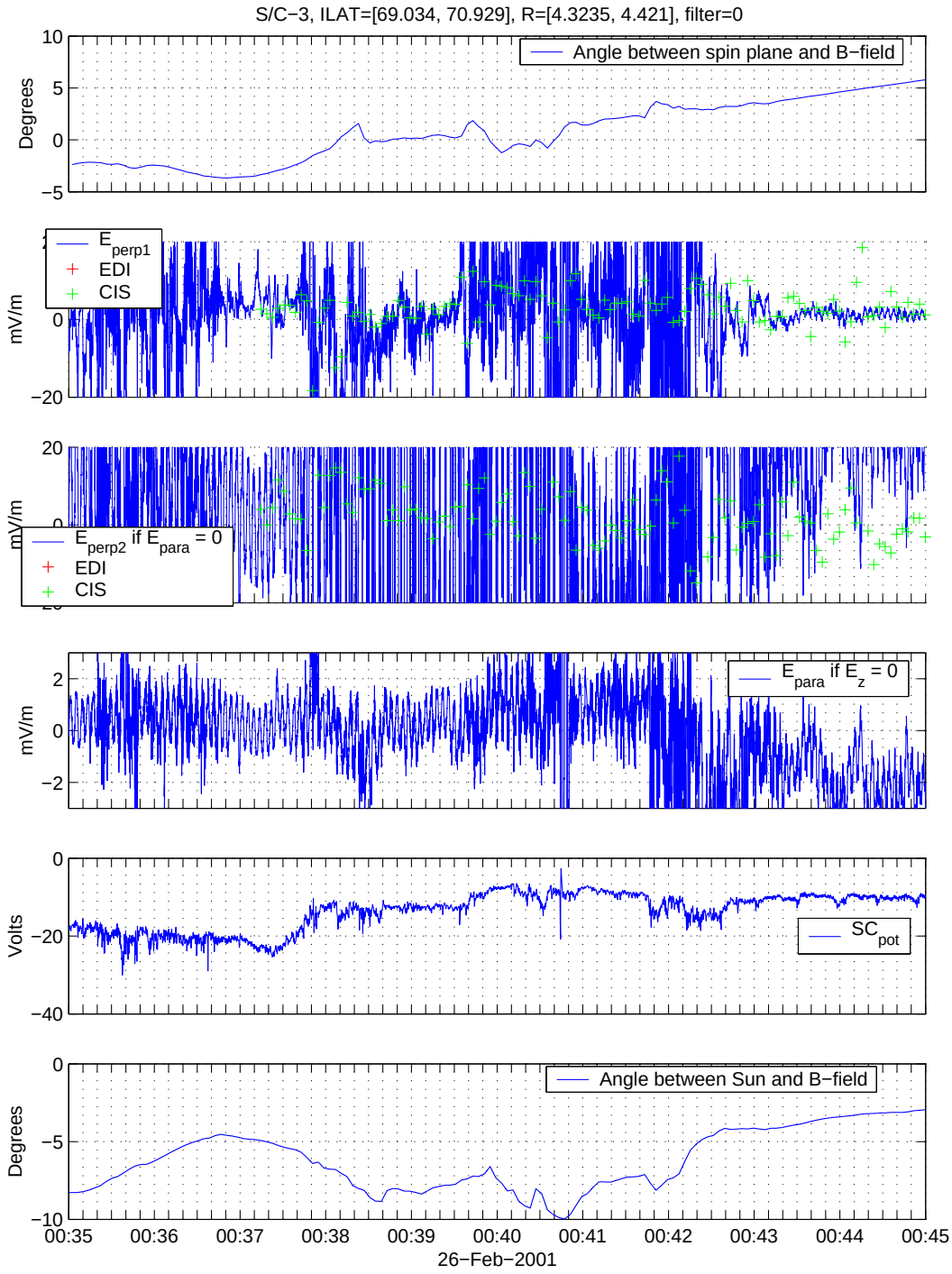
S/C−3, ILAT=[69.034, 70.929], R=[4.3235, 4.421], filter=0
Angle between spin plane and B−field
Degrees
E perp1
EDI
CIS
mV/m
E perp2 if E para = 0
EDI
CIS
mV/m
E para if E z = 0
mV/m
SC pot
Volts
Angle between Sun and B−field
Degrees
00:35
00:36
00:37
00:38
00:39
00:40
00:41
00:42
00:43
00:44
00:45
26−Feb−2001

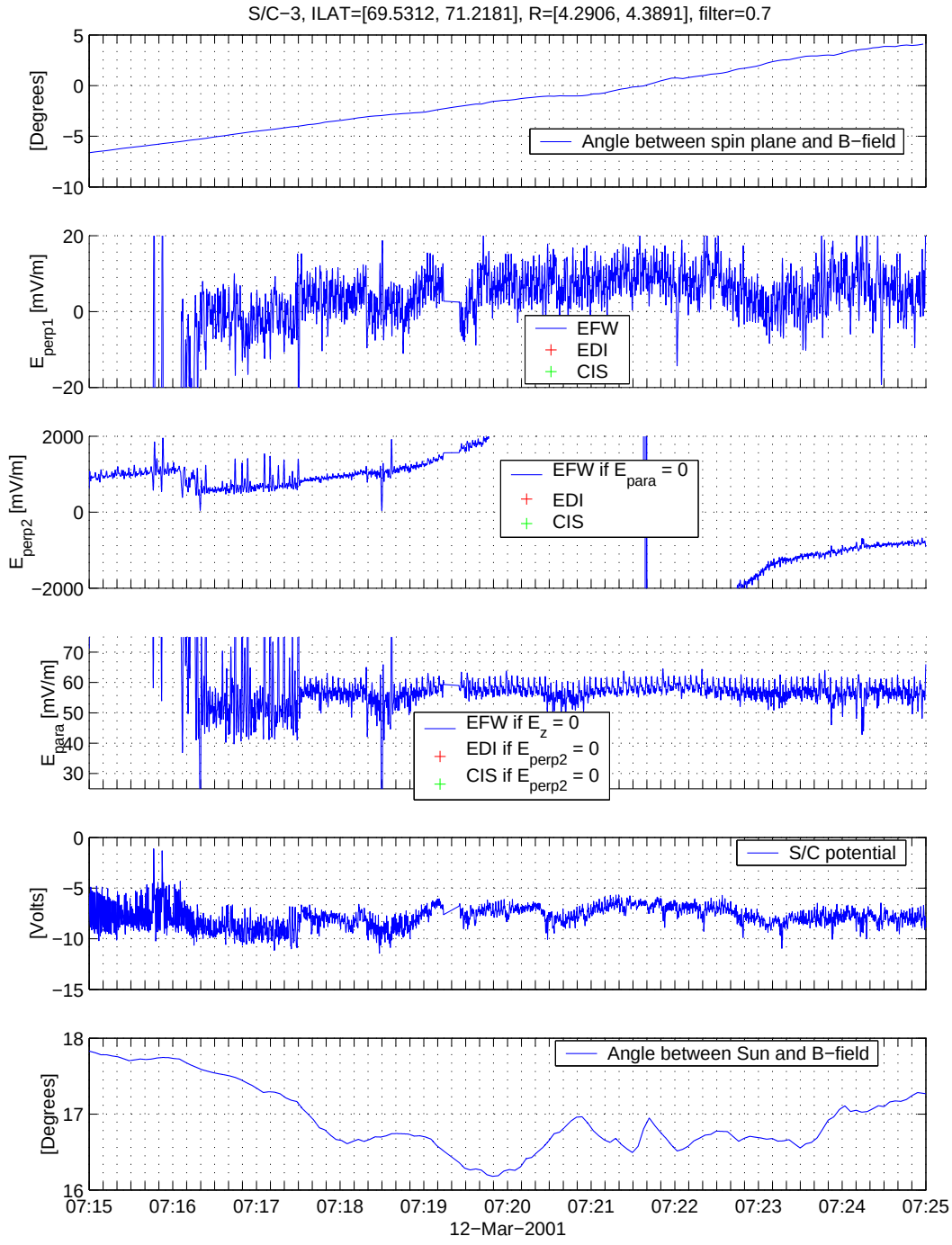
S/C−3, ILAT=[69.5312, 71.2181], R=[4.2906, 4.3891], filter=0.7
[Degrees]
Angle between spin plane and B−field
E perp1 [mV/m]
EFW
EDI
CIS
E perp2 [mV/m]
EFW if E para = 0
EDI
CIS
E para [mV/m]
EFW if E z = 0
EDI if E perp2 = 0
CIS if E perp2 = 0
[Volts]
S/C potential
[Degrees]
Angle between Sun and B−field
07:15
07:16
07:17
07:18
07:19
07:20
07:21
07:22
07:23
07:24
07:25
12−Mar−2001

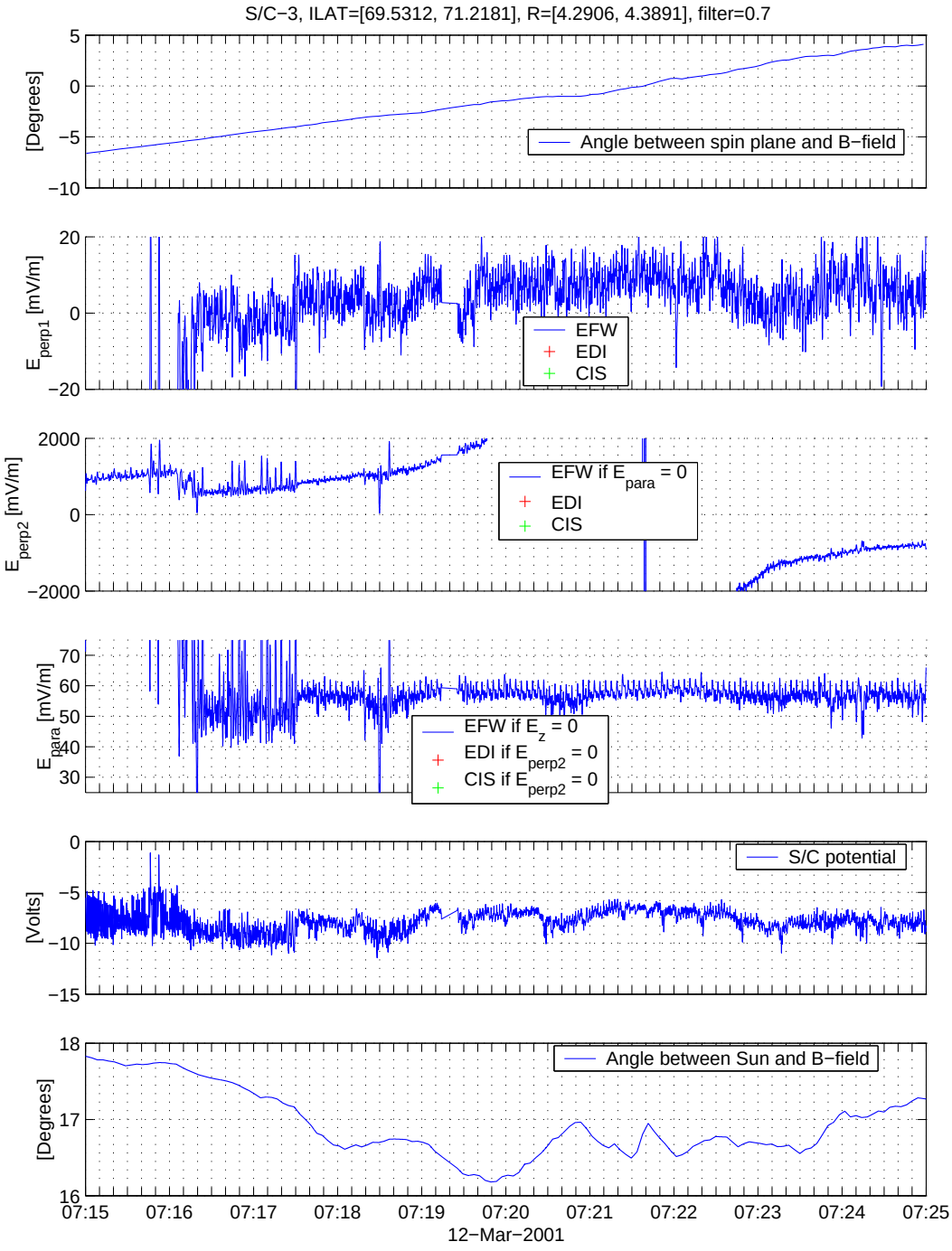
S/C−3, ILAT=[69.5312, 71.2181], R=[4.2906, 4.3891], filter=0.7
[Degrees]
Angle between spin plane and B−field
E perp1 [mV/m]
EFW
EDI
CIS
E perp2 [mV/m]
EFW if E para = 0
EDI
CIS
E para [mV/m]
EFW if E z = 0
EDI if E perp2 = 0
CIS if E perp2 = 0
[Volts]
S/C potential
[Degrees]
Angle between Sun and B−field
07:15
07:16
07:17
07:18
07:19
07:20
07:21
07:22
07:23
07:24
07:25
12−Mar−2001

Bibliography

[Alfven, H., 1958] Alfvén, H.: On the theory of magnetic storms and aurorae, Tellus, 10, 104, 1958

[Baumjohann and Treumann, 1996] Baumjohann, W., Treumann, R. A.: Basic Space Plasma Physics, London: Imperial College Press, 1996

[Block and Fälthammar, 1990] Block and Fälthammar: The role of magnetic field-aligned electric fields in auroral acceleration, J. Geophys. Res., 95, 5877, 1990

[Carlqvist and Boström, 1970] Carlqvist, P. and Boström, R.: Space-charge regions above the aurora, J. Geophys. Res., 75, 7140-7146, 1970

[Daly, P. W., 2002] Daly, P. W., Users Guide to the Cluster Science Data System, CSDS: DS-MPA-TN-0015, 2002

[Ergun et al, 2001] Ergun et al.: Direct observation of localized parallel electric fields in space plasma, Phys. Rev. Lett., Volume 87, Number 4, July 2001

[Eriksson and Boström, 1993] Eriksson, A. I. and Boström, R.: Are Weak Double Layers Important for Auroral Particle Acceleration?, Geophys. Monograph 80, p. 105-112, 1993

[Fälthammar, C.-G., 1983] Fälthammar, C.-G.: Magnetic-Field-Aligned Electric Fields, ESA Journal, vol. 7, no. 4, p. 385-404, 1983

[Gustafsson et al, 1977] Gustafsson, G. et al: The electric field and wave experiment for the Cluster mission, Space Sci. Rev., 79, 137-156, 1997

[Janhunen and Olsson, 2001] Janhunen, P. and Olsson, A.: Auroral Potential Structures and Current-Voltage Relationship: Summary of Recent Results, Physics and Chemistry of the Earth Part C, v. 26, iss. 1-3, p. 107-111, 2001

[Janhunen et al, 2001] Janhunen, P., Olsson, A., Laakso, H.: Altitude extension of auroral potential structures by event-based and statistical studies, Advances in Space Research, Volume 28, Issue 11, p. 1575-1580, 2001

[Janhunen and Olsson, 2000] Janhunen, P. and Olsson, A.: New model for auroral acceleration: O-shaped potential structure cooperating with waves, Annales Geophysicae, Volume 18, Issue 6, p.596-607, 2000

[Janhunen et al, 1999] Janhunen, P., Olsson, A., Mozer, F. S., Laakso, H.: How does the U-shaped potential close above the acceleration region? A study using Polar data, Annales Geophysicae, Volume 17, Issue 10, p.1276-1283, 1999

[Laakso et al, 2001] Laakso, H., Escoubet, C., Grard, R., Masson, A., Moullard, O., Andre, M., Eriksson, A. I., Gustafsson, G., Hull, A., Mozer, F., Lindqvist, P., Pedersen, A., Balogh, A., Dunlop, M., Fazakerley, A., Taylor, M.: Multi-Point Electric Field Observations in the High-Altitude Cusp Region, American Geophysical Union, Fall Meeting 2001, abstract #SM12C-09, Dec. 2001

[Lindqvist and Marklund, 1990] Lindqvist, P.-A. and Marklund, G. T., A statistical study of high-altitude electric fields measured on the Viking satellite, Journal of Geoph. Res., Volume 95, Number A5, p. 5867-5876, May 1990

[Lysak, R.L., 1990] Lysak, R. L.: Electrodynamic coupling of the magnetosphere and ionosphere, Space Science Reviews, vol. 52, p. 33-87, Feb. 1990

[Marklund, G., 1993] Marklund, G.: Viking investigations of auroral electrodynamical processes, Journal of Geophysical Research, vol. 98, no. A2, p. 1691-1704, Feb. 1, 1993

[McIlwain, C. E., 1960] McIlwain, C. E.: Direct measurement of particles producing visible auroras, J. Geophys. Res., 65, 2727, 1960

[Mozer et al, 1977] Mozer, F. S., more authors, Observations of paired electrostatic shocks in the polar magnetosphere, Phys. Rev. Lett., 38, 292, 1977

[Mozer and Hull, 2001] Mozer, F. S. and Hull, A.: Origin and geometry of upward parallel electric fields in the auroral acceleration region, Journal of Geophysical Research, Volume 106, Issue A4, p.5763-5778, April 1, 2001

[Mozer and Kletzing, 1998] Mozer, F. and Kletzing, C.: Direct observation of large, quasistatic, parallel electric fields in the auroral acceleration region, Geoph. Res. Letters, vol. 25, no. 10, p. 1629-1632, 1998

[Pedersen et al, 1998] Pedersen, A., Mozer, F. and Gustafsson, G.: Electric Field Measurements in a tenuous plasma with spherical double probes, in Measurement Techniques in Space Plasmas, AGU Geophys. Monograph 103, p. 1-12, 1998

[Pedersen et al, 2001] Pedersen, A., Decreau, B., Escoubet, C.-P., Gustafsson, G., Laakso, H., Lindqvist, P.-A., Lybekk, B., Masson, A., Mozer, F., Vaivads, A.: Four-point high time resolution information on electron densities by the electric field experiments (EFW) on Cluster, Annales Geophysicae, Volume 19, p.1483-1489, 2001

[Savage, C., 1994] Savage, C.: Aurora, Vancouver/Toronto: Douglas & McIntyre Ltd., 1994